EPFL

Thèse n° 7963

Microstructured biodegradable fibers for advanced controlled release

Présentée le 30 octobre 2020

à la Faculté des sciences et techniques de l'ingénieur
Laboratoire des fibres et matériaux photoniques
Programme doctoral en science et génie des matériaux

pour l'obtention du grade de Docteur ès Sciences

par

Shahrzad SHADMAN YAZDI

Acceptée sur proposition du jury

Prof. A. Fontcuberta i Morral, présidente du jury
Prof. F. Sorin, directeur de thèse
Dr L. Boesel, rapporteur
Prof. D. Milanese, rapporteur
Prof. E. Amstad, rapporteuse

École polytechnique fédérale de Lausanne

2020

To my Parents, Farideh and Mohammad,
Who sacrificed a lot so I could follow my dreams.

“As you start to walk on the way, the way appears”

Rumi

Acknowledgment

I wish to express my sincere appreciation to my supervisor, Professor Fabien Sorin, who has the mindset of a true mentor: he guided and encouraged me to be professional and he was understanding and supportive during the difficult times of my project. My experience of working with him starts since my master's program which was extremely fruitful, and later on doing the PhD at his lab on such exciting project was like a dream coming true. I would like to express my highest gratitude toward him not only because he offered me such life-changing opportunities but also because he believed in my strength and gave me the confidence to realize my ideas and to pursue my scientific interests freely. His supervision let me fully enjoy this experience and feel accomplished at the end. Moreover, I would like to thank him for all his encouragement in other aspects such as doing my first black slope on the ski day of the lab or following the french courses of the language center.

I am grateful to all members of my jury committee for the PhD exam: Prof. Anna Fontcuberta (president) and Prof. Esther Amstad from EPFL, Dr. Boesel Luciano from Empa St-Gallen, and Prof. Daniel Milanese from the university of Parma. I would like to thank you all for accepting to read my thesis and to attend my oral exam.

I am so thankful of both old and new members of FIMAP who are like friends to me: Anne Roy, Dr. Dang Tung Nguyen, Dr. Wei Yan, Dr. Alexis Page, Marco Volpi, Dr. Yunpeng Qu, Dr. Tapajyoti Dasgupat, Dr. Federica Sordo, Nicola Bartolomei, Chaoqun Dong, Louis Martin-Monier, Inès Richard, Dr. Bastien Schyrr, Andreas Leber, William Esposito, Pierre-Luc Piveteau, and Dr. Rajasundar Chandran. I feel honored to be able to work with such amazing people and to pass so many wonderful moments inside and outside of the lab. Because of them, I learnt how joyful it is to work in a team: to help each other without any reserve and to be able to laugh hard together during the breaks. Thank you so much all for tolerating my complaints, "my loud voice", and for creating so much funny time that could change my mood at hard times.

More specifically among them, I would like to thank my lab mate and my very good friend, Ines Richard. I worked with her closely during my project. We had so many fruitful and exciting discussions together, and I truly enjoyed all our scientific talks from learning the basic scientific concept together to comping up with new ideas for our experiments. Thank you Ines for always being there for helping me!

I would like to extend my thanks to all the technicians in the workshop of IMX and ATPR atelier: Yves Ruschetta and Alfred Thomas who were there to answer all my question, whether if it was the repetitive

questions regarding the use of machines or to design new ways of preform fabrication. Moreover, I would like to also thank the PhD students and postdocs of LPAC (Dr. Adrien Demongeot, Dr. Amael Maximillien, Alexandre Mordasini,…) and the staff of CIME (Gregoire Baroz, Colette Vallotton and Dr. Lucie Navratilova) for all the trainings, and more importantly for their precious time to give their input on my experiments for adopting the best setting of each machines.

I would like to also thank my friends inside and outside EPFL who made my life so colorful Chilchila, Lea, Rebecca, Marta, and Matt. I would like to also appreciate my Iranian friends as well who give me the feeling of home. Among them I would like to specifically thank Elmira who is like a life coach to me. Her valuable insights and guidance helped me to go through difficult times easier. She is like a sister to me with her genuine kindness. Also I would like to thank her husband, Mahmood who is very smart and kind. He also helped me so much to have the right attitude toward my PhD and to have an oriented career plan. Moreover, I would like to thank my other friends with whom every moment was a true delight and they gave me the energy to go on, Zahra (my love) and Ganga, Nakisa and Patrick, Maryam and Ramin, Sohrab, and so on.

I would like to express my deepest gratitude to my parents who are the most inspiring people in my life as well as my sister and brother. I would like to thank my father who always taught me to dream big, thank you for your support during all these years of my studies abroad. My mother, a true role model for women who always pushed me to follow my desires and supported all my decisions whatsoever. It is beyond words how much I am thankful of them for keeping up with all the frustration of being apart and the constant support they provided either through phone calls or all the delicious Persian food they accompanied with me after each visit. I would like to thank my sister who has been my best friend in all these years and my younger brother who has been the source of joy, fun and coolness in our family.

Moreover, I would like to thank my second family, the parents of my partner, and his sisters' family. They gave me so much love and support that was beyond my imagination. Thank you so much for all the nice meals and memories during the weekends and holidays which was so recharging.

Last but not least, I would like to thank the most special person in my life, Olivier. Definitely, my PhD work and experience would have not been the same without you. You are my true cheerleader and you give me so much purpose in life. I would like to deeply thank you for all the support. Your ultimate kindness and love helped me to go through the difficult moments with so much hope. I would like to deeply thank you for everything azizam…

Résumé

Les polymères biodégradables sont de plus en plus au cœur des dispositifs thérapeutiques. Sous la forme de longues et fines fibres, ils permettent une stratégie efficace de d'administration de médicaments pour diverses configurations biomédicales : sutures, supports de tissus biologiques, pansements, sondes chirurgicales et textiles intelligents. Pourtant, la fabrication de systèmes d'administration de médicaments sous forme de fibre n'a pas su répondre aux besoins de multifonctionnalité, de résistance mécanique, de concentration de médicament et de dynamique complexe de libération de plusieurs médicaments.

La première partie de cette entreprise consiste, pour la première fois, à identifier divers polymères thermoplastiques amorphes (poly (D,L-lactic-co-glycolic acid) – PLGA) ayant les bonnes propriétés rhéologiques et thermomécaniques pour pouvoir être étiré à chaud tout. Ainsi, nous démontrons diverses fibres entièrement ou partiellement biodégradables, ayant des sections circulaires ou rectangulaires, dont les matériaux peuvent avoir des dégradations différées. Ces fibres permettent l'administration de plusieurs doses ou substances dans l'intervalle de plusieurs semaines ou mois. Nous étudions expérimentalement leurs dégradation et dynamique de libération in vitro, et établissons un modèle pour le mécanisme de libération via une évolution morphologique de la dégradation des polymères. Nous montrons des exemples de fibres biodégradables étirées à chaud ayant des résistances mécaniques importantes par ajustement de la contrainte d'étirage, pouvant être utilisées dans des sutures actives. Le deuxième objectif qui émergea durant la thèse fut la modulation du temps d'administration de quelques semaines jusqu'à quelques jours. Un système composite comprenant des particules de verre de phosphate (Phosphate Glass - PG) (période de dégradation de 3 semaines) dans une matrice de PLGA (période de dégradation de 3 mois) fut étudié. Nous ajustâmes la composition afin d'atteindre un comportement rhéologique similaire à la matrice de PLGA, afin d'être compatible avec le procédé d'étirage à chaud. Il fut démontré que l'incorporation de différentes concentrations en particules de phosphate permit l'accélération de la dégradation du PLGA. De plus, le pH acide associé aux composés à base de PLGA est neutralisé au moyen de la suppression de la dégradation de la masse de PLGA et des éléments alcalins des particules de PG. L'intégration de ces composites dans les couches barrières des fibres permit en outre des dynamiques d'administration modulables allant de mécanismes entièrement gouvernés par la diffusion, ou inversement, par l'érosion.

La dernière partie de la présente thèse approfondit l'utilisation de fibres multi-matériaux pour l'administration par stimulation externe. L'effet de la température sur la cinétique de libération du PLGA est d'abord analysée afin de fournir un éclairage sur la réalisation de fibres pour l'administration thermo-stimulée de médicaments. L'accélération de la libération fut observée en exposant des fibres biodégradables à une augmentation de la température dans un four. Basé sur l'effet joule, une architecture novatrice de fibre

pour l'administration de médicaments déclenchée électriquement est proposée et approfondie. Ce travail établit une plateforme novatrice pour les fibres micro-structurées biodégradables pouvant servir d'implants, de sutures, de pansement, ou de support de tissu biologique, une avancée en pharmaceutique pour la réalisation de dispositifs actifs d'administration de médicaments.

Mots-clés : polymères biodégradables, fibres multi-matériaux, dispositifs pour l'administration de médicaments multidoses, cinétique de libération, procédé d'étirage à chaud, fibres composites, dispositifs pour l'administration de médicaments stimulée, sutures

Abstract

Biodegradable polymers are increasingly at the heart of therapeutic devices. Particularly in the form of thin and elongated fibers, they offer an effective strategy for controlled-release in a variety of biomedical configurations such as sutures, scaffolds, wound dressing, surgical or imaging probes, and smart textiles. So far however, the fabrication of fiber-based drug delivery systems has been unable to fulfill significant requirements of medicated fibers such as multi-functionality, adequate mechanical strength, drug loading capability and complex release profiles of multiple substances.

The first part of the work consisted in, for the first time, identifying various grades of biodegradable amorphous thermoplastic polymers poly (D,L-lactic-co-glycolic acid) (PLGA) with the proper thermomechanical and rheological properties to be thermally drawn. Based on this finding, we demonstrate a variety of partially or fully biodegradable fibers with cylindrical and rectangular cross-sectional geometries integrating materials of various biodegradable properties. These fibers are capable of releasing multiple doses or substances in the span of a few weeks to a few months. We experimentally study their degradation and release behavior in vitro, and model the release mechanism via morphological evolution of the degrading polymers. We show examples of thermally drawn biodegradable fibers with high mechanical strength as a result of drawing stress adjustment, that could be used as active sutures. The second objective that arose during the course of the thesis is the tailoring of the release time from a few weeks down to a few days. A composite system comprising PLGA (degradation period of 3 months) as the matrix, and phosphate glass (PG) particles (degradation period of 3 weeks) as filers was studied. We engineered the composition to reach rheological properties similar to the PLGA matrix, so that it can be compatible with the thermal drawing process. It is demonstrated that the incorporation of various contents of phosphate glass particles (5 to 40%) lead to the acceleration of PLGA degradation. Moreover, the acidic pH of PLGA degradation products is neutralized via the suppression of PLGA bulk degradation and the alkali elements of PG particles. The integration of these composites in the release barriers of the fibers also resulted in versatile release profiles ranging from fully diffusion-controlled to erosion-controlled mechanisms.

A final part of the thesis investigates the use of multi-material fibers to realize triggered release from external stimuli, the effect of temperature on the release kinetics of PLGA is first analyzed to provide insights for the realization of heat-triggered drug delivery fibers. The acceleration of release was observed upon exposing biodegradable fibers to an increase of temperature in an oven. Relying on joule heating, a novel architecture for electrically-triggered drug delivery fibers is proposed and investigated. This work establishes a novel platform for biodegradable micro-structured fibers for applications in implants, sutures,

wound dressing, or tissue scaffolds as well as a step toward the future of pharmaceutics in the realization of active and advanced drug delivery systems.

Key words: biodegradable polymers, multimaterial fibers, multi-dose drug delivery systems, release kinetics, thermal drawing process, composite fibers, stimuli-responsive drug delivery systems, sutures

Contents

Introduction

Throughout the history of pharmaceutics, drug delivery systems have been developed in different shapes, from a simple pill to sophisticated devices for the programmable administration of drug[1]. In recent decades, parenteral biodegradable drug delivery systems have gained increasing attention in therapeutics. Current devices however remain limited in the number of incorporated drugs and the non-versatility of release kinetics, which impact the desired therapeutic outcome. The development of complex drug delivery systems capable of serving multiple therapeutic functions is one of the significant remaining challenges in pharmaceutical fields[2]. Some of the medical complications requiring more advanced drug administration include delayed healing of chronic wounds due to prolonged inflammation and lack of growth factors[3], orthopedic implants failure due to peri-implant bone loss which requires systematic injection of drugs over months[4], and long-term administration of drugs in the treatment of diseases such as diabetes, tuberculosis and cancer, which is challenged by patient compliance[5], [6].

Fiber-based programmable drug delivery systems relevant to various applications such as sutures, wound dressing, orthopedic implants and healthcare textiles[2] hold a great promise in improving therapeutic efficacy. The fiber form factor has the potential to alleviate limitations associated with other drug delivery formats such as microcapsules[7], microsphere[8], [9] and nanoparticles[10] that are unable to integrate complex functionality due to lack of adequate surface area, mechanical strength and appropriate structure. Thus far however, although functional biodegradable fibers as drug delivery patches[3], [11], [12] and micro[13], [14]/nano[15] fibrous scaffolds have been established by fiber processing techniques such as electrospinning and wet spinning, the processes have entailed low viscosity which restrict the structural complexity to simple core-shell configurations. For example, when capillary effects dominate, it is difficult in any process to maintain a hollow micro-channel of small radius, especially over extremely long fiber lengths. As a result, simple configurations commonly found in biodegradable fibers limit the number of substance that can be delivered, as well as the complexity of release profiles which are key in several applications. These techniques also do not allow the co-processability of polymers with large variation of degradation rate, which is an important leveraging tool to realize fibers with complex release profiles. Moreover, Beyond the challenges associated with the fabrication approaches and the complexity of fiber architectures, programmable drug delivery fibers with control of both release kinetics and mechanical properties have not yet been investigated[6].

In this thesis, we rely on the thermal drawing process, a versatile fiber-processing approach capable of producing fiber with multi-material architectures with complex functionality[16]–[28]. In a first chapter, we

present some of the main principles and definitions that are relevant to the project at hand. As we will explain, we focused a first part of our work on the well-known poly(glycolide-co-L-lactide) (PLGA) polymers for several reasons: widely used and proven material in the field of delivery, amorphous microstructure potentially compatible with the thermal drawing process, tunable mechanical properties, and ability to engineer several properties (rheological, biodegradability etc…) by changing the composition and molecular weight. A literature review of PLGA drug delivery systems and fibers will be presented and the novelty of our work will be discussed in details (chapter 1). As the initial objective, we investigate the feasibility of the thermal drawing of various PLGA compositions and molecular weights based on their rheological properties. After the identification of appropriate PLGAs, we demonstrate the scalable fabrication of micro-structured biodegradable fibers with multiple reservoirs of arbitrary size and position, spanning the entire fiber length (chapter 2). Next, we characterize the release kinetics and biodegradation properties of the identified PLGAs, from which the control release of unprecedented complexity can be achieved. We propose a model to account for the PLGA degradation after thermal drawing, via morphological evolution of the degrading polymers and a phenomenological reaction-diffusion degradation model. The proposed model is defined based on the Fickian diffusion equations and includes an effective diffusion coefficient which is subject to change throughout the degradation. Moreover, we show examples of thermally drawn biodegradable fibers with high mechanical strength as a result of drawing stress adjustment, that could be used as active sutures. Also, in order to tackle the well-known shrinkage problem of fibers highly aligned polymer chains, methods such as a heat treatment procedure and codrawing of the amorphous PLGA with a semicrystalline polymer are developed (chapter 3).

After the throughout study of the thermal drawing of micro-structured PLGA and its exploitation to engineer complex release profiles, we will turn towards composites materials that can bring another dimension to tailor processing and release properties. In particular, we develop a novel composite of PLGA and biodegradable phosphate glass (PG) microparticles to fabricate innovative thermally drawn drug carrying fibers. Engineering the release kinetics through the tailoring the morphology and degradation chemistry of the PLGA via the incorporation of various contents of PG particles is shown (Chapter 4). Finally, our last objective is to exploit the multi-material thermal drawing platform to realize stimuli-responsive drug delivery fibers, to trigger the release on demand. We propose fiber configurations with two stainless steel electrodes in the vicinity of PLGA films, which allowed the generation of elevated temperatures via the joule effect, with a direct impact on the release kinetics. The release studies showed that upon the application of a high voltage (4V), the diffusion of macromolecular drugs is inhibited due to the rubbery state of PLGA, however, the use of smaller drug size and thinner PLGA films are found to be promising factors to stimulate the release in such configurations (chapter 5).

In a last chapter, we will summarize our findings and discuss several directions of research to exploit these novel building blocks that we could establish in the course of this thesis.

Chapter 1 State of the art

In this chapter we present a review of some of the critical studies previously done as well as the theories relevant to our research. First, the potential of the thermal drawing process is described through an example of photodetecting fibers, and a review of recently published biodegradable thermally drawn fibers is presented. Next, the degradation mechanism and different classifications of biodegradable polymers are described. In order to provide insights on the release profiles of our PLGA drug delivery fibers, the release kinetics of various PLGA drug delivery systems are presented and compared. Next, different models for the description of drug delivery systems governed by various release mechanisms are presented and their weaknesses and strengths are discussed. We will then emphasize the need for the development of our proposed complex drug delivery fibers through some previous works on multi-reservoir drug delivery systems. As the fourth chapter focuses on the development of PLGA and phosphate glass particle composites, the degradation mechanism and biomedical benefits of phosphate glass particles are also described. To introduce our ultimate goal of the realization of responsive drug delivery systems, the common employed triggers and responsive polymers are presented. Finally, to demonstrate the potential application of our fibers in sutures, the tensile properties of the absorbable sutures based on their compositions are shown.

1.1 Thermal drawing of biodegradable fibers

The advent of thermal drawing dates back to the emergence of silica-based optical fibers [29], [30]. Despite its long history, thermally drawn fibers have only recently found applications in other fields beyond optical transport and sensing. Recently indeed, fibers that can detect light [31], [32], heat [33], sound [34], and chemicals [35] have been realized using this fabrication process. An example of photodetecting fibers is shown below in Figure 1.1b where different class of materials such as metals, semiconductors, and insulators are integrated in prescribed position and feature sizes in the fiber cross-section. The fabrication process involves heating a preform that is a macroscopic version of the final fiber [36] (Figure 1.1a). Preforms are fabricated using simple apparatus that are used to assemble different materials at the centimeter to sub-millimeter scale. Brought to the furnace of a draw tower, the assembly is heated and pulled into kilometers-long fibers (Figure 1.1c). For a successful draw, as we discuss in more details below and in chapter 2, materials with high viscosity at the processing temperature are required to counter balance capillary effects and ensure the preservation of complex architecture down to the micro-meter scale.

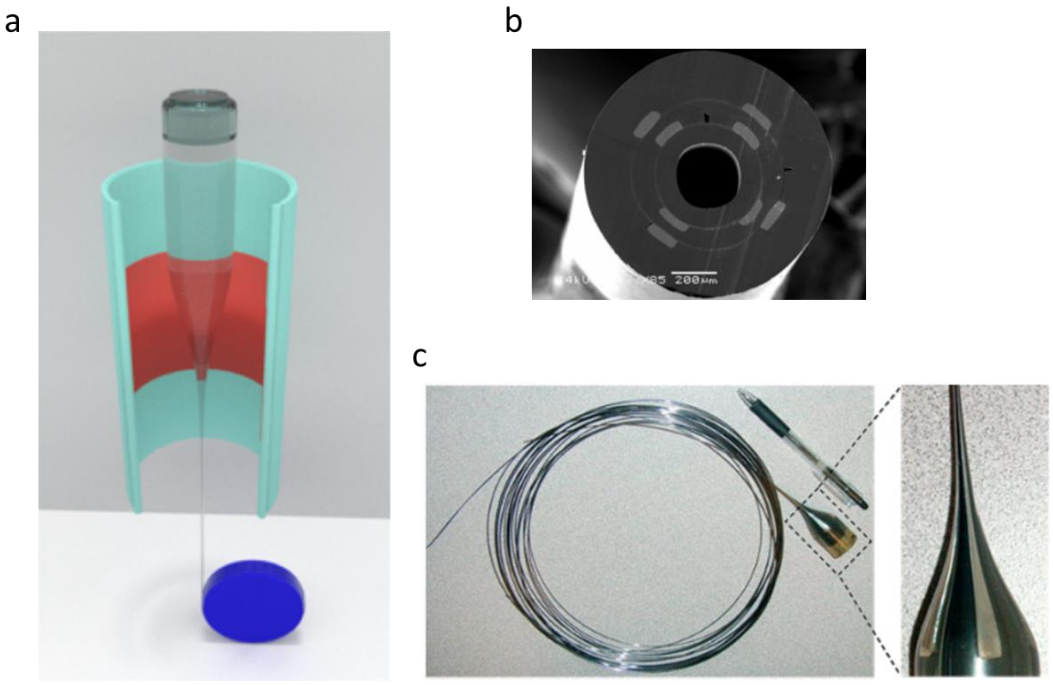

Figure 1.1 a) Schematic of thermal drawing process, b) scanning electron miscorscopy of the cross-section of a fiber device[32], c) structure of a macroscopic preform drawn down to meters-long fiber devices[37]

Despite the vast variety of materials that have been shown to be compatible with the thermal drawing process, including inorganic metals, glasses, elastomers, porous materials or even piezoelectric materials[38], [39], the fabrication of thermally drawn biodegradable fibers is still at it infancy. For a long time indeed, the lack of a broader rheological criteria governing the compatibility of materials with the thermal drawing process has made it difficult to find compatible materials with novel attributes. In a recent paper however, Qu et.al[17] described a simple yet powerful criteria for thermoplastics to be suitable for thermal drawing: a large loss modulus (G") that is greater than the storage modulus (G') within the processing temperature window, and with G" decreasing slowly with temperature in this range. This rheological property is well illustrated in Figure 1.2 for a polycarbonate (PC), a conventional polymer extensively used in thermally drawn fibers. The temperature at which the crossover of G" and G' occurs is used to set the drawing temperature profile.

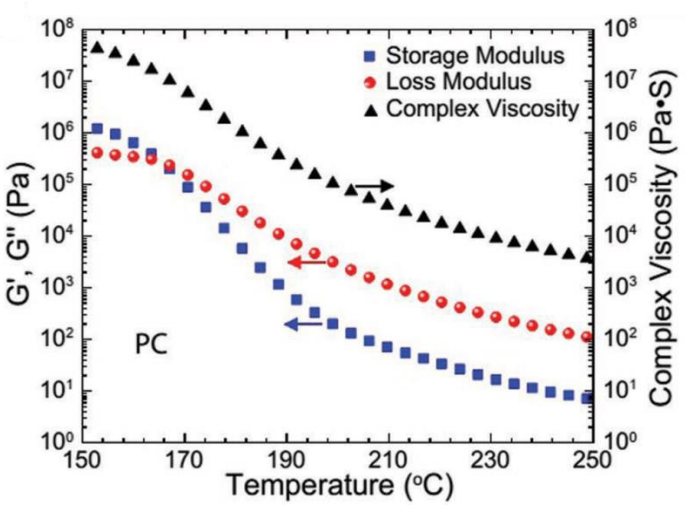

Figure 1.2. Rheological properties of polycarbonate (PC)[17]

Thus far, biodegradable polymers such as Polylactic acid (PLA) and Polycaprolactone (PCL) have been integrated in the thermal drawing process albeit within an amorphous cladding. Indeed, their semicrystalline microstructure results in a sudden drop of viscosity with the increase of temperature due to the melting of the crystalline part, which makes it very difficult to draw such materials on their own. Some of the examples include porous PCL and PLA fabricated by the combination of thermal drawing and salt leaching using a polystyrene cladding (Figure 1.3)[40] and porous PCL fibers fabricated by the combination of thermal drawing and thermally induced phase separation (TIPS) using a cyclic olefin copolymer (COC) as the cladding (Figure 1.4)[41].

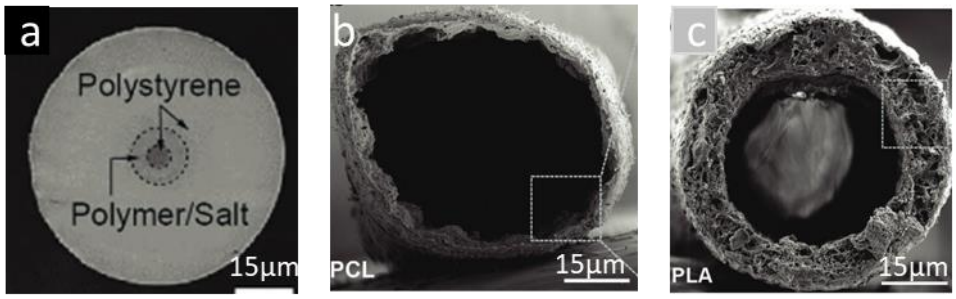

Figure 1.3. a) Cross-section of preforms containing PCL/NaCl composite and polystyrene as sacrificial core and cladding, b,c) porous PCL and PLA fiber channels respectively[40]

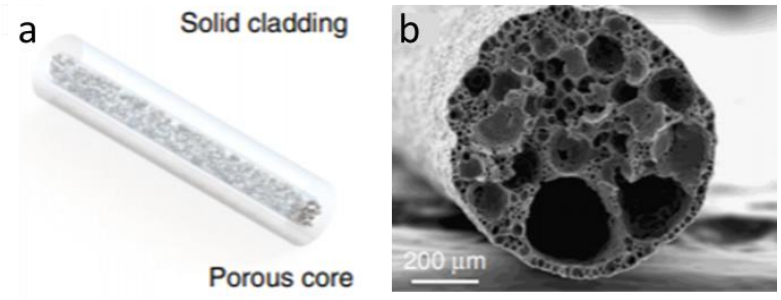

Figure 1.4. a) section of drawn fiber containing porous core with dense cladding, b) SEM of porous PCL fiber[41]

Despite these interesting examples, the control of microstructures in such fibers requires additional processing steps and the obtained architectures are too simple and limited. Moreover, the incorporated polymers possess a very slow degradation rate which limit the types of applications that could be envisioned. Therefore, a novel material system is required to address these challenges and to couple tailored biodegradation properties with the versatility of the multi-material thermal drawing process.

1.2 Biodegradable polymers

Biodegradable polymers used in the drug delivery systems can be divided into two subsets: natural and synthetic[42]. Examples of natural biodegradable polymers could be found in classes of proteins and polysaccharides such as Albumin[43], Cellulose[44] and Starch[45]. Synthetic biodegradable polymers generally contain bonds such as ester-, amide- and anhydride bonds which degrade either through hydrolysis or enzymatic reactions[46]. While controlling the release behavior through natural biodegradable polymers is not easy, synthetic biodegradable polymers offer a variety of tools to control the release. The degradation can occur in two different mechanisms: 1) surface degradation where the erosion starts from the outer part of the material and is faster than water diffusion[47], 2) bulk degradation where the bulk of material

undergoes the erosion process[1]. The bulk degradation can be further divided into homogenous or heterogeneous erosion depending on the rate of water diffusion. The schematic of these two mechanisms is illustrated in Figure 1.5.

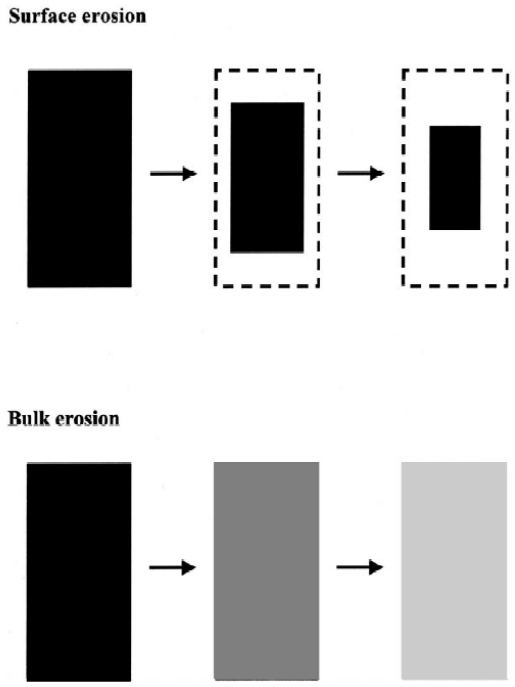

Figure 1.5. schematic of two mechanisms of degradation: surface erosion and bulk erosion[47]

The hydrolysis degradation consists of series of complex steps such as: the diffusion of the water inside the polymer, the creation of monomers and oligomers and the diffusion of monomers out of the system which leads to the erosion of the polymer[42]. Since the chain scission starts from the very early stage of the degradation, the relation between the molecular weight and time is used to define the degradation kinetics, described by zero-order or pseudo first-order equations[46]. Bioerosion occurs when the hydrolysis is advanced enough that polymer chains possess the critical molecular weight which is equivalent to the oligomers up to nanomers[48] or the number average molecular weight (Mn)=13,500 for PLGA. At this stage the polymer chains can dissolve in water and lead to weight loss. While the two definitions of degradation and erosion are interrelated, they occur at different time scales and thus different release behaviors are obtained from each of them. In this work we aim to study the release properties of various types of PLGA in thermally drawn fibers, and in particular investigate if similar degradation mechanisms will be at play at the fiber level.

1.3 Release kinetics of PLGA drug delivery systems

PLGA shows different release kinetics depending on the geometry and architecture of the device. Nevertheless, in all cases the governing mechanism is based on both diffusion and erosion. The typical release profile of PLGA is a sigmoidal or a classical S shape. The initial stage of the release profile is mainly controlled by the device geometry (film thickness etc…) and the concentration gradient while the later stage is driven by the degradation kinetics of the PLGA[49].

In Figure 1.6, several examples of PLGA drug carriers exhibiting a sigmoidal shape are presented. The release profile of Sirolimus from a PLGA coating layer exhibits the two phases of slow release and fast release with different drug loadings[49] (Figure 1.6a). As can be seen, the release rate in the diffusion phase is very slow and the degradation is the governing mechanism for the complete release. This was attributed to the hydrophobicity of Sirolimus and its uniform distribution in the film. In another study on the release behavior of fluorescein isothiocyanate labeled dextran (FD), a hydrophilic drug, from PLGA microspheres of diameter of 30-40 μm[8], a sigmoidal shape profile was also obtained for different molecular weights of FD (Figure 1.6b). The effect of drug type on the release kinetics from PLGA pellets was also investigated. Two-phase profiles were obtained for all types[50] (Figure 1.6c); the fastest diffusion phase corresponded to Aspirin, the most hydrophilic of all while Haloperidol, a hydrophobic drug, exhibited much slower diffusion phase. While these interesting observations were found in this study, no clear and strong relationship could be derived for other types of drugs with respect to their release kinetics.

From the analyses of the release kinetics of different systems, it can be concluded that in the cases where the size of PLGA carrier is large (more than a few microns), or the incorporated drug is hydrophobic or a supramolecular substance, degradation plays an important role in the release and therefore the release curves have a sigmoidal shape. This prevalence of the degradation mechanism in the release kinetics can be explained by the inhibition of drug diffusion through the polymer chains due to reasons including long diffusion pathways, large size of the drug, or high affinity of the drug to the polymer.

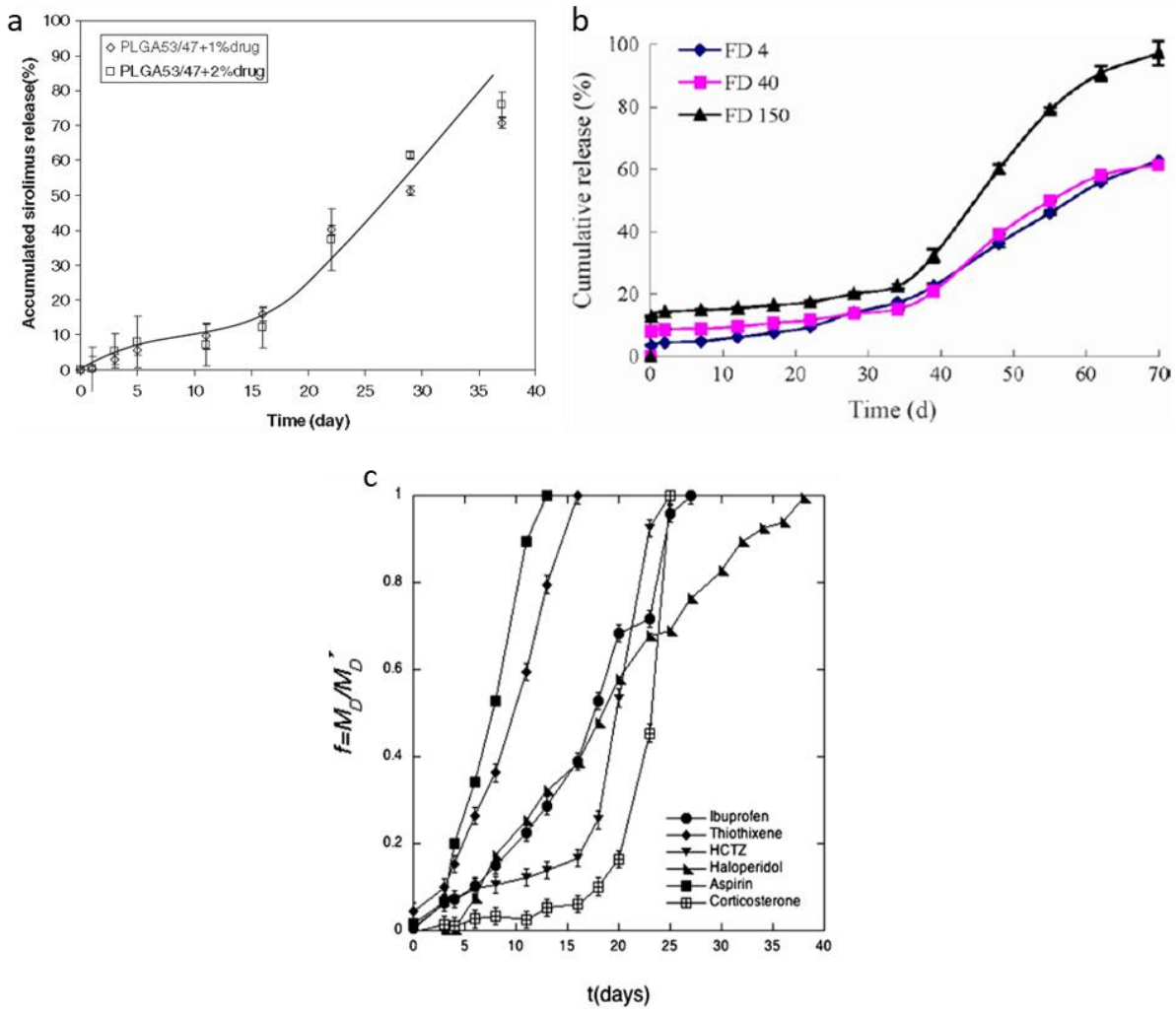

Figure 1.6. a)The cumulative release of Sirolimus from PLGA 53/47 for different drug loading[49], b) the release curves obtained for different molecular weights of FD from PLGA microspheres[8], c) The release curves of six different drugs from PLGA pellets containing the same weight fraction[50]

1.4 Understanding and modeling the release mechanism

In order to design a novel material system for controlled drug delivery, it is crucial to understand the underlying mechanism in drug transport. The development of an appropriate mathematical description could help predicting the release kinetics before the realization of the device, as well as interpret and better exploit experimental data. Different models have been developed to describe the drug release governed by diffusion and degradation mechanisms. In a drug delivery system, the drug can be loaded inside a matrix or a reservoir[51]. Depending on the matrix if it is degradable or non-degradable, the release mechanism varies.

In the case of a non-degradable matrix, the release is governed by Fickian diffusion which takes into account parameters such as the concentration gradient, diffusion distance and swelling[52]. A general model used to describe these phenomena is[53]:

$$\frac{M_t}{M_\infty} = kt^n \quad (1.1)$$

Where M_t and M_∞ are the amount of drug released after time (t) and an infinite time respectively. *k* is a constant, *t* is the release time, and *n* is an exponent for the characterization of the release. The interplay between the two mechanisms of diffusion and swelling in drug transport can be divided into the following scenarios and is reflected in the value of *n* which determines the shape of the release profiles.

1) Fickian diffusion describes the drug transport when the characteristic relaxation time (t_r) is not equal to the solvent diffusion time (t_d) and therefore the diffusion coefficient is not constant[1]. (n is equal to ½)
2) Anomalous or non-Fickian describes the diffusion of drugs when the relaxation time and the solvent diffusion time is almost equal ($t_r \approx t_d$)[1]. (n is between ½ and 1)
3) Case II transport mechanism in which the drug release is mainly derived by swelling relaxation characteristic of the polymer[54]. (n is equal to 1)

The relaxation time is based on the reptation theory[55]. It describes the polymer chain entanglement by a relationship between molecular mass and chain relaxation time. For a given polymer and solvent, the relaxation time depends on the solvent concentration and temperature[1].

The most commonly used model for the description of controlled release systems based on the Fickian equation is the Higuchi equation[56]. This model describes the release of water soluble drugs into a semi-solid and/or solid mixtures. The hypotheses are that the drugs are uniformly dispersed in the matrix as the diffusing media, there is no dissolution and swelling of the matrix, and the diffusion occurs in one-dimension. The model results in the dependency of the released drug with the square root of time.

On the other hand, the mathematical modeling of the erodible systems is much more complex than the diffusion- or swelling- controlled release systems[57]. The complexity comes from the variety of chemical reactions and physical mass transport phenomena which can induce the release. Moreover, due to the degradation, their parameters are constantly changing with time. As the release barrier in our system is a thin PLGA film characterized by bulk degradation and a non-uniform pore structure, the developed models which consider these phenomena are presented here. These models are based on phenomenological empirical models or diffusion-reaction theories. It is crucial to analyze the strength and weakness of each model and recognize the dominating step in each case to apply an appropriate model to our system.

The mechanistic models are highly accurate and predictive models that take into account all the involved processes. In contrast empirical equations focus on the final release rate resulting from the superposition of all the involved phenomena during degradation[47]. Therefore, while the mechanistic models are more powerful, they are also more difficult to deal with. An example is the work of Zhu et. al.[58] where they studied the drug release from PLGA coating on stents. They introduced the interesting concept of drug diffusivity through both the polymer phase and the liquid-filled pores. The release through each medium determines the shape of slow and fast release phases in the PLGA release profile. The schematic is displayed in Figure 1.7. A model for the effective drug diffusivity was derived based on polymer molecular weight (MW) change, drug partitioning coefficient and the porosity change, and subsequently used to describe the release equation. This model is not adapted for our system as their degradation model neglects the autocatalytic effect due to the short length scale of the coating (the order of 10 μm).

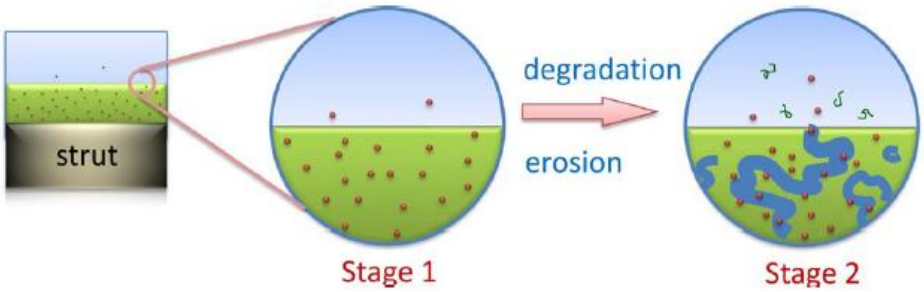

Figure 1.7. Two stage release from a drug loaded PLGA coating, stage 1: diffusion through the polymer matrix, stage 2: simultaneous diffusion through polymer matrix and the pores[58]

Heller and Baker developed a model for the description of bulk-eroding polymers such as PLGA when the drug is dispersed inside a matrix[59]. The first phase of their model was described by the Higuchi equation, implying purely diffusion-controlled release followed by a first-order release profile resulting from the degradation process. The characteristic release curves of the two models are shown in Figure 1.8. In the case of Higuchi curve, the release rate decreases with time due to the increase of diffusion pathways, while in the release curve by Heller and Baker, after the first phase, the release rate starts to increase due to the progression of erosion[47]. While their model included the effect of bioerosion and the increase of drug permeability with time, the release was described for the polymers as a carrier matrix while neglecting the degradation effect in the initial phase.

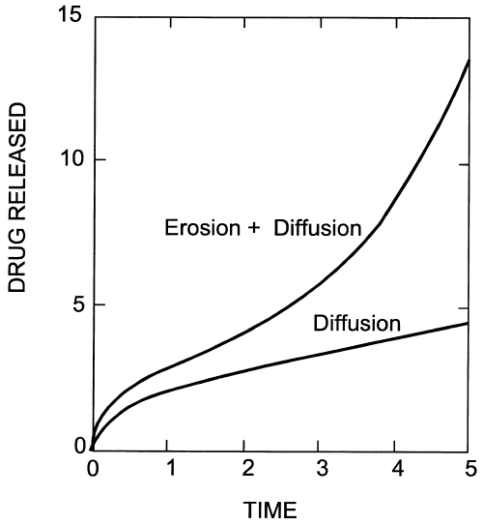

Figure 1.8. The release curves describing model of Heller and Baker (erosion+diffusion curve) and the classical Higuchi equations (diffusion curve)[47]

Batycky et al. has also developed a theoretical model for the description of drug release from PLGA bulk-eroding microspheres[60]. The interesting parameter in this study is the correlation of evolving pore structure with the diffusing species which is crucial in the release of macromolecular drugs. The size of the pores was calculated based on the mass and molecular weights of the degrading polymer chains and classified into the subsets of micro-, meso- and macro- pores. They described that after a certain time called induction time[61], the micropores coalesce and their radius become large enough to permit the release of macromolecule drugs. Finally, a continuous release equation was derived based on the Fickian diffusion of drugs though the pores. While this model takes into account the morphological evolution of the polymer for drug release, it requires experimental measurements or the estimation of a long list of parameters. Moreover, the system is defined for drug-loaded microspheres rather than a reservoir-type system.

Autocatalytic effect has a significant impact on the release kinetics as it induces faster degradation in thicker films, however surprisingly this effect has been rarely implemented in the release models. One example is the model of Thombre, Joshi and Himmelstein[62] which considers the acceleration of the degradation by acid-producing species in poly(ortho ester)-based drug delivery systems. They considered the presence of 4 species: water, acid generator, acidic catalyst and drug; their reaction and diffusion were coupled and described by partial differential equations. In these systems the acid generator species were a third substance aside from the polymer and the drug and not a product of the degradation itself. In case of PLGA, autocatalysis occurs by the acidic oligomer as the byproducts of the degradation itself. Non-empirical models such as Monte Carlo approaches have also been developed[63], [64] to describe the release kinetics from the polymers possessing both surface and bulk degradation mechanism. These models treat the

degradation as a random event[47]. Due to the lack of an appropriate model for mathematical description of the release from autocatalysed bulk eroding release barrier, we adopted a phenomenological degradation model from the work of Wang et al.[65] and derived the release equation based on it. This will be discussed in Chapter 3.

1.5 Advanced drug delivery systems (multi-dose or multi-drug)

This category of devices represents active preprogrammed controlled release systems and capable of producing complex release profiles such as multiple pulses or regimes in a programmable pattern. The development of such devices constitutes one of the main focus of the pharmaceutical field as their integration in biomedical devices could significantly help the therapeutic efficiency both in local and systematic therapies.

One strategy for the fabrication of complex drug delivery systems is the integration of multiple materials in a single device where the desired release profile could be engineered based on the physicochemical properties, geometry and position of each component. For example, pulsatile release profiles for the release of Parathyroid hormone was achieved by stacking surface-erosion polymers alternating with drug-loaded layers inside a hollow cylinder as the sealant filling made up of biodegradable PLA[66]. The schematic of the device with the corresponding pulsatile release profile for different polyethylene glycol (PEG)-containing anhydrides is presented in Figure 1.9.

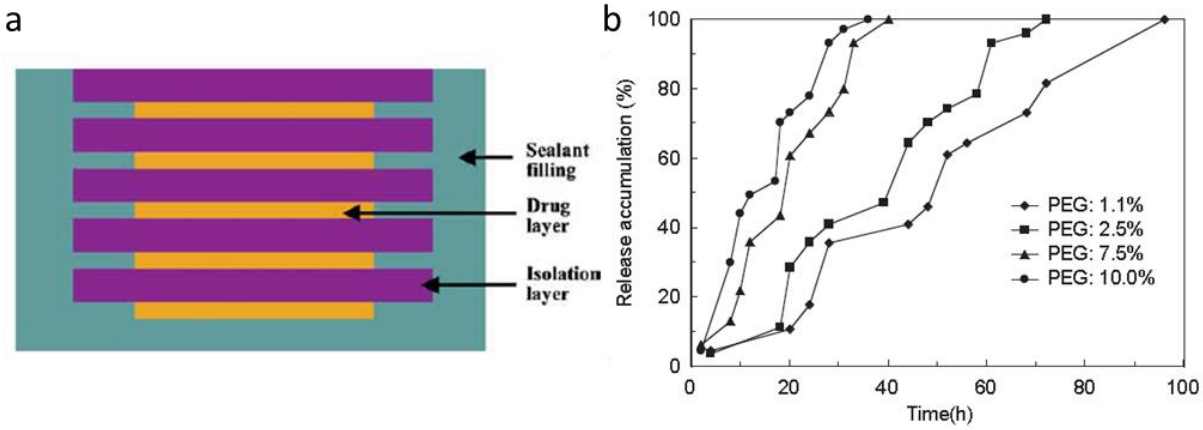

Figure 1.9. Schematic of alternating layer of polymers with drug-loaded layers and the corresponding multi-pulse profile for different PEG% in anhydrides, using BSA as the drug model[66]

With a similar concept, Grayson et al.[67] developed multi-pulse biodegradable microchips containing microreservoirs sealed with PLGAs of differed molecular weights. The schematic and the cumulative

release profile from four of the reservoirs filled with dextran is shown in Figure 1.10. In these works, the fabrication process consists of multiple techniques such as 3D-printing, compression molding, and hot-pressing performed separately for each component. Such processing steps remain cumbersome, inflexible, irreproducible or un-scalable.

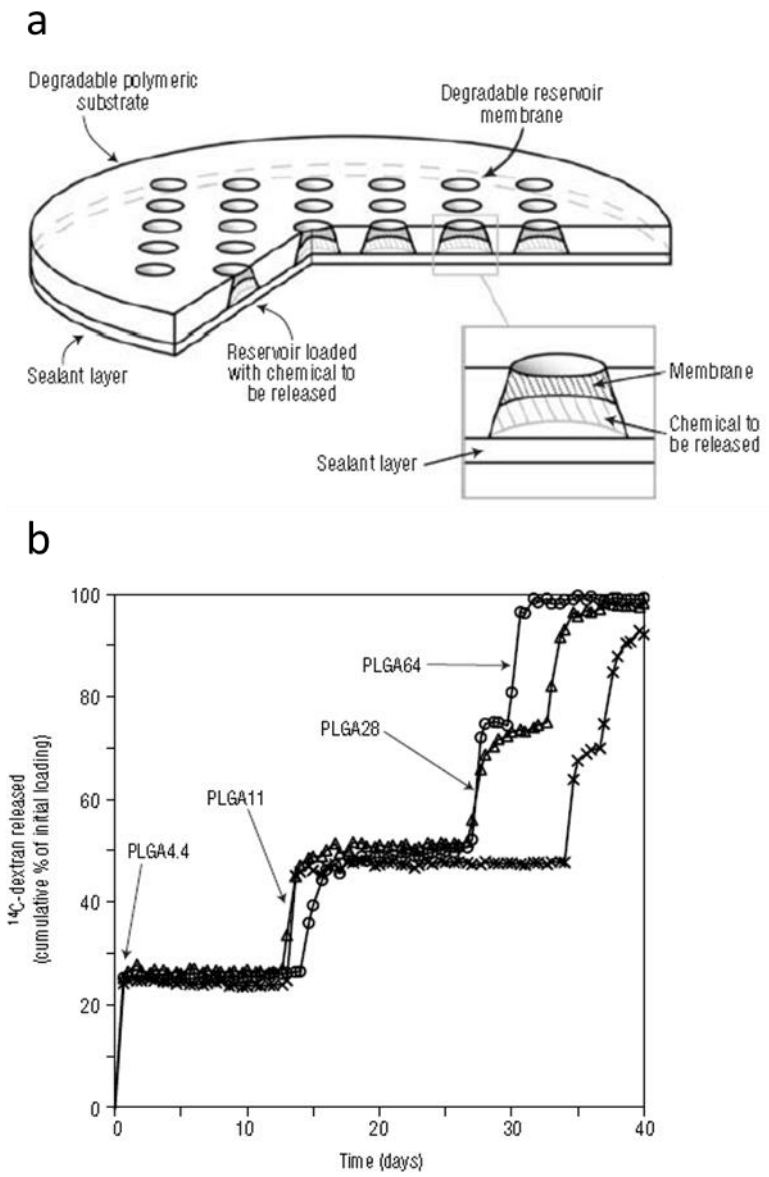

Figure 1.10. a) Schematic of microchip devices made up of a degradable substrate containing reservoirs with membranes and sealant, b) cumulative release of C-dextran released from microdevices each containing 4 reservoirs[67]

Another engineering method for these systems includes biomedical microelectromechanical systems (BioMEMS) such as microneedles, micropumps, microvalves and microfluidics[68]. Such microfabrication

techniques are adapted from the semiconductor processing which also consists of a series of steps and produced in a limited throughput. In addition, in most of these systems, the integrated components are not fully biodegradable and the design is based on complex geometries[69].

There have been several attempts to produce complex drug delivery systems in the fiber format. Examples are electrospun nanofibers coated with micelle nanocarrier capable of dual releasing[70], core-shell nanofibers produced by coaxial electrospinning[71], and fibers filled with biodegradable nanoparticles fabricated by both wet and dry-wet spinning[72]. Due to the solution/melt nature of these processing conditions, these techniques cannot process multiple number of materials or any types of drug. This could consequently influence their functionality and their level of structural complexity. Moreover, such fibers are in nano/microscale which could not be easily implemented in applications such as sutures or textiles.

1.6 Ceramics and glasses: Phosphate glasses

The most widespread use of bioceramics and bioglasses has been in tissue engineering. Biocomposites composed of biocompatible polymer matrix and fillers have been developed to achieve superior properties such as increasing the elastic modulus[73], [74], decreasing the degradation rate[73], [74], improving tissue adhesion[75] and osteoinductive potential[76]. The most common used fillers in bioapplications are hydroxyapatite (HA)($Ca_{10}(PO_4)_6(OH)_2$)[77], [78] and bioactive glasses (e.g. bioglass with the composition of 45% SiO_2, 24.5% Na_2O, 24.4% CaO and 6% P_2O_5 in wt%)[79]. The utilization of these fillers is due to their similar chemical properties[80] to bone and their bioactivity[81]. While these fillers have appealing properties, their degradation rate is too fast in the case of HA[82] or too slow in the case of bioglass[83] to be adjusted with the lifetime of the target implant.

In contrast to bioglasses and HA, phosphate glasses (PG) containing at least 50% P_2O_5[84] have tailorable chemical properties which could be engineered to achieve dissolution rates over several orders of magnitude[85]. There has been a significant amount of work on the dissolution of phosphate glasses in ternary systems P_2O_5-CaO-Na_2O[86]. The properties of these PGs are derived from $PO4^{3-}$ tetrahedron structural units where three oxygen atoms are bonding with the neighboring tetrahedral to form a 3-D network and the terminal oxygen is connected to the phosphorous atom[87], shown in Figure 1.11. These bridging oxygens can be broken by modifying oxides such as alkali and alkali earth metal oxides[88] to depolymerize the glass structure. In general, divalent cations such as Ca^{2+} and Mg^{2+} can improve the durability of the glass more than monovalent cations such as Na^{+} by creating ionic crosslinks between non-bridging oxygens[89]. Particularly with the substitution of CaO by MgO an increase in pH was observed and the weight loss was delayed [90]. This is because Mg^{2+} is able to create even stronger bonds compared

to Ca^{2+} because of its smaller radius and thus higher field strength[91]. Moreover, this composition is also advantageous as the very high solubility rate of the glass could cause inflammatory reaction[92]. In this work the phosphate glass has this composition: P_2O_5 (50%), Na_2O (11.5%), B_2O_3 (2.5%), CaO (10%), SiO_2 (3%), MgO (23%)

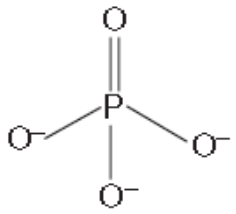

Figure 1.11. Phosphate anion tetrahedra[93]

It was suggested that the mechanism of dissolution is based on the hydration of phosphate chains rather than hydrolysis[89]. The degradation process of PGs consists of two steps: a slow degradation due to the diffusion of water molecules inside the glass followed by a uniform degradation which depends on the rate of the detachment of hydrated part from the partially hydrated part[93].

Phosphate glasses have been widely employed owing to their biocompatibility with the hard and soft tissues and also excellent optical properties[85], [91]. Some of the common clinical applications of PG could be found in bacterial control devices[94], nerve repair[95] and oral healthcare[96]. Even though tailoring the degradation rate via composites have been widely studied[91], [97], this attribute has been rarely implemented in the drug delivery devices. Some examples of systems in which PG was utilized as the medium of drug transport include the followings and their release profiles are presented in Figure 1.12: 1) Figure 1.12a presents the release profiles of hollow core PG fibers loaded with different types of drugs which were all released in the period of 18 min[84]. 2) Figure 1.12b shows the sustained release profile obtained for PG nanoparticles incorporating different La_2O_3 content (PL0, PL5, and PL10) and loaded with ciprofloxacin as the drug[98]. 3) Figure 1.12c corresponds to the release profiles of a composite of PG/PMMA with different PG contents and loaded with an antibiotic drug[99]. Although dissolution of different PGs successfully resulted in the drug transport in the aforementioned works, this property was not fully exploited to achieve tailorable release kinetics.

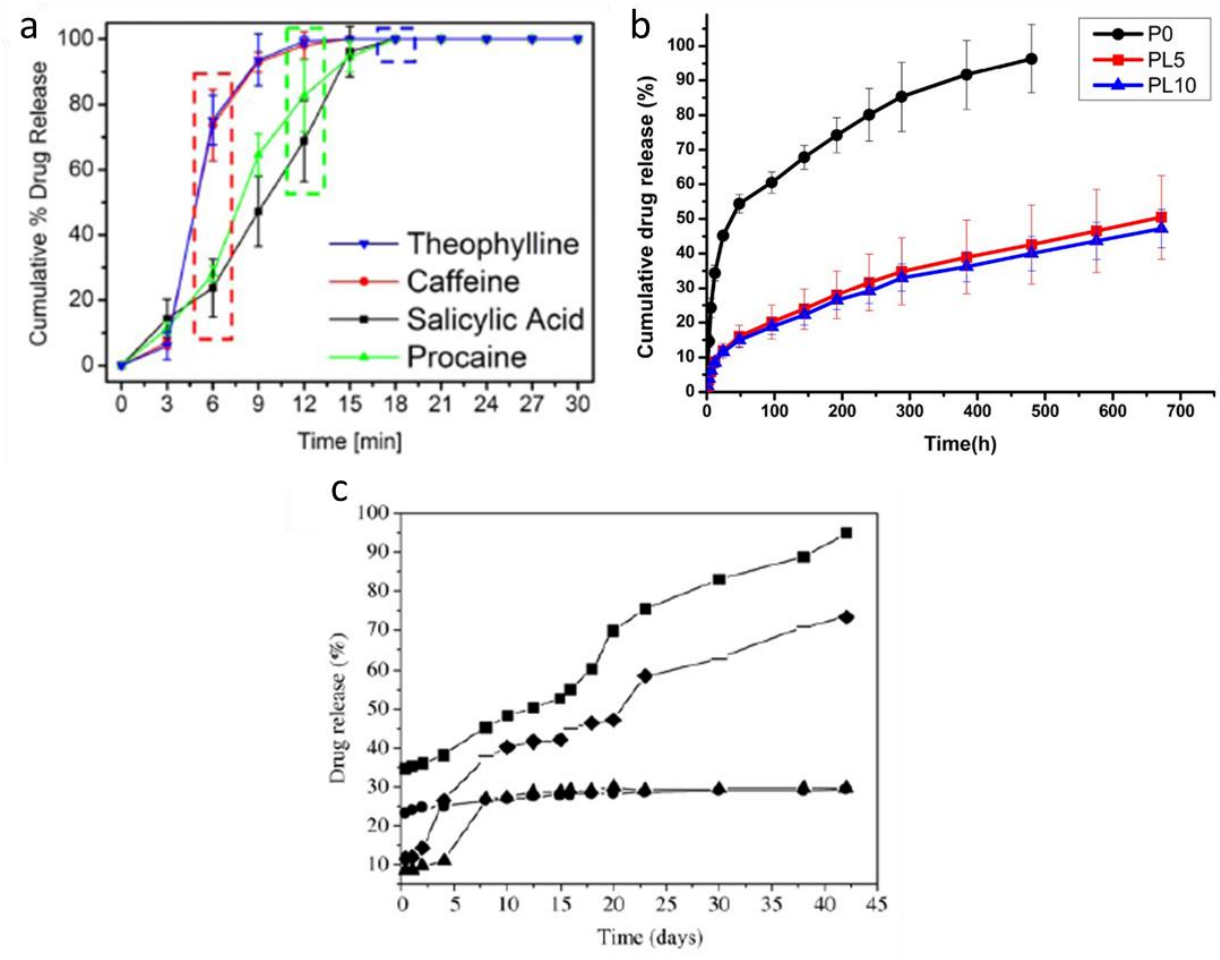

Figure 1.12. Release curves from various phosphate glass systems: a) PG hollow core fibers filled with various drugs[84], b) PG nanoparticles of various La_2O_3 contents: 0% (P0), 5% (PL5), and 10% (PL10) loaded with Ciprofloxacin[98], c) PMMA/PG composites of various PG content: 30 wt% PG (▲), 60 wt % (♦), 70 wt% PG (■), and 0 wt% PG (●) loaded with Vancomycin[99]

1.7 Stimuli-responsive drug delivery devices

In order to achieve drug release in a targeted manner or on-demand, drug delivery devices responsive to chemical (pH, ionic strength), physical(electrical current, magnetic field, mechanical stress) and biological (enzymes, biomolecules) stimuli have been designed[68]. These stimuli can be further classified to intrinsic (naturally exists in the body) and extrinsic (man-made)[100] categories. These devices represent active self-programmed controlled release systems and require responsive polymers to exhibit a change in their physiochemical properties by a specific stimulus. The most common intrinsic triggers are the pH and enzymes[46] since a change in their level is affiliated to a disease. As an example, solid tumors lead to the accumulation of acidic metabolites and thus a pH fluctuation[101]. The outcome of release patterns from stimuli-responsive devices could be a pulsatile release or the acceleration of the initial release profile. The

examples are a zero-order release from poly (ethylene glycol) hydrogels in the presence of an enzyme[102] and a faster release rate from poly (ortho ester amides) in an acidic pH[103].

Drug delivery systems based on external stimuli such as temperature, light, magnetic field and ultrasound have been widely investigated. The external stimuli-based systems allow higher control over the precision of both released dosage and rate compared to the intrinsic stimuli. Among these stimuli, temperature is an effective trigger in changing the behavior of polymers. The temperature-sensitive polymers could manifest behaviors such as the increase in water solubility[104], a change in physical and chemical properties[105], and the acceleration of the degradation rate. The heating source in these systems relies on sophisticated mechanisms such as magneto-calorification or photothermal transformation[100]. This method of release activation is mainly employed in the treatment of cancer as the increase of the temperature is also beneficial in damaging the tumor tissues.

While the development of new formulations of responsive polymers has led to major advances in the growth of functional drug delivery systems, the structure and functionality of such devices remain simple. The reason lies in the lack of an appropriate fabrication technique to introduce the external trigger in complex configurations. In Chapter 5 of the thesis, we will present a simple design for heat-induced release via Joule heating in thermally drawn fibers.

1.8 Mechanical properties of absorbable sutures

One of the most promising applications of our developed fibers is sutures. Since they are load-bearing devices, their mechanical strength is crucial to ensure the closure of the wound and mechanical support during healing. The required values for the mechanical strength differ based on the wounded site such as ophthalmic, pediatric, gynecology and cutaneous surgery. Tensile test is the common procedure to describe important parameters such as breaking load at failure and elongation[106]. The stress-strain curves of commonly used absorbable sutures are shown in the Figure 1.13. The common absorbable sutures such as Maxon and Vicryl are composed of semicrystalline polymers: polyglyconate and polyglactin 910, respectively. Polyglactin 910 is the semicrystalline copolymer of glycolic and lactic acid with the formula of poly(glycolide-co-L-lactide) 90/10 and exhibits mechanical strength of 1300 MPa in unknotted configuration. This value is the highest tensile strength among the absorbable sutures after Rapid polyglactin 910[106]. However, it should be noted that this value corresponds to braided sutures which offer enhanced strength compared to monofilament sutures. The other sutures possess much lower mechanical strength (a few hundred MPa) and the natural sutures such as plain gut and chromic gut lie in the lowest range.

The drawback with these semicrystalline polymers is that they are not easy to process into fibers with micro-structured cross-section or multi-material architectures, and their degradation rate cannot be easily tailored. Additional processing such as coating and radiation[107] are required to increase their degradation rate. On the other hand, amorphous polymers such as PLGA offer fast degradation rate but possess low mechanical strength. In this work, we thrive to improve the mechanical property of PLGA through the alignment of the polymer chains during the drawing process.

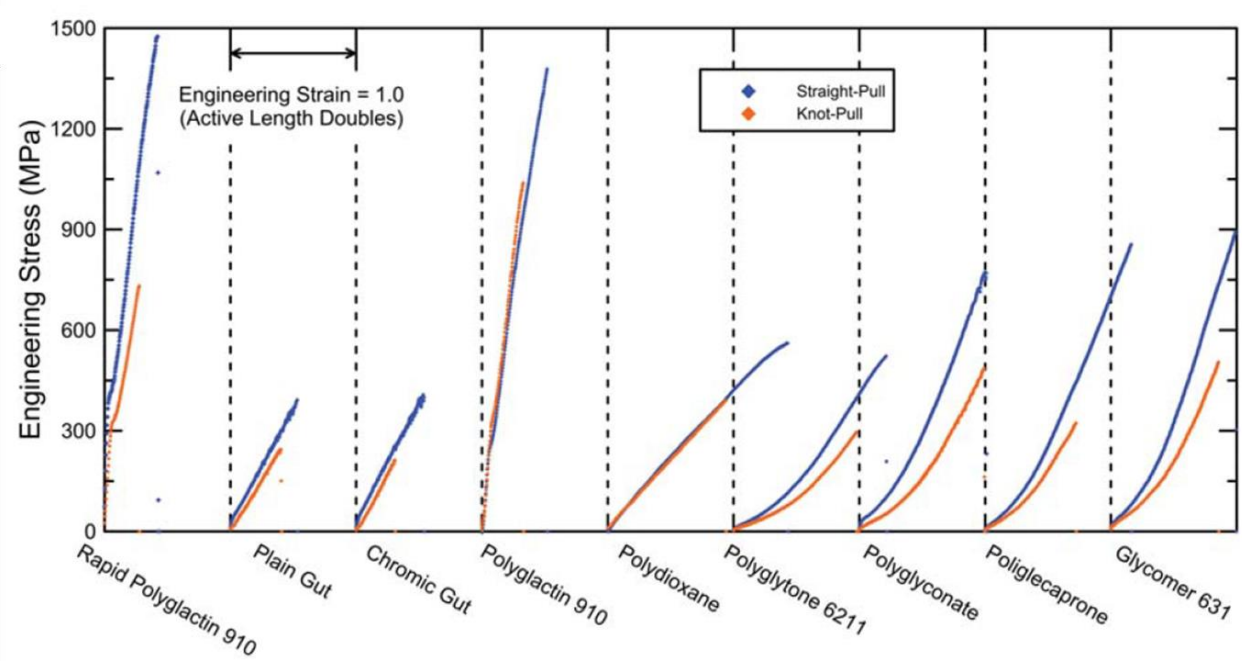

Figure 1.13. Stress Vs. strain curves for absorbable sutures in straight and knot configurations[106]

Chapter 2 Thermal drawing of biodegradable polymers

In this chapter, the rheological and thermal properties of PLGA75 (containing 75% lactide and 25% glycolide) are first analyzed to verify its compatibility with the thermal drawing process. The measurements are done on various forms of PLGA75 (as-bought pellets, hot-pressed pellets, solvent-cast film) to study the effect of processing on the polymer morphology. Next, multimaterial PMMA-PLGA fibers using the PLGA films fabricated by hot-pressing and solvent-casting are thermally drawn and their final structures are compared. Next, the rheological properties of other PLGA compositions and molecular weights are investigated in order to provide a wide selection of materials and a guideline for the thermal drawing of complex multimaterial fibers. Finally, the true potential of thermal drawing through the fabrication of unprecedented microstructured fibers in biodegradable compositions is illustrated. The cross-sections of some of the obtained fibers are presented. The sections 2.1 and 2.5 are largely borrowed from the paper [6].

2.1 Viscoelastic characterization of solvent-cast and hot-pressed PLGA films

Conventionally, polymers with high viscosity (above 10^3 Pa.s) at the drawing temperature [17]are favorable as capillary effects can be counter balanced, and they can maintain the integrity of the structure during the drawing. Highly viscous boundaries also allow for the integration of multiple materials from various classes such as metals, semiconductors, and polymers in complex architectures[17], [108]–[110]. The rheological requirement of the thermal drawing can be extracted from oscillatory shear rheology where the relation between storage and loss muduli (G' and G") determines the ideal drawing temperature window[17]. It was found that the temperature window where G" decreases slowly and dominates G', enables to control the flow and to achieve microstructured features[17], [23].

This criterion required to identify amorphous biodegradable polymers possessing viscoelastic properties suitable to preserve microstructures. It was found that some compositions of Poly (D, L-lactic-co-glycolic acid) (PLGA), a well-known amorphous biodegradable thermoplastic, satisfies this condition. PLGA degrades through hydrolysis by breaking down to its constituting elements, lactic acid and glycolic acid[111], [112]. PLGA75, containing 75% lactide and 25% glycolide, was the first PLGA candidate to study its compatibility with the thermal drawing process, owing to its amorphous nature and thermoplastic properties. Rheological characterization of PLGA75 (Figure 2.1a&b) confirms the transition from elastic to viscous phase at the crossover of G' (storage modulus) and G" (loss modulus) which is 106°C for hot-pressed PLGA film and 101°C for the solvent-cast film. It has been previously shown that the temperature range above the cross over is ideal for the thermal drawing of PLGA[17]. The relation between the complex viscosity and the storage and loss modulus is shown below:

$$\eta^* = \eta' + j\eta'' \quad (2.1)$$

where the dynamic viscosity is defined by : $\eta' = \frac{G''}{\omega}$ (2.2)

and out of phase viscosity is defined by: $\eta'' = \frac{G'}{\omega}$ (2.3)

η* is the complex viscosity, η' and η'' are the real and imaginary parts, and ω is the angular viscosity. The dynamic viscosity (η') measures the elasticity or stored energy . The imaginary part (η'') represents the steady state viscosity and measures the rate of energy dissipation. Each of these viscosities could be further calculated from the real and imaginary parts of the shear modulus[113].

In order to study the behavior of the two PLGA films under various deformation rates, a frequency sweep over a large span was performed. Since drawing temperature could vary depending on the preheating time and the combination with other materials, the measurements were done at three temperatures of 50, 80 and 150°C (Figure 2.1c). The results show almost no difference between the hot-pressed and solvent-cast films. A clear shear thinning implementing non-Newtonian behavior is evident at 50 and 80°C while at 150°C, no effect of shear frequency on the viscosity is seen. This suggests that the viscosity is too low at 150°C and that drawing speed will have no effect on the stability of PLGA films.

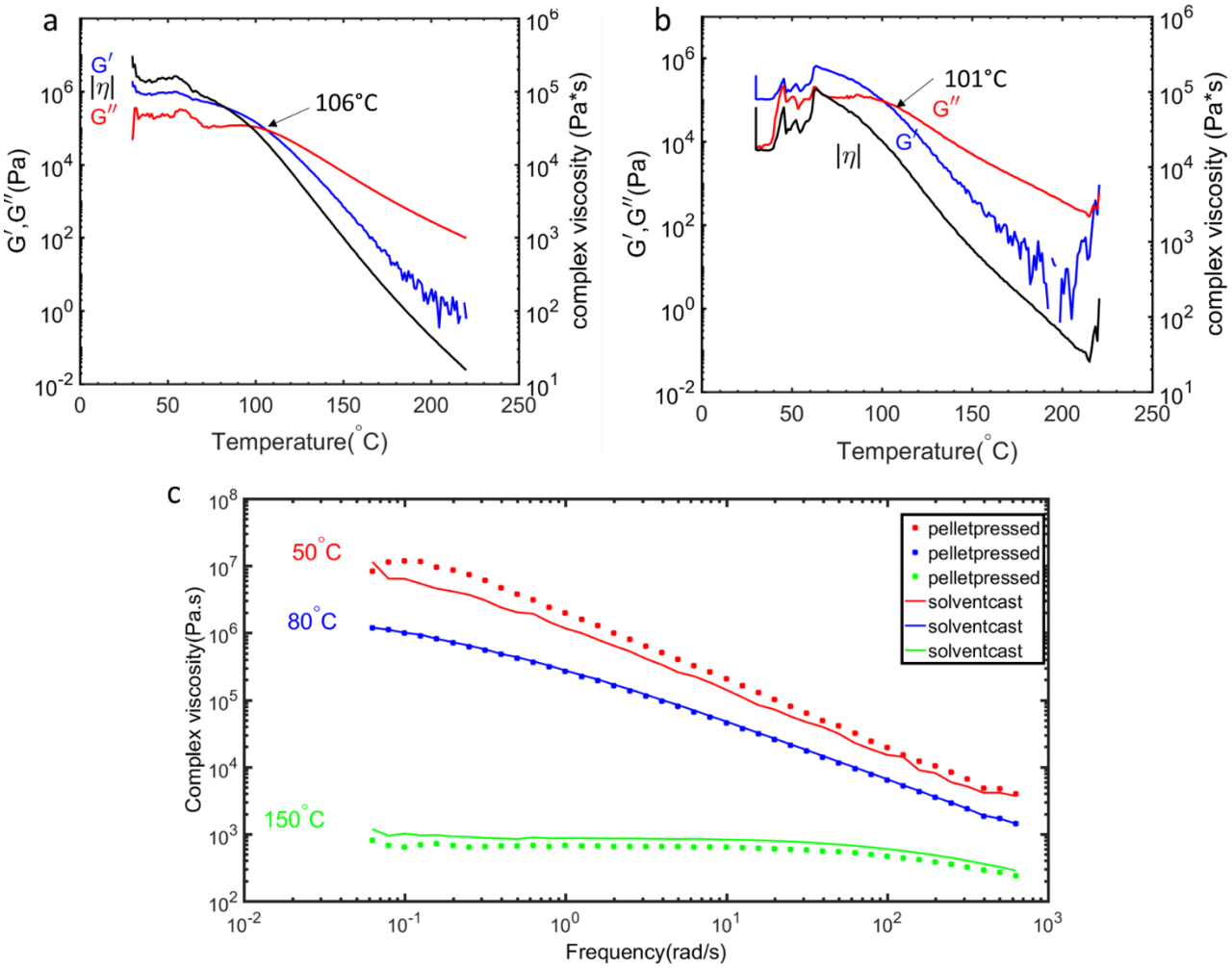

Figure 2.1. The rheological characterization of PLGA75 films, a, b) The oscillatory shear curves of hot-pressed and solvent-cast PLGA films respectively, c) The shear thinning of hot-pressed and solvent-cast PLGA films at 50, 80 and 150°C

In dynamic mechanical analysis (DMA), the viscoelastic property of the polymers can be analyzed in tension. In this mode, an oscillatory stress could be applied on the sample and strain behavior analyzed over a temperature ramp. Figure 2.2a shows the temperature range at which the material softens and transits into a rubbery state. This temperature range is crucial in the thermal drawing because it defines the viscosity profile along the drawing direction. Moreover, the value of storage modulus gives us insight on the intermolecular interaction. The energy dissipated in the material can be presented by the tangent of the phase angle (delta) which is the ratio of loss and storage moduli[114]. As can be seen, the transition temperature profile for the two films of hot-pressed and solvent-cast PLGA is the same. However, a difference in the storage modulus could be seen. The solvent cast film exhibits higher storage modulus in both the glassy and rubbery state which suggests a higher stiffness of the solvent-cast film compared to the hot-pressed film.

Figure 2.2b also shows slightly higher damping behavior for the hot-pressed films which further supports the results of the storage modulus behavior. The analysis of viscoelastic behavior of the two films by DMA suggests that the hot-pressed film could be a better candidate for the thermal drawing due to its capability to better dissipate energy.

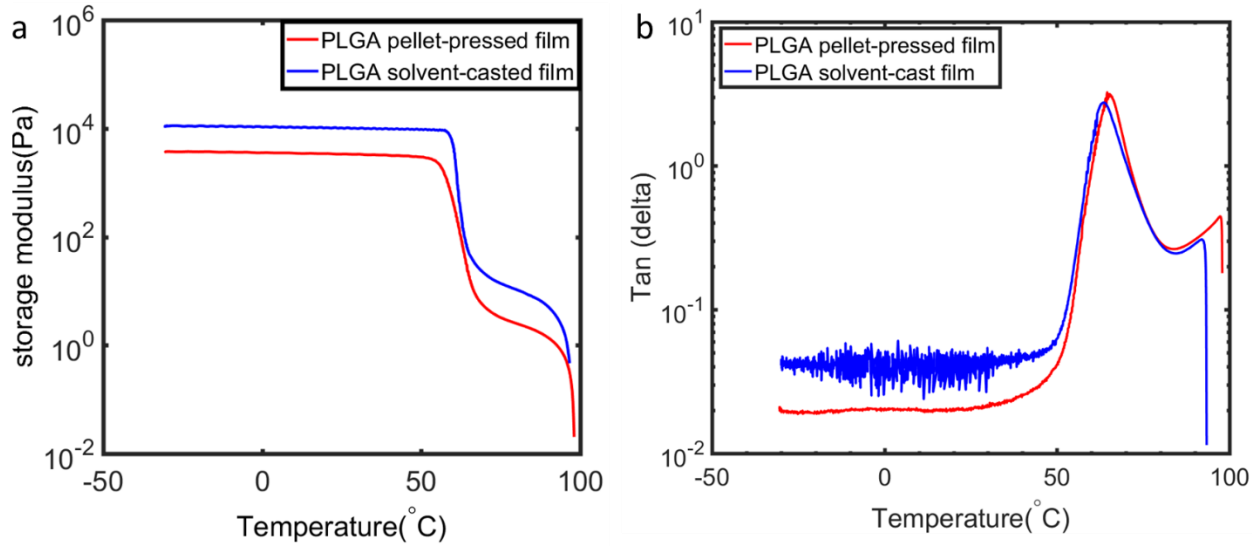

Figure 2.2. The dynamic mechanical analysis of hot-pressed and solvent-cast PLGA75 film in a temperature ramp: a) the response of storage modulus, b) the damping factor

2.2 Thermal characterization of solvent-cast and hot-pressed PLGA films

Differential scanning calorimetry (DSC) was employed to measure the glass transition temperatures (T_g) of the various PLGA films, and provide information about the effect of different preform fabrication methods on the morphology of the polymer. Figure 2.3a shows the DSC curves for the hot-pressed and solvent-cast PLGA films. The results exhibit the evidence of enthalpy relaxation close to the glass transition temperature range for the two films. This effect appears as a small peak instead of a smooth step-wise glass transition curve. In standard DSC, the heat flow to the sample is measured at a constant heating or cooling rate, and it gives information on the sum of all thermal phenomena such as glass transition, melting, and crystallization. This can lead to misinterpretation of data when these phenomena overlap. Modulated DSC (mDSC) would be able to disassociate the overlapping events while maintaining high sensitivity.

In modulated DSC, the sample is heated with oscillation in constant rate at a predefined temperature amplitude. Using mDSC, the effect of enthalpy relaxation is separated as non-reversing heat flow, therefore the T_g can be determined accurately from the reversing heat flow curve. From this method, the heat capacity component (reversing heat flow) could be extracted as well. The non-reversing heat flow (kinetic

component) is the total heat flow subtracted from the reversing heat flow[115]. The total heat flow is equivalent to the heat flow measured in standard conventional DSC. The relation between the total heat flow and its component is shown below[116].

$$\frac{dH}{dT} = C_p \frac{dT}{dt} + f(T,t) \quad (2.4)$$

Where $\frac{dH}{dT}$ is the total heat flow rate, C_p is the heat capacity, $\frac{dT}{dt}$ is the heating rate, and $f(T,t)$ represents the kinetic heat flow which is the function of temperature and time. In modulated DSC, there are three governing parameters[116]:

1) The average heat rate (˚C/min)
   It is usually less than 5˚C/min. There should be 4-6 modulation period during the glass transition interval.
2) Amplitude of temperature modulation (±˚C)
   (typically between ± 0.1 ˚C and ±2 ˚C)
3) Period of temperature modulation (s)
   (typically between 40s to 100s)

In Figure 2.3b&c, the impact of two different sets of values for these modulation parameters are analyzed. In Figure 2.3b, the modulation conditions are at 2°C/min with amplitude of 0.5°C every 100s. As can be seen, this condition does not provide enough number of cycles in the transition range and the enthalpy peak is still present at the glass transition. Therefore, the heating rate and period were changed to 0.5°C/min and every 60s (Figure 2.3c). This combination of parameters could result in enough number of cycles in the transition period and a smooth step-like glass transition could be achieved. Moreover, the amplitude is increased to 1°C to improve the sensitivity[117].

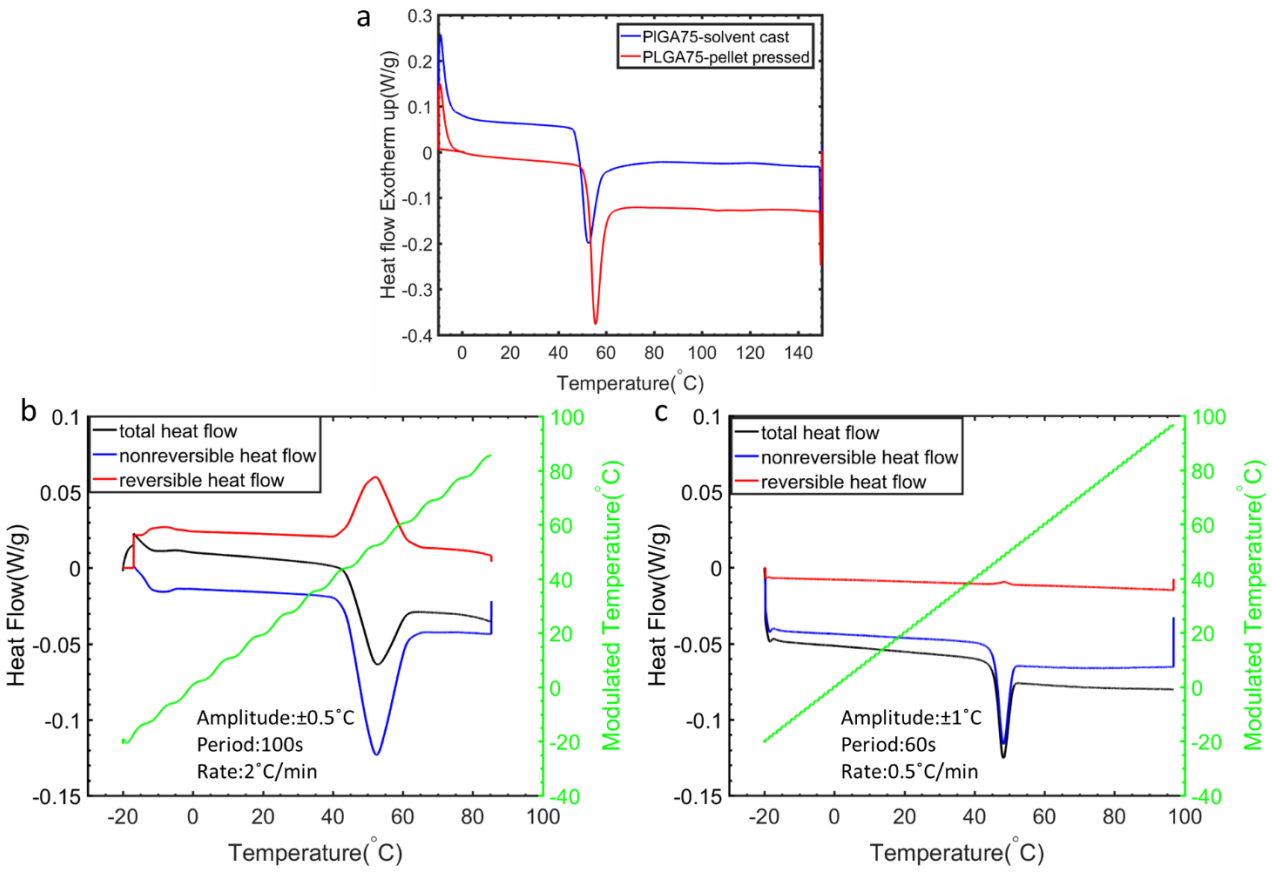

Figure 2.3. The thermal characterization of hot-pressed and solvent-cast PLGA75 films, a) The DSC curves, b, c) The modulated DSC curves with different sets of parameters

Figure 2.4 presents the results of mDSC using the optimized parameters for PLGA75 in the forms of pellets (as bought), annealed pellets, hot-pressed film, and solvent cast film. Interestingly, the glass transition of as-bought pellets (Figure 2.4a) is still accompanied with an enthalpy peak at this modulation peak. However, when the pellets are annealed in an oven at 50°C overnight, this enthalpy peak almost vanished, and the associated T_g was measured at 47.5°C (Figure 2.4b). Figure 2.4c shows the mDSC curve for the hot-pressed PLGA film made from the pellets. Its T_g was measured at 47.4°C which is equivalent to the T_g of annealed pellets. However, the pellet-pressed film shows more evidence of the heat history (larger deep the in heat flow curves) compared to the annealed pellet due to the prior heat treatment. Solvent-cast film exhibits significantly lower T_g (28˚C) compared to the pellet-pressed film (Figure 2.4d). This difference can be attributed to the rearrangement of polymer chains as a result of the interaction with solvent. Our results of mDSC could clearly show the thermal history of each PLGA format based on the processing and preparation method. Moreover, these kinetic phenomena could be successfully deconvoluted and the intrinsic properties of the polymer could be revealed.

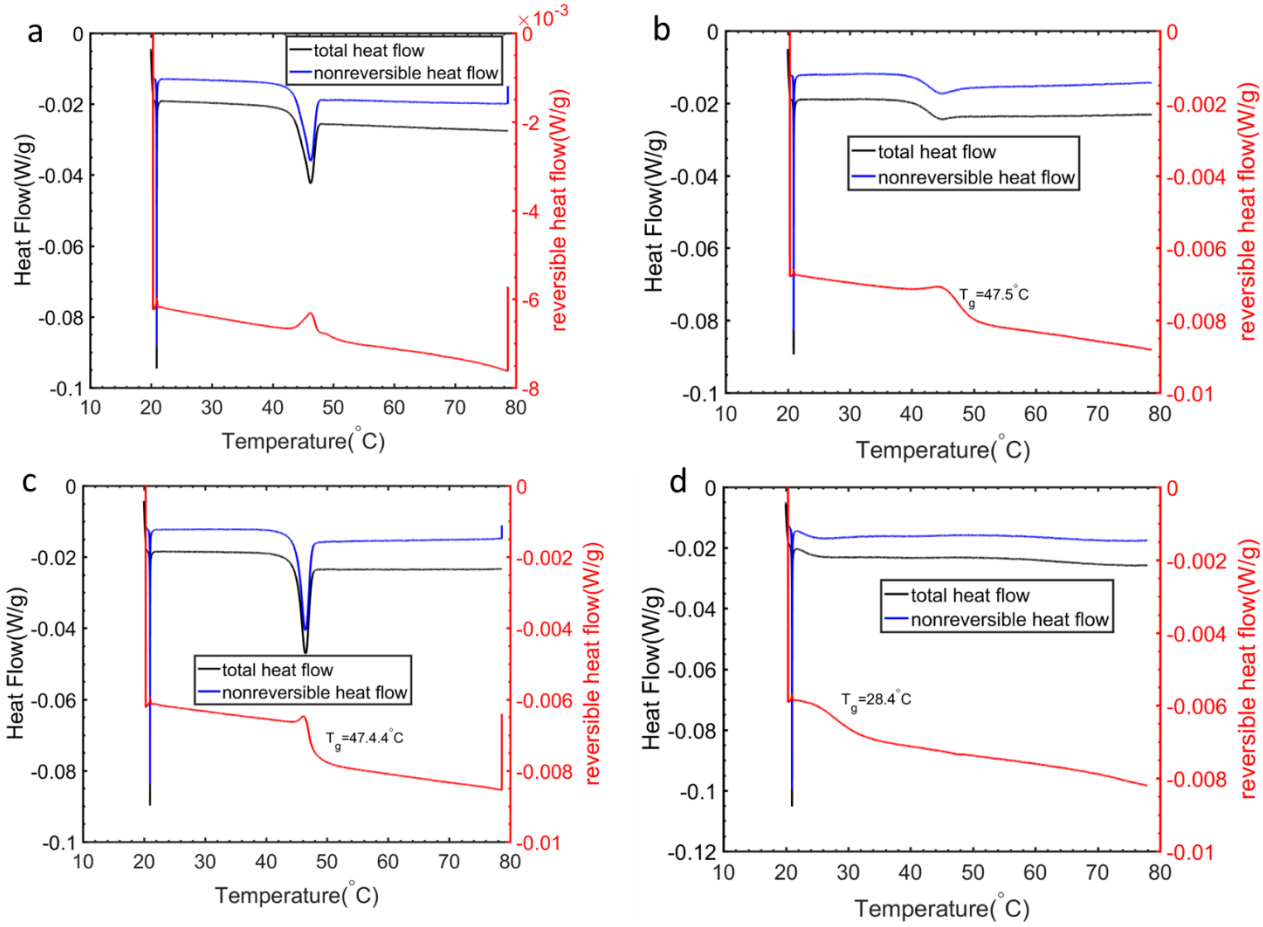

Figure 2.4. The modulated DSC curves for different formats of PLGA75, a) as-bought pellets, b) annealed pellets, c) hot-pressed film, d) solvent-cast film

2.3 Thermal drawing of hot-pressed and solvent-cast PLGA films

To assess the compatibility with the thermal drawing process of prepared PLGA films, we first co-process them with another thermoplastic such as poly (methyl methacrylate), PMMA. This will allow us later to exploit the properties of other thermoplastics in complement to the biodegradability of PLGA. It also enables us to characterize the release mechanism of thin PLGA layers later used as encapsulant for fiber-integrated drug reservoirs. We establish the co-drawing of PMMA plate containing a hollow channel with the PLGA films fabricated by hot-pressing and solvent-casting (Figure 2.5a&b). For PLGA films of the same thickness (500µm) at the preform level but prepared differently, different behaviors can be observed at the fiber level. For fibers of about 1200µm width, the solvent-cast film was broken on top of the channel while the hot-pressed film could maintain its integrity down to 10µm in thickness above the hollow channel. This

observation could potentially be attributed to the higher storage modulus of solvent-cast films or possible presence of solvent in the film which led to its rupture.

After the successful co-drawing of PMMA with hot-pressed PLGA films, the effect of thickness of PLGA film on its stability at the fiber level is explored. As shown in Figure 2.5c, two PMMA plates were hot-pressed together, and a hollow channel on each side was milled and covered with PLGA films of different thicknesses: 500 and 1000 µm. The cross-section of the fiber shows that the thick film (1000 µm) was significantly deformed and overflew inside the channel while 500 µm film kept its shape. This indicates that PMMA provides a good adhesion and support for PLGA when the thickness is small enough however, with a larger thickness of PLGA, its low viscosity at the high drawing temperature of PMMA (130°C) leads to the reflow inside the channel. Since the drawing was done under the exact same conditions, this result was used in the designs to engineer the PLGA thickness in various architectures. For all PMMA-PLGA fibers in this work, a thickness between 500 and 1000 µm is designed for PLGA films at the preform level.

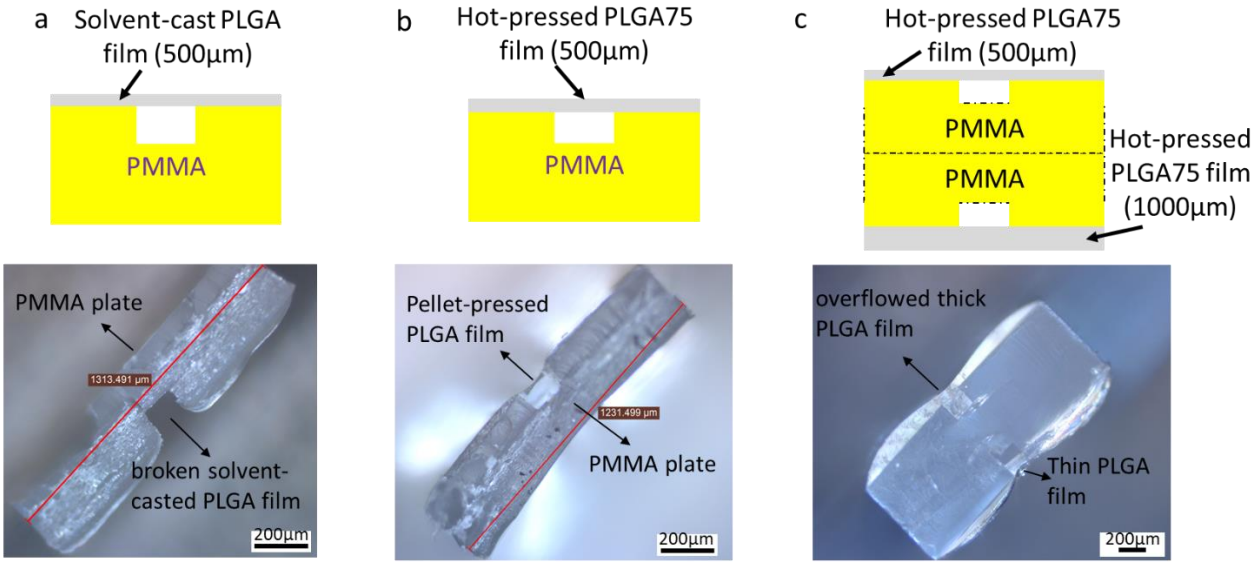

Figure 2.5. The structure of multimaterial PMMA-PLGA fibers, a) PMMA plate composed of one channel and 500 µm solvent-cast PLGA75 film as the release barrier, b) PMMA plate composed of one channel and 500 µm hot-pressed PLGA75 film as the release barrier c) a thick PMMA plate composed of two channels and the release barriers of 500 and 1000µm hot-pressed PLGA75 films.

2.4 Rheological characterization of various PLGA grades

Beyond film thickness, in order to fabricate fibers with various release rate, PLGA films of different compositions and molecular weights are also investigated: 1) PLGA 75(79k g/mol), 2) PLGA50(47k

g/mol), and 3) PLGA85(160k g/mol) 3) a blend of two different molecular weights (MW) of PLGA75 in two compositions of (80% 79k g/mol and 20% 13k g/mol), named PLGA75blend8020 and (50% 79k g/mol and 50% 13k g/mol), named PLGA75blend5050. This composition of PLGA75blend was found to accelerate the degradation rate of the pure high MW PLGA75. However, their viscoelastic behavior should be analyzed to verify if they possess the proper rheology for thermal drawing. Figure 2.6a&b&c&d shows the rheological curves of PLGA85, PLGA50, PLGA75blend8020, and PLGA75blend5050 where the crossover of G' and G" occurs at 136, 99, 84 and 76°C respectively.

Figure 2.6e presents the comparison of the complex viscosity of these films. PLGA85 exhibited the highest viscosity followed by PLGA75, PLGA50 and PLGA75blends respectively. Since the viscosity and loss modulus of PLGA75blend5050 fall rapidly, its composition was found to be incompatible with the thermal drawing. However, other films exhibited a relatively slow decrease of viscosity and their thermal drawing is demonstrated in the next sections. In general, it can be concluded that for a PLGA of higher molecular weight and lactide content, the viscosity is higher and the crossover between the two moduli occurs at higher temperature. This is an important information for the design of future architectures regarding their position and geometry.

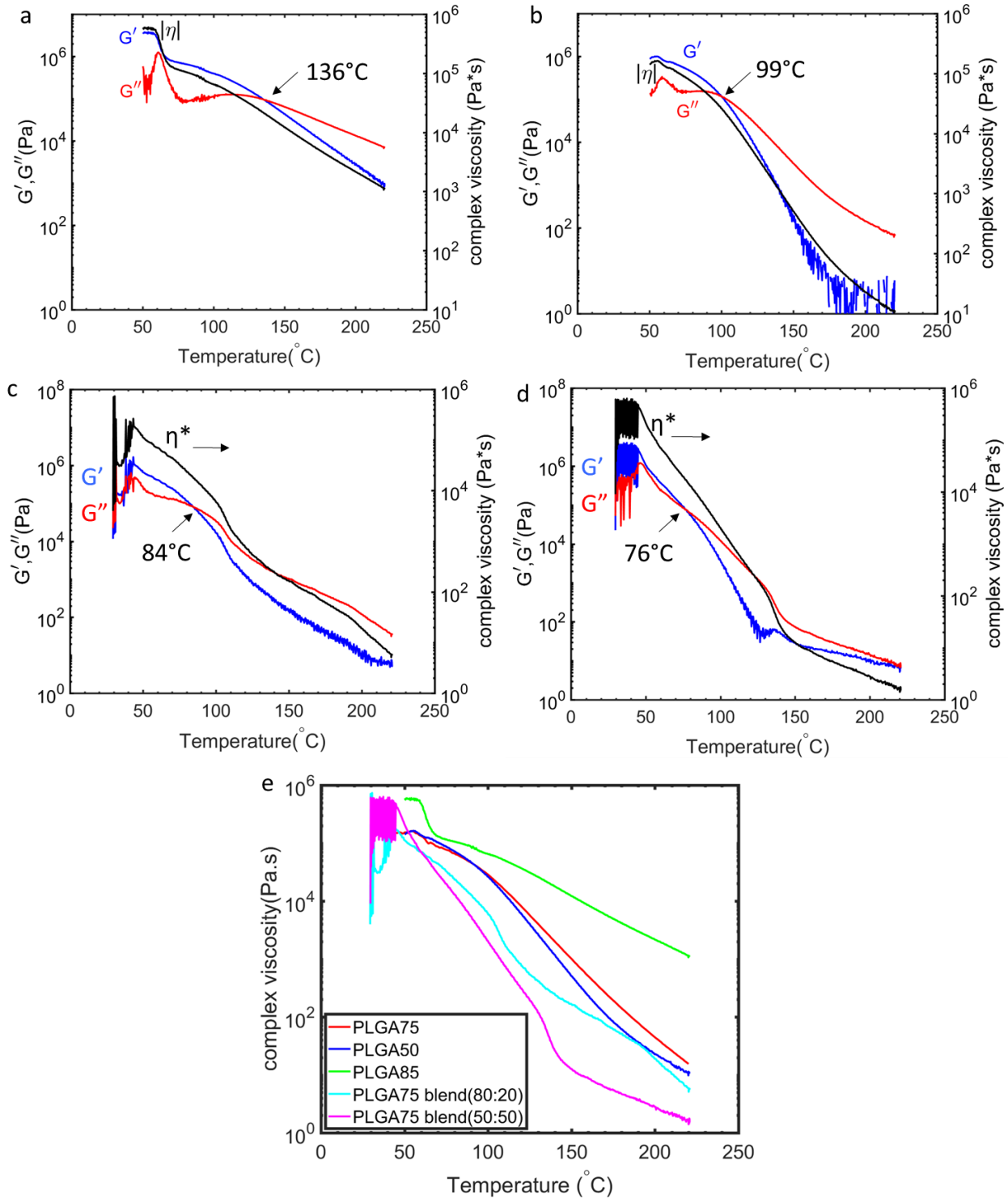

Figure 2.6. The oscillatory shear rheology of different PLGA grades, a) PLGA85, b) PLGA50, c) PLGA75blend8020, d) PLGA75blend5050 where the crossover of G' and G" occurs at 136, 99, 84, and 76°C respectively, e) The comparison of their complex viscosity

2.5 Thermal drawing of microstructure drug delivery fibers

Building on the knowledge obtained in the characterization of each PLGA grade, we could successfully thermally draw microstructured biodegradable fibers with complex architectures. Some of the cross-sections are showcased in Figure 2.7. Figure 2.7a demonstrates the thermal drawing of PLGA75 where the initial rectangular structure at the preform level was well preserved, revealing a thermal drawing in the viscous state at relatively high viscosity. Figure 2.7b&c depict the feasibility of drawing of PLGA75 into microstructured fibers of different geometries, cylindrical shape containing two channels and rectangular shape containing one channel, respectively. The predefined architecture of the fibers at the preform level is well preserved and PLGA microstructures down to a few micrometers are obtained in a single drawing step. This level of control over biodegradable fiber architecture is unprecedented and contrasts drastically from solution based or semi-crystalline polymer based processes[24], [25], [118], [119]. Furthermore, the feasibility to integrate such microchannels enabled the fabrication of multi-release drug delivery fibers containing multiple drug reservoirs, as we show below. Figure 2.7d shows the cross-section of a multimaterial rectangular fiber made up of PMMA and PLGA50 (50% lactide). PMMA is the core material and contains a hollow channel, on top of which PLGA50 film is placed. The PLGA film ($T_g \sim 45°C$) preserved its integrity to a high extent despite of drawing at a higher temperature with PMMA ($T_g \sim 110°C$, which indicates the excellent adhesion between PMMA and PLGA[6].

Figure 2.7e shows a similar structure as Figure 2.7d, a ribbon with a micro-channel covered by a biodegradable film. However, this time the whole structure is made up of PLGA75, making it fully biodegradable. Figure 2.7f is an example of fully biodegradable multimaterial fiber. Since PLGA85 has the highest viscosity among the studied PLGA grades, it is used in the bulk of the fiber. It is also the composition that takes the longest to degrade, so that it can ensure the integrity fiber while constituents are being released. A hollow channel is integrated in the plate and PLGA50 film is placed on top of the channel to act as the release barrier. This structure shows the unique potential of the thermal drawing process that can co-process different materials to obtain a complex structure with domains of various degradation properties. PLGA85 and PLGA50 indeed have respectively the slowest and fasted degradation rate among the studied PLGA grades, and their physicochemical properties differ drastically. Despite of these differences, the integrity of the PLGA50 film is well-preserved over the wide opening of the channel and along the fiber length. We will exploit these types of structures in the next chapter to realize complex multi-dose drug delivery fibers.

Finally, we leverage the unique attributes of the fiber drawing process to demonstrate configurations opening novel opportunities for biodegradable fibers and fabrics. Figure 2.7g shows an intriguing example

of fiber structure composed of a hollow channel in the center intended to be used as a conduit for cell or nerve and four other smaller channels as drug reservoir. In Figure 2.7h, we present a hollow-core PLGA fiber with a textured inner surface, using an approach previously developed[26], [120]. The structure is composed of a hollow core fiber made up of PLGA85 in which the inner surface of the channel is textured down to a few micro-meters. Textured biodegradable implants can offer novel opportunity to facilitate the growth of tissues while tailoring delivery of nutrients by adjusting degradation rate to the growth rate of cells and neurons[6], [121].

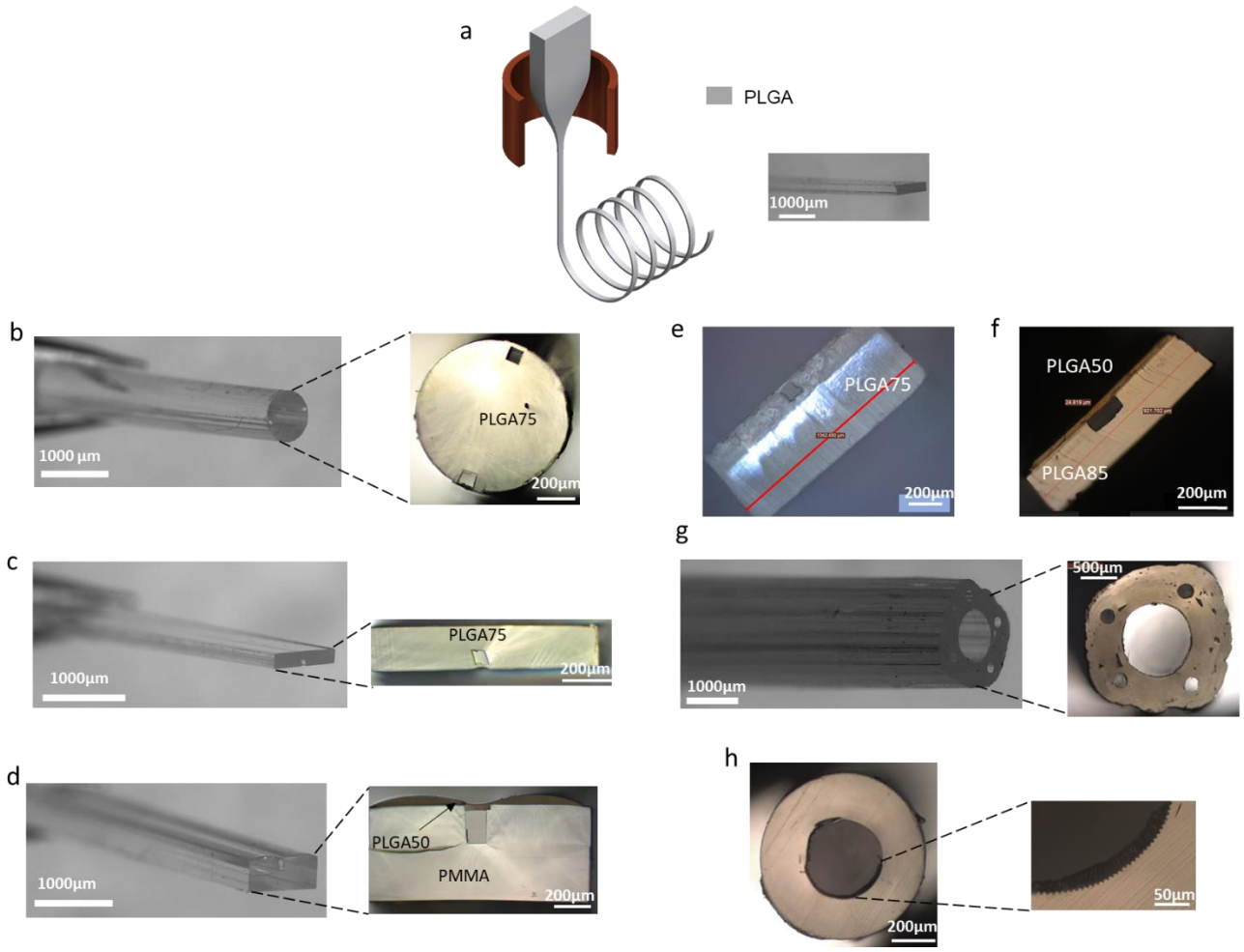

Figure 2.7. The cross-sections of the thermally drawn microstrcutured fibers. a) The schematic of the thermal drawing and and rectangular PLGA75 fibers, b) a cylindrical PLGA75 fibers contaning two channles, c) a thin rectangular PLGA75 fiber containing one channel, d) a multimaterial PMMA-PLGA50 fiber contaning one channel, e) a thick rectangular PLGA75 fiber contaning one channel, f) a multimaterial

PLGA85-PLGA50 fiber, g) a hollow core PLGA75 fiber containg four other channels, h) A hollow core textured PLGA85 fiber

Figure 2.8a illustrates the scalability of the technique where tens of meters-long PLGA fibers were obtained in a single draw. Furthermore, the flexibility of these PLGA fibers is demonstrated through their knotting ability (Figure 2.8b) for potential suture applications and weaving ability (Figure 1.8c) for potential wound dressing applications. Such weaved structure of fibers could form ideal substrates for an effective delivery system of therapeutic agents[122] in a variety of contexts such as wound dressing or prosthesis[6].

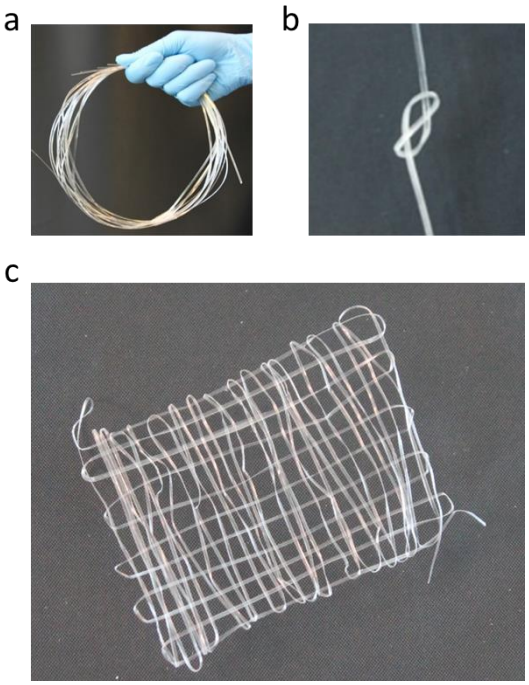

Figure 2.8. Demonstration of the scalability and flexibility of the thermally drawn fibers: a) Meters-long microstructured PLGA fibers, b) Knotting ability and c) Weaving ability of PLGA fibers

2.6 Experimental

Here, we give a more precise account of the experimental procedures followed to fabricate and characterize the different materials and biodegradable fibers discussed in this chapter:

Materials: Low molecular weight Polylactic-co-glycolic acid, PLGA75 (RESOMER® RG 752H), PLGA50 (RESOMER® RG 504 H), PLGA85 (RESOMER® RG 858 S), and Polycaprolactone (PCL), RESOMER® C 212, were purchased from Evonik, while the high molecular weight PLGA75 (PURASORB® PDLG 7507) from Corbion Purac. Poly(methyl methacrylates) (PMMA, or Plexiglas), plates were purchased from Evonik Röhm GmbH while PMMA rods were purchased from Plexacryl SA.

PLGA75blend microextrusion: The high and low molecular weight PLGA75 were mixed in weight ratio of 80:20 and hot-pressed prior to microextrusion. This step was done to solidify the flake format of low molecular weight to ease its handling. The non-uniform pressed blend was fed to the microextruder (DSM Micro 5) in batches of 2-3 g and mixed at 140 °C to obtain uniformly dispersed PLGA75blend.

Sample storage: Prior to any processing, the polymers were stored at 25 °C under vacuum in an oven (VT 6060 M from Thermo scientific) for minimum of two weeks in order to ensure the evaporation of any residual water vapor.

Hot pressing PLGA film: The hot-pressed PLGA films were each prepare by hot-pressing predetermined weight of PLGA pellets in a rectangular mold of 2.4×17 cm under conditions of 100 °C, 5 N cm^{-2} under vacuum for 10 min to obtain the desired thickness (1g~300 µm film)

Solvent casting PLGA films: The solvent-cast films were prepared by mixing 10 g of PLGA75 pellets in 40 g dichloromethane solvent. The solution was mixed via magnetic stirring for an hour until all the PLGA pellets dissolved completely. The solution was then cast on a Teflon film, and immediately a roller was applied on the solution to spread it. In order to evaporate the solvent, the cast film was left in a hood for 1 day, and in a vacuum oven at 25°C for 4-5 days, then the film was peeled. In order to obtain the films of desired thickness, the films were hot-pressed.

Rheological Characterization: the rheological measurements were done on a TA Instrument AR 2000ex (USA) rheometer. The tests were performed at the oscillatory temperature ramp, frequency of 1Hz, strain of 1% and the heating rate 2°C/min. For the tests parallel Aluminum plates of 25mm diameter with Peltier Plate heating system was employed.

DMA measurement: The viscoelastic properties of the films were measured in multi- frequency-strain mode with oscillation strain of 0.01% and frequency of 1 Hz in a temperature ramp from -30 to 200°C with the rate of 2°C/min. However, the measurement was stopped before 100°C due to the softening of the PLGA films.

DSC measurement: The DSC measurement was performed by a DSC Q100 TA. The samples were heated from -10°C to 150°C at a constant speed of 10°C/min.

Preform fabrication:

1) PMMA-PLGA preforms: two PMMA plates of 5.8 mm were hot-pressed (Lauffer Pressen UVL 5.0) together at 130 °C, 10 N cm^{-2} for 20 min to obtain a thicker plate with dimensions of 2.4 cm width,1.2 cm thickness and 16 cm length. A groove of 4 mm depth×2 mm width was milled along the preform. The PLGA film and PMMA plate were hot-pressed at 90 °C and 4 N cm^{-2} with presence of a Teflon

bar in the channel to prevent the deformation of PLGA film. The Teflon bars were removed prior to drawing.

2) Thick and thin rectangular PLGA75 containing one channel: For 1 cm-thick and 5 mm-thick PLGA75 plates, respectively 50 g and 30 g pellets were hot-pressed in a rectangular mold (L: 16 cm and W: 2.4 cm). The conditions were set at 120°C with pressure of 24 N/cm^2 and at vacuum. Then, a 2 mm x 2 mm groove was milled in the center and along the plate. A Teflon bar was inserted in the channel and the prepared solvent-cast PLGA75 film was hot-pressed on the plate at 100°C for 15 min. Then, the Teflon bar was withdrawn.
3) PLGA85-PLGA50 preform: The PLGA85 plate was obtained by hot-pressing the previously hot-pressed pieces of PLGA85 at 120°C with pressure of 8 N/cm2, at vacuum for 40 min. A groove of 2 mm x 2 mm was milled in the center and along the plate. The PLGA50 film was obtained by hot-pressing 4 g pellets at 110°C with pressure of 5 N/ cm^2 for 10 min which resulted in thickness of 500 µm. A Teflon bar was inserted in the channel and the PLGA50 film was hot-pressed on the plate at 70°C for 10 min. Then the Teflon bar was withdrawn.
4) Hollow core PLGA75 preform containing 4 channel: This preform was made by rolling thin PLGA75 films around a rod. After a certain diameter 4 smaller tubes were added and more films were rolled around to provide enough material surrounding the rods. Next, it was put in an oven at 100°c to consolidate the rolled films. The preform was progressively turned around to make sure the efficient transfer of heat.
5) Hollow core textured PLGA85 preform: The hollow core PLGA85 cylinder and textured PLGA85 film were fabricated separately. For the fabrication of textured PLGA film, first a plain PLGA85 film was fabricated by hot-pressing 4 g of PLGA85 pieces at 140°C, with pressure of 10 N/cm^2 for 15 min. At this step the film was about 500 µm thick. Then, the textures were created by hot-pressing the prepared film on a 100 µm textured PDMS at 120°C with pressure of 10 N/cm^2. This resulted in 350 µm thick texture PLGA85 film. On the other hand, the hollow core PLGA85 cylinder was made in a pre-designed mold with a diameter of 2 cm including a 1cm-dimater rod at the center. The PLGA85 pieces were first grounded to obtain a powder-like consistency. This step was found to help the material to melt efficiently and to prevent the creation of bubbles. The mold was filled with the powder and pressed in a consolidation oven with some heavy weights. The temperature was set at 180°C for one hour and then, it was reduced to 160°C and the consolidation was continued for a few more hours. More material was added progressively upon melting of the material. After the preparation of the hollow core PLGA85 cylinder, the prepared textured film was cut in a rectangular shape with a width equal to the circumference of the inner core of PLGA cylinder (3.14 cm). The film was rolled and inserted into the hollow core. This step requires a small thickness of the film so that it would be flexible enough and not

break. The 350 µm film in our case was found to have an appropriate. No heat was applied at this step in order to ensure to integrity of the textures. It was observed that the film was welded to the PLGA cylinder upon heating during the drawing.

Thermal drawing: The preforms were drawn with a custom draw tower consisting of a three-zone furnace. The set temperatures PMMA-PLGA preforms were (100-260-90 °C). The PLGA75 preforms were drawn at (70-135-50 °C) while the PLGA85 preforms were drawn at (70-170-50 °C).

Optical microscopy: The cross-sections of the fibers for the optical microscopy images were prepared using ultramicrotomy, and images taken with LEICA DM 2700 OM equipped with a LEICA MC170 HD camera.

Thickness measurement: The thickness of PLGA films in PMMA-PLGA fibers were measured by the optical microscopy.

Molecular weight measurement: The molecular weight of PLGA grades was measured using gel permeation chromatography (GPC). The measurements were done on solutions of 3mg PLGA samples in 1ml Tetrahydrofuran (THF). The calibration was done based on Polystyrene (PS) and the detector was based on measuring the refractive index.

2.7 Summary and Conclusion

In this chapter we established characterization techniques to screen PLGA grades compatible with thermal drawing. Although understanding the material behavior during thermal drawing is still in its infancy, our studies of rheology and thermal properties could provide some insights. The previously proposed theories on the rheological behavior of the polymer as a prerequisite for the thermal drawing was verified on PLGA polymers. It was confirmed that a slow transition of loss modulus gives a higher flexibility in controlling the ultimate feature size and even the morphology of the polymer film during thermal drawing. Conventionally glass transition temperature (T_g) is thought to be an important parameter in the processing of polymers. However, depending on the process, T_g by itself cannot entail the complexity of the polymer behavior under heating. It was found that the crossover temperature of storage and loss modulus is a better indicator of polymer deformation in the thermal drawing and could be utilized to set the drawing temperature. Moreover, the study of the thermal properties revealed the thermal history and morphological differences of various PLGA formats based on their processing conditions. The occurrence of these phenomena was differentiated by modulated DSC. It was found that the heat history of the PLGA pellets could be erased by annealing them. Moreover, the T_g of the PLGA films could significantly differ if they were heat treated or processed by solvents.

Finally, the comparison of viscosity values of different PLGA grades was utilized to designing and realizing multimaterial fibers with unprecedented microstructures.

Chapter 3 Release and mechanical properties of drug delivery fibers

This chapter constitutes the core objective of the thesis based on which the developments in next chapters are carried out. Firstly, an appropriate drug model is selected and is used to study the release properties of the thermally drawn PLGA films. The release mechanism is elucidated by analyzing the morphological evolution of the PLGA film during the degradation period using SEM. To mathematically describe the obtained release profiles, a release model based on an existing phenomenal degradation model is developed. The obtained release kinetics with respect to the physicochemical and geometry of the integrated PLGAs are exploited to realize multimaterial fibers capable of releasing drugs in multiples doses. Next, the effect of two different sizes of drug models on the release profiles is shown. WAXS measurements are performed on the PLGA films before and after the drawing to verify if the microstructure of polymer changed during the processing and had any influence on the degradation kinetics. Finally, the tensile properties of the thermally drawn PLGA fibers are improved by increasing the drawing stress. It will be shown that these highly aligned PLGA fibers are subject to shrinkage in the conditions of the release study. Two methods of heat treatment and co-drawing with a semicrystalline polymer are proposed to eradicate this problem. DMA measurements will be conducted to show that the shrinkage of the fibers could be reduced or completely removed when these methods are applied. The sections 3.2, 3.3, and 3.4 are largely borrowed from the paper [6].

3.1 Selection of an appropriate drug model

The interaction between the drug and the polymer carrier has a significant impact on the kinetics of the release profile. As the first step of the release study, we thrive to identify a fluorescent-labelled drug model where its release mechanism would be dependent on the PLGA degradation. Since the release barrier is the hydrophobic PLGA, a hydrophilic drug model should be chosen to have a higher affinity (partition coefficient) with water and therefore do not interact with PLGA. For example, Rhodamine B is hydrophobic and when injected in the hollow channel of the fibers, the evidence of the absorption in PLGA was observed (Figure 3.1). This interaction is undesirable as it inhibits the release while the PLGA morphology is continuously changing due to the degradation.

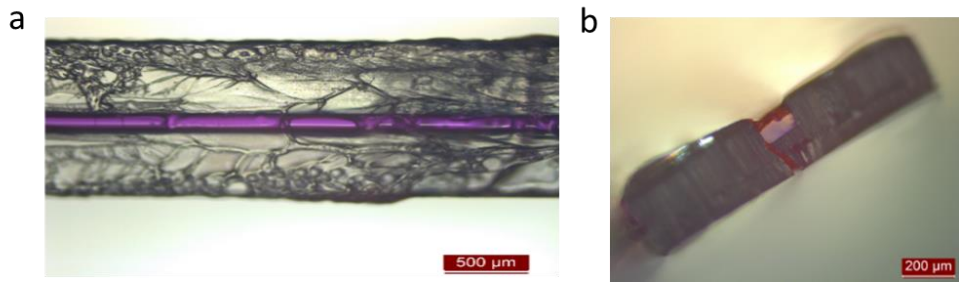

Figure 3.1. Optical microscopy showing the absorption between Rhodamine B and the degrading PLGA in PMMA-PLGA75 fibers, a) top view and b) cross-sectional view

Another criterion is the size of the drug model which could influence the release mechanism significantly. This is why pharma scientists are constantly looking for new drug carriers upon the discovery of a novel drug. Since, we would like to engineer the release kinetics through the degradation properties of PLGA, a macromolecular drug model is selected so that its release could solely occur through the degradation of PLGA and not through the other mechanisms such as diffusion. Fluorescein isothiocyanate (FITC) labeled dextran (MW=70kg/mol), abbreviated as FD70, is found to meet these requirements, and could be employed as the representative of macromolecular substances such as proteins.

Moreover, the drug model should keep its properties over long degradation times (several weeks) while capsulated. As the released concentrations are determined based on the florescence intensity of the drug model, the stability of the fluorescence intensity throughout the release study has to be verified. Two solutions of FD70 in PBS in low and high concentrations ($1.09x10^{-8}$ mol/L and $2.23x10^{-4}$ mol/L) are prepared and kept in an oven at 37°C and their fluorescence intensity were measured every few days for 104 days (Figure 3.2). As can be observed, the dye exhibited a good stability over such an extended period. However, low concentration FD70 solutions show higher stability than high concentration ones. Therefore, the concentration of the initial injected FD70 solution in the channel was chosen so that the concentration of the released dye stay in the order of 10^{-8} mol/l throughout the study. This low concentration also prevents the agglomeration of the dye and possible loss of fluorescent intensity.

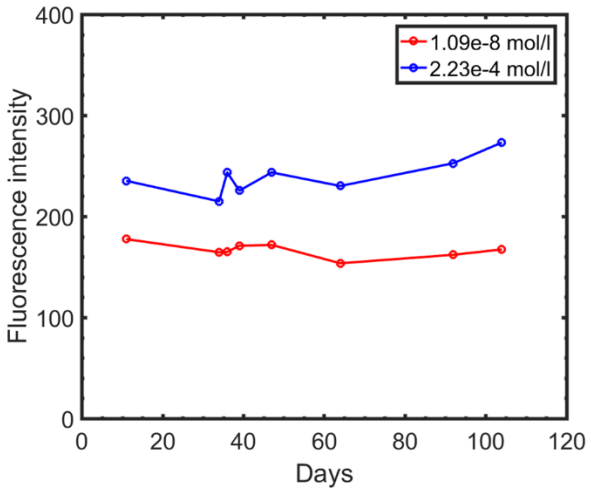

Figure 3.2. Intensity stability of low (1.09×10-8 mol/l) and high (2.23×10-4 mol/l) concentrations of FITC-dextran (70 kDa) over the course of 104 days

Lastly, the concentration of FD70 in PBS is calibrated based on the emitted fluorescence in low concentrations. To measure the fluorescence of such dilute solutions, the slit length is increased so that the spectra of all the expected released concentrations during the degradation of PLGA could be measured with the same parameters (Figure 3.3a). The peak intensities of the spectra at emission wavelength of 516 nm are plotted with respect to their corresponding concentrations (Figure 3.3b). As can be seen, a linear correlation is obtained which ensures the validity of the calibration curve.

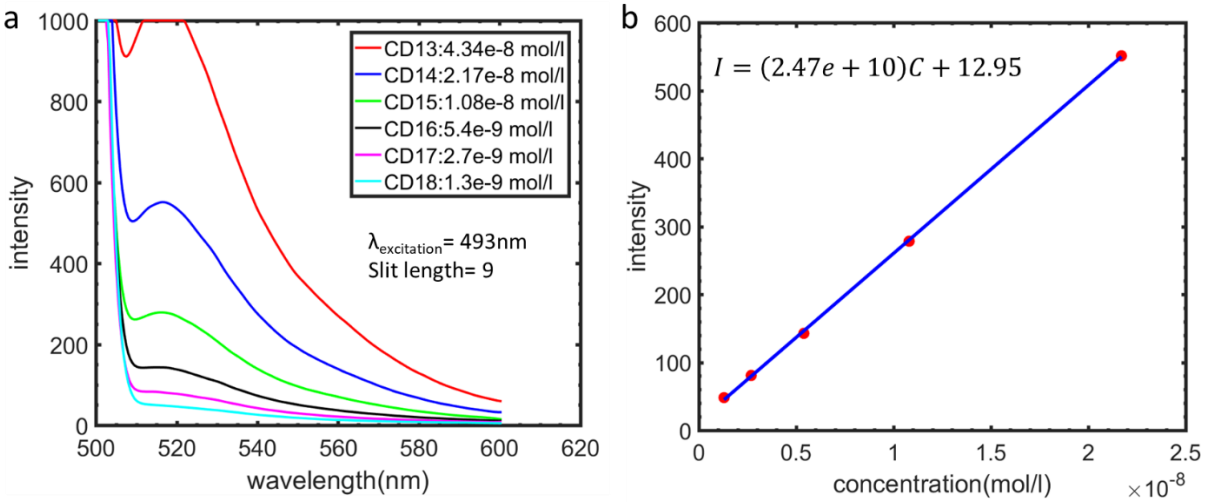

Figure 3.3. a) The spectra of fluorescence emission intensity for different concentrations of FITC-dextran(70kDa) and b) the fluorescence calibration curve

3.2 Release characterization of thermally drawn PLGAs

In order to study a selection of polymers with various degradation rates for the fabrication of multi-dose drug delivery fibers, various PLGA-based polymers were co-drawn with a non-degradable thermoplastic. As explained above, PMMA was chosen as the core integrating a hollow channel above which the PLGA film acts as the barrier between the drug reservoir and the release environment. The fabrication considerations of this structure was discussed in details in chapter 2. The presence of PMMA in the core allows us to study the release kinetics of each film solely without the effect of the core degradation. In order to fabricate fibers with various release rates, PLGA films of different compositions and molecular weights were integrated: 1) PLGA 75, 2) PLGA50(47k g/mol), and 3) PLGA75blend8020, as discussed previously in chapter 1. Moreover, the thickness of the PLGA films was varied for each composition to achieve further control of the release rate. The size of the PLGA film is an effective tool in tuning the degradation rate due to the well-known bulk degradation mechanism of PLGA [123]–[126] which results in the faster degradation of thicker films[6].

After the drawing process, FD70 was injected into the hollow channels. The fibers were incubated at 37°C in phosphate buffer saline (PBS) and the fluorescence spectroscopy was performed at predetermined times on the release medium. In parallel, over the course of degradation, the evolution of the morphology of the degrading PLGAs was analyzed by SEM to understand the release mechanism. Figure 3.4 shows the release profiles and the SEM images obtained from three PMMA-PLGA fibers in which the release barrier consists of PLGA50, PLGA75, and PLGA75blend films in two different thicknesses. The release profiles follow the biphasic release kinetic reported in a number of PLGA delivery systems: 1) slow release phase due to the diffusion through the polymer chains and 2) fast release phase through the water-filled pores created upon erosion [6], [8], [9], [127].

In PMMA-PLGA75 fibers, the release study was performed on a small variation of thickness: 60μm and 67μm (Figure 3.4a). The results showed very similar release rates in the first phase; however, the onset of the second phase was shifted to earlier time in thicker films due to the bulk degradation. In fibers of 60μm-thick PLGA75, the second phase started on day 70 whereas the onset in fibers of 67μm-thick is shifted to day 65. This is due to the presence of long diffusion pathways in the thicker films which trap the produced acidic oligomers and induce more significant autocatalysis, leading to faster degradation and thus faster release[6]. The SEM images of degrading PLGA75 (Figure 3.4b) further confirms the effect of bulk degradation as the surface of PLGA75 remains fairly smooth with the appearance of a very few pores throughout the degradation period. At week 10, the first breakage appears which corresponds to the start of the fast release phase and it is due to the increased accumulation of trapped oligomers in the bulk of the polymer. The same release rate was seen in the first phase for the two thicknesses due to the insignificant

contribution of the diffusion mechanism. This can be explained by the absence of enough number of pores and dense network of long PLGA chains that leads to delay of the release to the time when the autocatalysis dominates.

The thickness of PLGA50 films in the two PMMA-PLGA50 fibers was 39µm and 110µm. Figure 3.4c shows the biphasic trend of the two release profiles. Surprisingly, the two fibers exhibited very similar release profiles despite of the large difference in their thicknesses. This behavior can be attributed to the presence of high number of pores from the early stage of degradation which suppresses the bulk degradation[9] and allows the produced oligomers to diffuse out of the film. Therefore, the effect of the autocatalysis is counterbalanced by the long diffusion pathways in thick PLGA50 films and similar release profiles are obtained for the two films[6]. The corresponding SEM images in Figure 3.4d exhibit typical porous morphology of degrading PLGAs[128]. This observation implies that the release mechanism in the first phase is through the simultaneous diffusion of the drug from both polymer chains and the pores[58]. In the course of the degradation, the number of pores continues to increase and protrusions and gaps are created as a result of swelling and erosion (day 10). The swelling of the film concomitant with the increased connection of pore network [128] lead to the creation of the cracks on the film and thus a fast release phase occurs (day17).

The release study on PLGA75blend was performed on two thicknesses of 47µm and 33µm (Figure 3.4e). The release kinetics of the 33µm PLGA75blend film deviated from the biphasic phase and showed a trend closer to linear regime indicating diffusion-controlled release according to the Higuchi model[129], [130]. The 47µm film resulted in a diffusion phase up to day 36, however, the fast release phase did not start immediately after the diffusion phase; it was hindered by a flat plateau, started on day 53 and completed by day 77. It should be noted again that the PLGA75blend contains only 20% low MW PLGA75 compared to the PLGA75 film in Figure 3.4a, and yet a significant difference in the release kinetic was obtained. This difference can be explained with an analysis of SEM images of the top view of the 47µm-film where it is in contact with the release medium. As it can be seen in Figure 3.4f, PLGA75blend film is distinguished by the presence of pores from the early stage of degradation (week4). On week 5, the film starts to swell which is the sign of an increase in the osmotic pressure[65], [126], [131]. The swelling is the result of the fast degradation of low molecular weight PLGAs and thus the appearance of critical molecular weights[126] which increase the pore density through water penetration. As it is evident in the SEM image of week 6, the film continues to swell further and a non-uniformity appears due to the thinner center of the films on top of the channel. Interestingly, the swelling period corresponds to the flat plateau in the release profile. This “no release” period can be explained by the dense network of the polymer chains which reduces the internal porosity[8] and thus the drug diffusion. However, at the same time due to the degradation, the density and

size of the pores keeps increasing until the film loses its stability and local break-ups happens at different parts of the film evident on SEM image of week 9. The complete rupture of the film occurs on week 11 which corresponds to the end point of the release period. Such an in-depth understanding of release mechanisms through morphological analysis Figure 3.4 enables us to engineer novel compositions for adjusting the release profiles according to the target application[6].

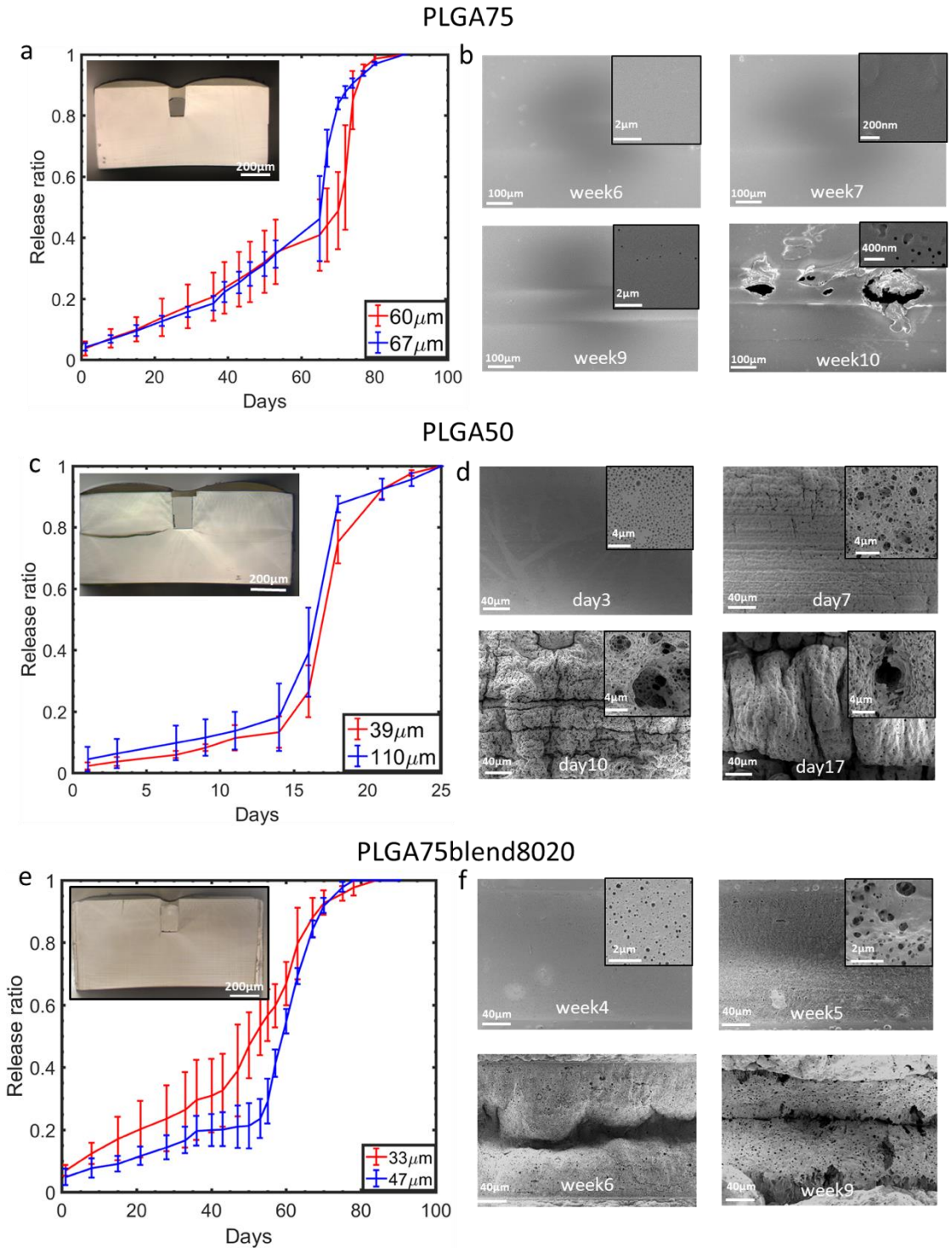

Figure 3.4. The release profiles and corresponding SEM images of degrading PLGA of a&b) PMMA-PLGA75 fibers where PLGA75 film acts as the release barrier in two thicknesses of 60 and 67μm, c&d) PMMA-PLGA50 fiber where the PLGA50 film acts as the release barrier in two thicknesses of 39 and

110µm, e&f) PMMA-PLGA75blend fibers for release barriers of 47 and 33µm PLGA75blend films respectively

3.3 Modelling the release kinetics

As observed, controlling the degradation rate and release kinetics through the dimension of the device is not straightforward and the size-dependency varies based on the physiochemical properties of the original polymer. In order to optimize the design of the device, we go further to elucidate the underlying release mechanism through an analytical model. We adopt the phenomenological diffusion-reaction degradation model from the work of Wang et al.[65] to predict the degradation rate of the PLGA films. A set of partial differential equations was proposed to show the interplay between non-catalyzed hydrolysis, catalyzed hydrolysis and monomer diffusion. Due to the ability of the model to show the competition between these governing factors, non-specificity of the model to a certain polymer system, and its simplicity, we adopted this model for the description of our system[6]. The equations consist of production rate of monomers and reduction rate of ester bounds[65]:

$$\frac{dC_e}{dt} = -(k_1 C_e + k_2 C_e C_m^n) \quad (3.1)$$

$$\frac{dC_m}{dt} = k_1 C_e + k_2 C_e C_m^n + div\left\{D_0\left[1 + \alpha\left(1 - \frac{C_m + C_e}{C_{e0}}\right)\right] \times grad(C_m)\right\} \quad (3.2)$$

Where C_e and C_m are the mole concentration of the ester bounds and the monomers remaining in the device, respectively. k_1 and k_2 are the reaction rate constants for non-catalyzed and catalyzed hydrolysis, respectively. n reflects the dissociation of the acidic groups. D_0 is the initial diffusion constant in the polymer and α is a constant ($\alpha = 4.5$).

In order to model the release kinetics of the active ingredients from the thermally drawn fibers, we implemented a Fickian release equation coupled with the proposed degradation equations. The key parameter in coupling the degradation and release is the effective diffusivity coefficient

$$D = D_0\left[1 + \alpha\left(1 - \frac{C_m + C_e}{C_{e0}}\right)\right] \quad (3.3)$$

which is the function of formation rate of pores and is defined by the diffusion rate of monomers out of the film. This value is subject to change throughout the degradation which affects the degradation itself and thus the release. As release is dissociated into diffusion through two different pathways: degrading polymer phase and the liquid-filled pores[58], we break down the effective diffusivity parameter into two parts in the proposed release equation[6]:

$$D_p = D_{0,d,p}\left(\frac{C_e}{C_{e0}}\right)^{-2} \quad (3.4) \qquad and \quad D_l = D_{0,d,l}\alpha\left(1-\frac{C_m+C_e}{C_{e0}}\right) \quad (3.5)$$

where $D_{0,d,p}$and $D_{0,d,l}$ are the initial diffusion coefficient of the drug in the polymer phase and the liquid phase respectively. The first part (Equation 3.4) reflects the diffusion coefficient in the degrading polymer phase. According to reptation theory[132], the diffusivity is defined based on the ratio of average MW which was assumed equivalent to the ratio of polymer concentration. The second part (Equation 3.5) reflects the diffusion in the liquid-filled pores and is defined based on the same pore formation rate described in the degradation equations. By including these two parts into the effective diffusivity term of the Fick's law, we obtain:

$$\frac{dC_d}{dt} = div\left\{\left[D_{0,d,p}\left(\frac{C_e}{C_{e0}}\right)^{-2} + D_{0,d,l}\alpha\left(1-\frac{C_m+C_e}{C_{e0}}\right)\right]\times grad(C_m)\right\} \quad (3.6)$$

In order to account for the constrictivity effect, which describes the hindrance in diffusion due to the similar size of macromolecular drugs and the pore size[58], the diffusion through the liquid-filled pores (Equation4) was taken into account in the release equation beyond a critical pore fraction. Critical pore fraction was selected as 12% which accounts for the time when the pore number starts to accelerate rapidly and the diffusion through the liquid-filled pores dominates. This effect was previously treated by introducing an induction time based on the pore size[60].

The partial differential equations of degradation are numerically solved by using the Galerkin method proposed in the same work [65]. Consequently, the release equation is solved with appropriate initial and boundary conditions. The schematic of the release system is shown in Figure 3.5.

At t=0: $C_d=C_{d0}$ when $x < 0$, and $C_d=0$ when $x > 0$,

for $x < x_{min}$: $\frac{\partial C_d}{\partial x}$ =0, and for $x > x_{max}$: $\frac{\partial C_d}{\partial x}$ =0

x_{min}= -6*L, and x_{max}= 1000*L where L= thickness of the film

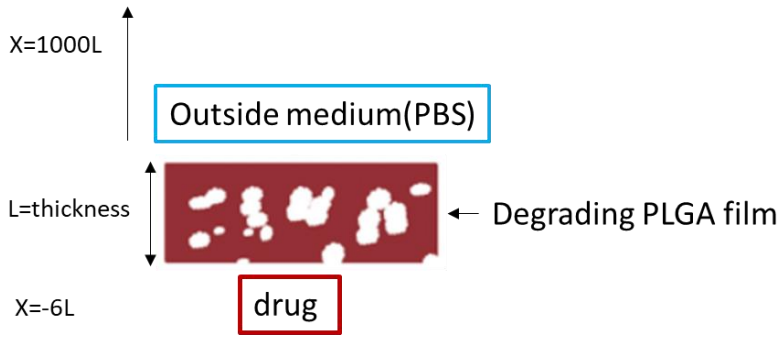

Figure 3.5. The schematic for the description of drug release through the PLGA release barrier in the fibers

The 4 parameters of k_1, k_2, D_0 and n are set as the fitting parameters and their values are iterated relatively for each film based on the experimental observations within their theoretical range:

Fitting parameters	PLGA75	PLGA75blend	PLGA50
$\boldsymbol{k_2}$ ($M^{-n}.s^{-1}$)	4.5×10^{-3}	2×10^{-3}	1.2×10^{-3}
$\boldsymbol{n}$	0.25	0.4	0.7
$\boldsymbol{D_0}$ ($m^2.s^{-1}$)	1×10^{-14}	6×10^{-15}	2×10^{-14}
$\boldsymbol{k_1}$ (s^{-1})	8×10^{-4}	2×10^{-3}	5×10^{-3}

Table 3.1. The values of fitting parameters for modeling the release profiles of each PLGA film

The results of the fitting for PLGA75blend are presented in Figure 3.6a&b. The model successfully describes the diffusion domination in the thinner film (33µm) through a linear regime, and autocatalysis domination in the thicker film (47µm) through a more pronounced sigmoidal shape[6].

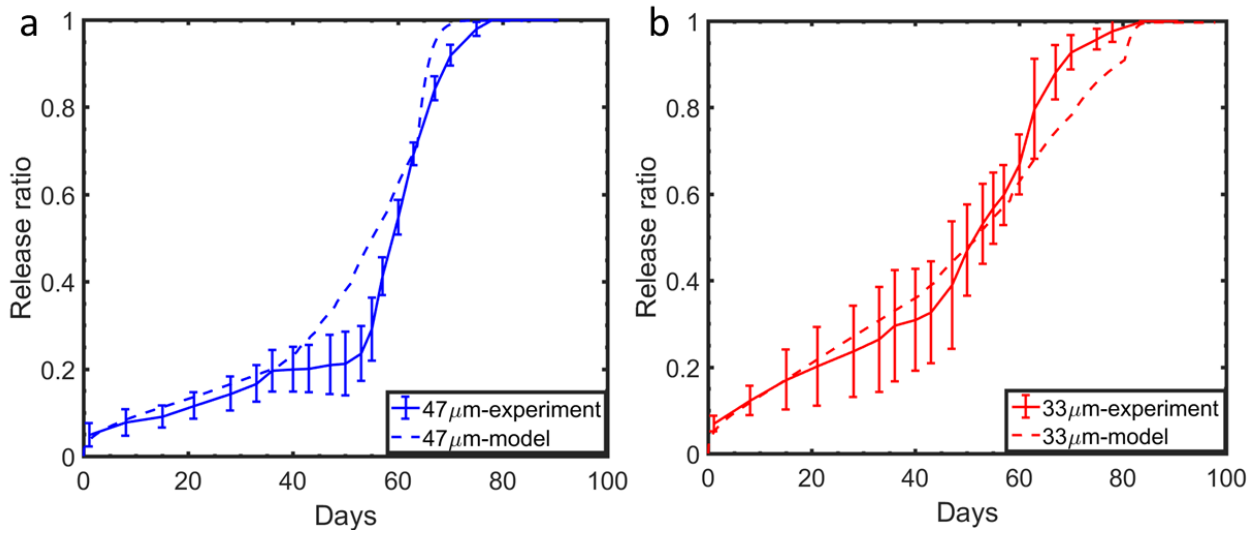

Figure 3.6. Comparison of the release profile based on the experiment (solid line) and the model (dashed line), a) 47µm PLGA75blend film, b) 33µm PLGA75blend film

The model could also be used to fit the experimental results of PLGA75 and PLGA50 films (Figure 3.7a&b), however with some discrepancies. Even though the model could illustrate the same total release time for the very different thicknesses of PLGA50, the rate of slow and fast release phases could not be matched together. Interestingly, the model could illustrate the enhanced release rate due to the bulk degradation in thicker films of PLGA75. However, as can be seen, the model is limited in showing the extent of this accelerated release.

Overall, we could illustrate the main phenomena governing the degradation and release rate through a degradation model. For each PLGA barrier, a set of fitting parameters were found which could successfully describe the release kinetics in different thicknesses, however the range of thickness for which the model could be fitted is limited. Moreover the model neglects all the reaction steps, detailed morphological and structural changes[65] such as swelling and spatial porosity distribution which leads to the observed discrepancy between the model and the experimental release profiles.

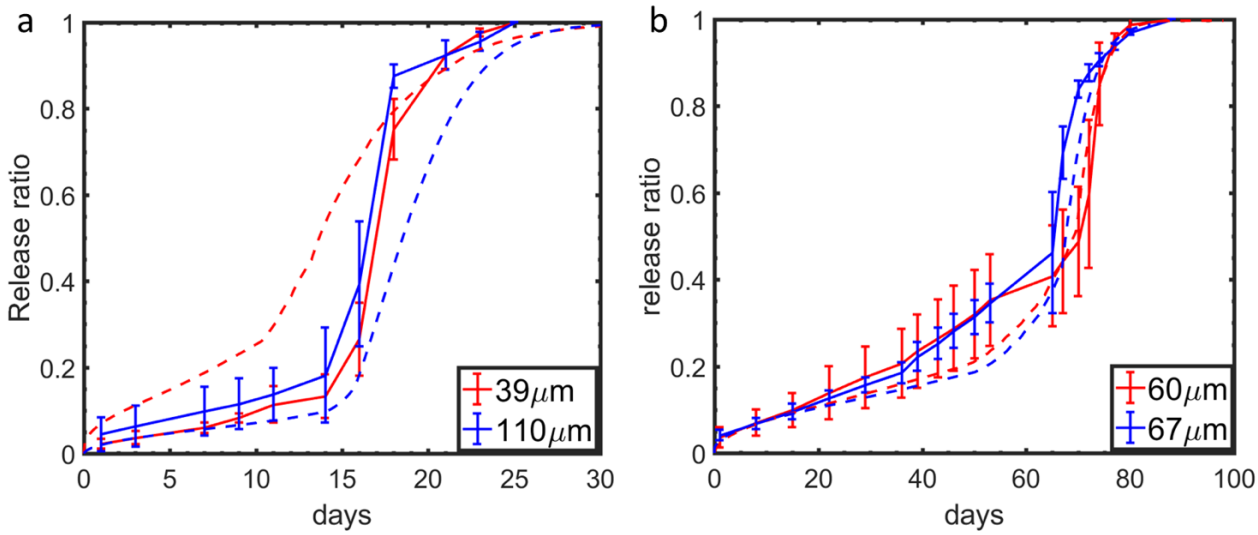

Figure 3.7. Comparison of the release profile based on the experiment (solid line) and the model (dashed line), a) PLGA50 for two thicknesses of 39 and 110 µm, b) PLGA75 for two thicknesses of 60 and 67 µm

3.4 Complex drug delivery fibers

To illustrate the true potential of thermal drawing for the fabrication of advanced biomedical devices, programmable drug delivery fibers capable of releasing predictable dosages of active ingredients at particular time intervals are developed. Figure 3.8a presents a schematic of thermal drawing of a hybrid cylindrical fiber composed of PMMA core containing two channels and PLGA75 and PLGA50 films with the same thickness (~40µm) as the release barrier (Figure 3.8b). The two reservoirs were injected with FD70 and the release study was performed. The release profile presented in Figure 3.8c reveals two sigmoidal profiles corresponding to PLGA50 film in a shorter time period and PLGA75 film in a longer period. 40µm PLGA50 resulted in the first diffusion phase up to day 18 followed by a sharp release phase up to day 25. This result perfectly matches to our findings in Figure 3.4c where the same exact results were obtained for 40µm PLGA50 film. Moreover, the release ratio is 50% upon full degradation of PLGA50 film suggesting that the loaded drug in one reservoir has completely released. This makes the release of the remaining drug solely dependent on the degradation of 40µm PLGA75 film. The degradation of PLGA75 resulted in a slow diffusion phase until day 96 followed by a faster release until day 146. Comparing the obtained results for PLGA75 in Figure 3.4a, the release was significantly delayed due to the smaller thickness of PLGA75 films. This result further supports the significant effect of bulk degradation for different thicknesses of PLGA75[6].

At last, we demonstrate an intriguing example of a fully biodegradable programmable drug delivery fiber. The functionality of this fiber results from the engineered architecture of the cross-section which involves careful selection of the incorporated materials and their corresponding dimensions and positions. In this design, we aim for the core material to have higher viscosity to ensure the stability of the structure during the drawing, and also to have the lowest degradation rate to preserve the integrity of the fiber during degradation. It was found that PLGA85 (85% lactide content) meets these requirements and based on the results of complex viscosity measurement in chapter 2, PLGA85 exhibited the highest viscosity followed by PLGA75, PLGA50 and PLGA75blend respectively. Therefore, PLGA85 was chosen as the main body of the device and 4 microchannels were incorporated as the drug reservoirs (Figure 3.8d&e). In order to achieve release at 4 different time intervals, PLGAs of different thicknesses in accordance with their expected release rate were placed on top of each channel. Thanks to our fabrication approach, we can control the position, thickness and composition of different biodegradable materials in a single fiber: 1)53µm PLGA50 2)130µm PLGA75blend 3)95µm PLGA75 4)47µm PLGA75[6].

After thermal drawing, a heat treatment step ((10min at 80°C+10min at 25°C) x 3times+ 2hours at 80°C) was performed on the fibers to release potential residual stress and to ensure their dimensional stability in PBS and 37°C. Next, the four channels were loaded with FD70. Release experiments resulted in 4 sigmoidal release profiles, labeled with their corresponding barrier (Figure 3.8f). The first step up to day 27 corresponds to 53µm PLGA50 film which is consistent with the release timelines of PMMA-PLGA50 fibers, as for any thickness value in the range of 39-110µm, a similar release profile is expected. The second step up to day 50 corresponds to 130µm PLGA75blend. This release timeline is significantly faster than the release rate obtained from 33 and 47µm PLGA blend film (Figure 3.4e) which further highlights the significance of bulk degradation. The third step up to day 71 corresponds to 95µm thick PLGA75 and the remaining release corresponds to 47µm PLGA75. The delayed release of 47µm PLGA75 up to day 126 aligns well with our findings for 60 and 67µm PMMA-PLGA75 fibers (Figure 3.4a) where a faster release was observed for the thicker film. Reversely, for thinner films, the onset of the fast release is expected to occur at later stage which is evident in the fourth step corresponding to 47µm PLGA75 film. It can be seen that the release ratio at the end of each step is slightly more than one fourth of the loaded chemical; this is because all the films are characterized by a slow diffusive release in their first phase which cannot be differentiated and their release is identified by their fast accelerated release phase[6].

In this study, we demonstrated a multi-phase release in a single micro-structured fiber. Clearly, the potential of the fiber does not stay within the release of only one active ingredient, each channel could be loaded with various therapeutic agents such as anti-inflammatory agents to reduce edema, antibacterial agents to prevent infection and growth factor to boost skin regeneration[3], [6].

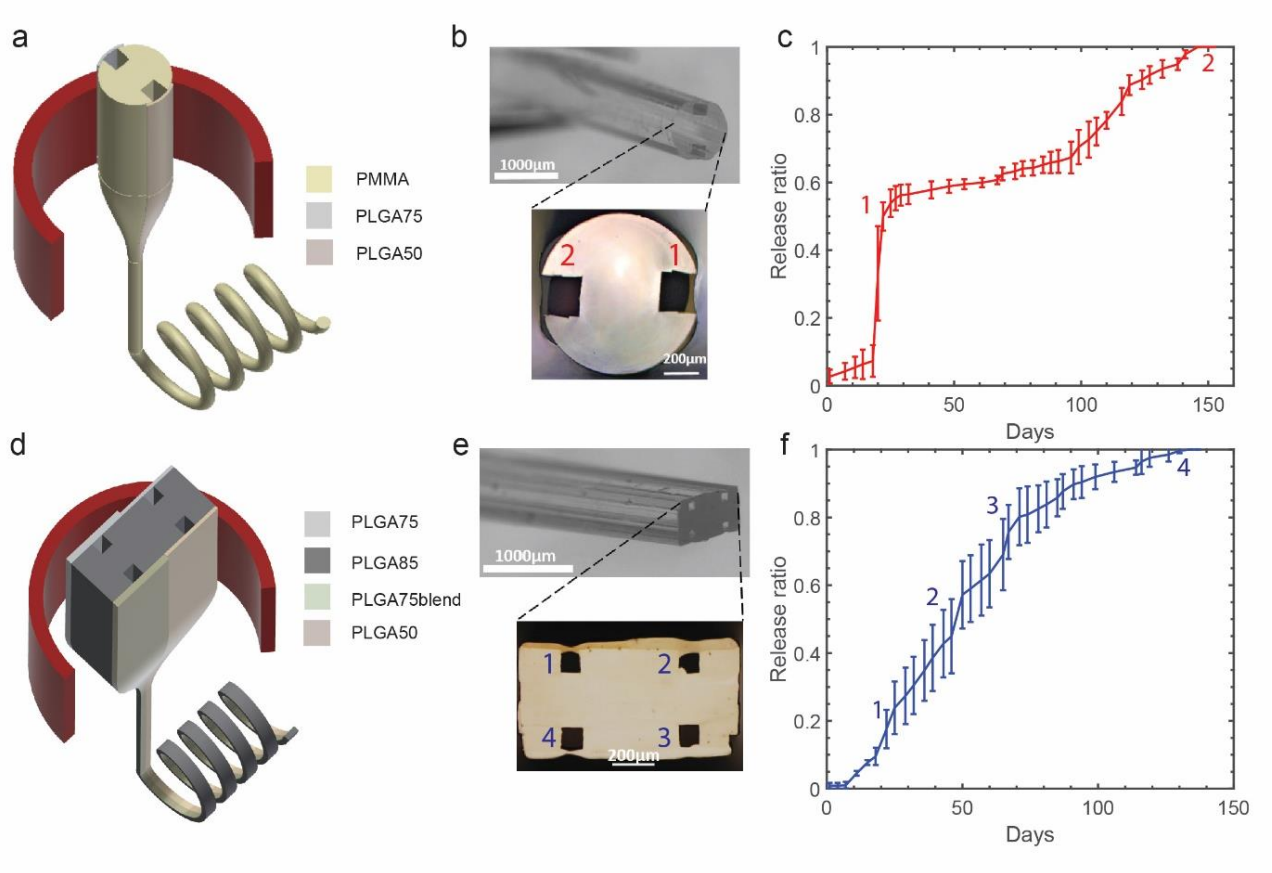

Figure 3.8. Multi-dose drug delivery fibers in partially and fully biodegradable compositions. a) Schematic of the thermal drawing of hybrid PMMA-PLGA75-PLGA50 fibers, b) OM of the corresponding fiber where PMMA is in the bulk encapsulating 2 channels and PLGA75 and PLGA50 films in the same thickness act as the release barrier for each channel, c) The obtained multi-dose release profile of the fiber where two segments corresponding to PLGA50 and PLGA75 barriers are labeled, d) Schematic of thermal drawing of fully biodegradable PLGA85-PLGA75-PLGA75blend-PLGA50 fibers, e) OM image of the corresponding fiber where PLGA85 is in the bulk encapsulating 4 channels and PLGA75 blend , PLGA50 and PLGA75 of two different thicknesses (thin and thick) act as the release barrier for each channel, f) The obtained multi-dose release profile where 4 segments corresponding to PLGA50, PLGA75blend, thick PLGA75, and thin PLGA75 barriers are respectively labelled.

3.5 Effect of drug size on the release kinetics

All the previous measurements were performed using FITC-dextran with MW of 70k Da. In order to study the effect of drug size, some of the previous fibers were injected with a smaller size FITC-dextran with MW of 40k Da (FD40) and their release kinetics compared with the profiles obtained for FD70. Figure 3.9a&b show the two different release profiles obtained from the multi-channel and single-channel fibers. As it is evident, the difference of size between the two molecular weights of 40k Da and 70k Da is not large enough to show a significant difference between the release profiles. However, in the diffusion-controlled phases of the release profiles, the smaller dye molecules (40k Da) exhibited faster release. In order to truly illustrate the influence of drug size, a much smaller MW of FITC-dextran, perhaps 4k Da, should be employed.

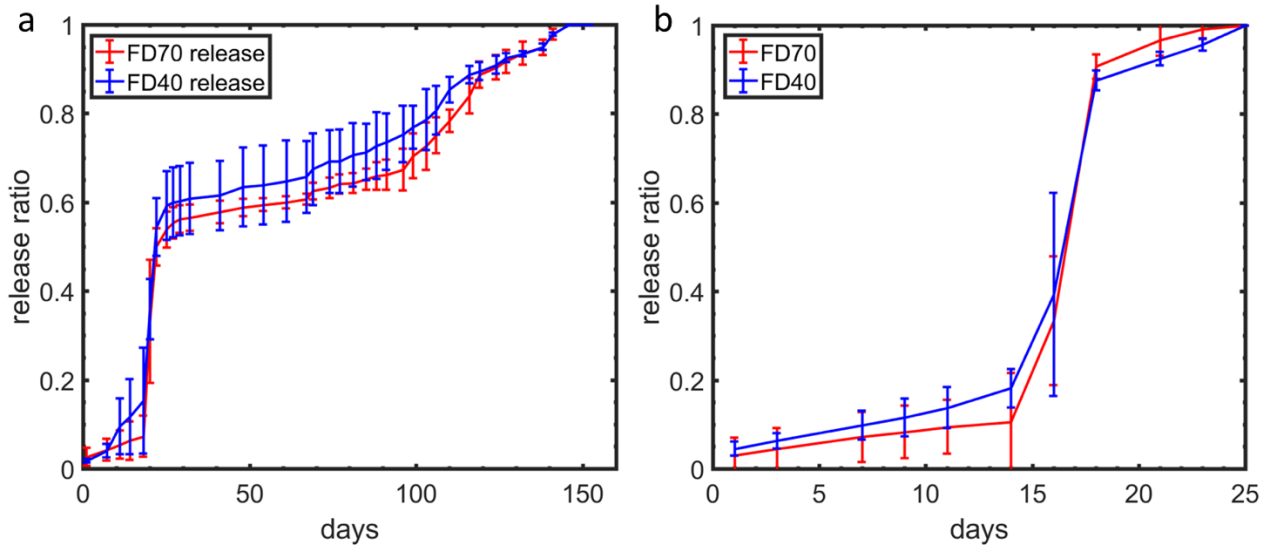

Figure 3.9. Effect of two sizes of FITC-dextran (40kDa and 70kDa) on the release profiles of a) cylindrical fiber PMMA-PLGA50-PLGA75 and b) rectangular PMMA-PLGA50

3.6 Chain orientation of PLGA release barriers in the thermal drawing

Since the thermal drawing could induce polymer chain alignment, it is essential to analyze the internal microstructure of PLGA before and after the thermal drawing in the studied fibers to verify if the thermal drawing could have any impact on the biodegradation kinetics. Since PLGA is an amorphous material and partially ordered microstructures are expected to be created during thermal drawing, wide-angle X-ray scattering (WAXS) is a technique of choice. The WAXS measurements were done in collaboration with Empa St-Gallen, and particulary Anjani Maurya who performed the measurements, on PLGA50 films after different processing conditions: PMMA-PLGA50 fiber, PLGA85-PLGA50 fiber and hot-pressed PLGA50 film.

Figure 3.10a&b show the extracted profiles along and perpendicular to the fiber axis respectively. The red arrows correspond to PMMA peak positions and the green arrow to the PLGA film. As can be seen, the PMMA and PLGA peaks are very close to each other and therefore identifying and deconvoluting them is challenging in transmission mode. Grazing-incidence S/wide-angle X-ray scattering (GIS/WAXS) should be done to measure the properties of the PLGA50 film only. However, since codrawing of PLGA50 with PMMA was done at higher temperature with PMMA than with PLGA85, in the case of presence of any ordered microstructure, the peak of PLGA50 should be lower in PMMA-PLGA50 fibers than in PLGA85-PLGA50 fibers.

Nevertheless, based on the identified peaks, it can be seen that the difference between the peak positions of the PLGA in the film and in the fiber when analyzed perpendicular or parallel to the fiber is insignificant. This indicates that the morphology of PLGA50 is intact when drawn with PLGA85 or PMMA. This is because the two fibers were drawn at much higher temperature than the one required for PLGA50 that experienced drawing at low viscosity, and therefore no stress was induced on PLGA50 film during the drawing. The 2D SAXS profiles for the three compositions in Figure 3.10c&d&e also show the isotropic scattering profile. While this result is reassuring in using the results of the release kinetics of thermally drawn PLGA50 barriers in different fibers to predict the release behavior of complex fibers with different cores, the same analysis should be done for other PLGA compositions. This is because different PLGAs have different viscosities and other grades could experience higher stress during the drawing with PLGA85 than with PMMA.

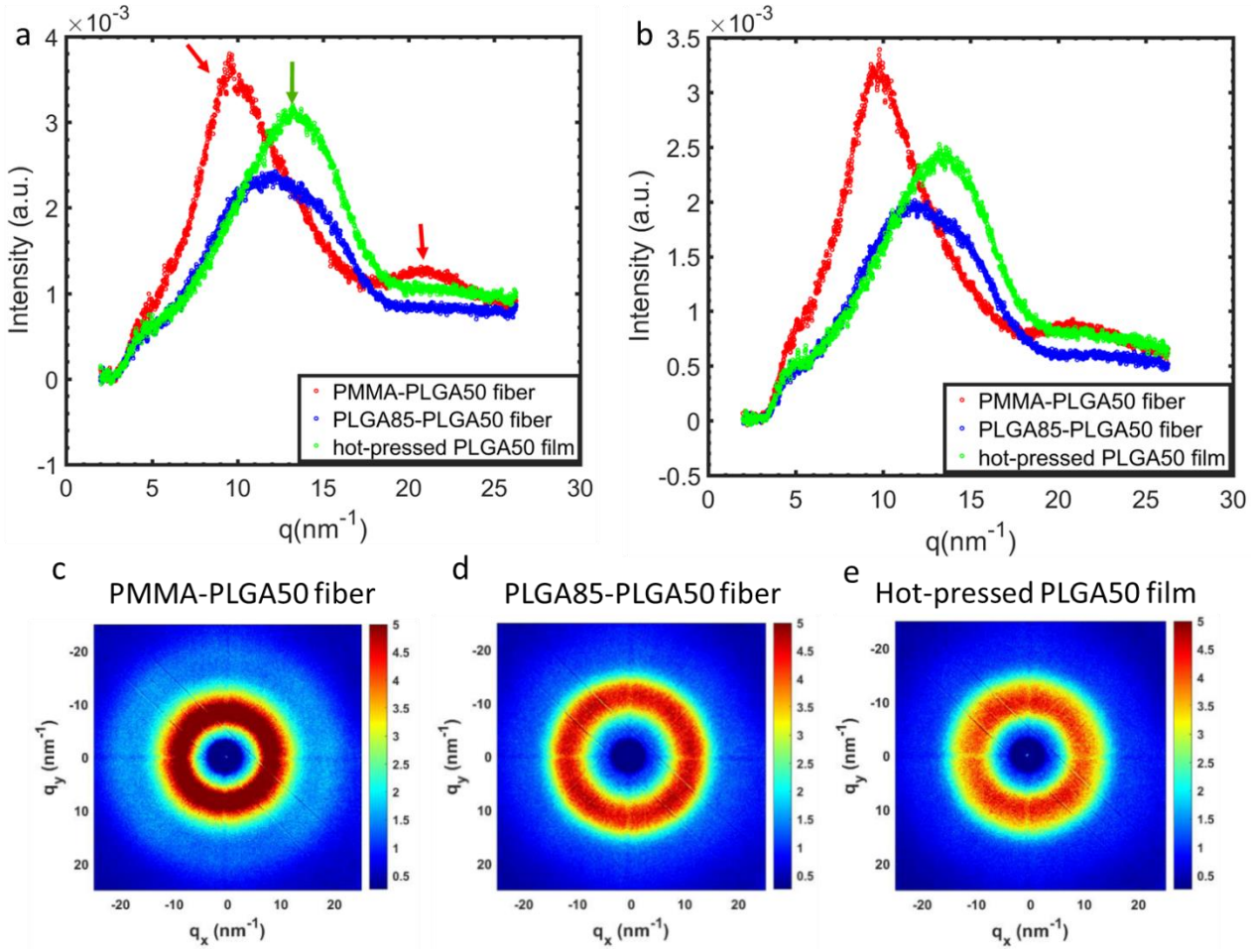

Figure 3.10. SAXS data on PLGA50 films a) along the fiber axis and b) perpendicular to the fiber axis, c,d,e) 2D SAXS profiles for PLGA50 film of PMMA-PLGA50 fiber, PLGA85-PLGA50 fiber and hot-pressed PLGA50 film respectively.

3.7 Mechanical properties of thermally drawn PLGA fibers

In this part, the mechanical properties of PLGA-based fibers are investigated that are key for biomedical devices[133], [134] such as sutures[106] and implants. By thermally drawing fibers at high stress, polymer chains tend to align along the drawing direction which results in high mechanical strength[135]–[138]. Figure 3.11 shows the representative stress-strain curves from fibers of rectangular PLGA85 at different drawing stresses: 2.6, 3.2, 5.06, 6, and 7.8 MPa. All the tensile curves are characterized by a small linear region after which the fibers experience necking manifested by a flat plateau. Then the curves exhibit a strain hardening ramp with characteristic fluctuations which suggest the occurrence of structural rearrangement and shear banding[6], [139], [140]. The ultimate tensile strength of the fibers could be improved from 120 MPa to 220 MPa, when drawn at higher stress. Since the dimensions of the fibers get

smaller with increasing drawing stress due to the increase of the draw down ratio (or the drawing speed) at a constant drawing temperature, they are less ductile. Therefore, less shear banding occurs and they can resist higher force to achieve even higher alignment of polymer chains during the cold drawing of tensile test. This leads to a smaller elongation of the fibers at higher stresses. Nevertheless, the elongation of the fibers is considered advantageous for suture application in case of edema[106] or spikes in loading[141].

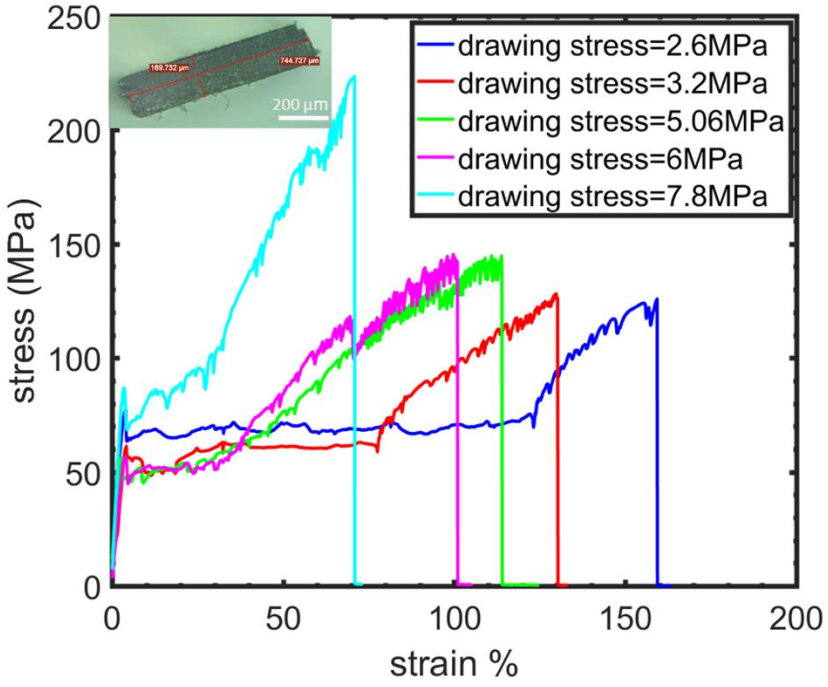

Figure 3.11. The tensile curves of the rectangular PLGA85 fibers drawn at 2.6, 3.2, 5, 6, and 7.8MPa

The effect of the drawing stress on stress-strain curves of cylindrical PLGA85 fibers is also investigated and shown in Figure 3.12. It can be seen that the significant increase of drawing stress from 2.6 to 11 MPa leads to the increase of the strain hardening modulus. This resulted in failure strength as high as 276 MPa for 247µm-diameter PLGA fibers (Figure 3.12c). This failure stress for such fiber size is comparable to the tensile properties of commonly used absorbable sutures[106], [141]. In order to better compare the mechanical behavior of the fibers drawn at different stresses, the strain hardening modulus of the curves were extracted based on the engineering stresses using Gaussian equations[142]. Gaussian equations assume that the polymer coils do not stretch to it maximum length during the strain hardening[142]. The extraction of strain hardening modulus is shown in Figure 3.12b based on:

$$\sigma_{Eng} = {}^{Y}/_{\lambda} + G_p\left(\lambda - {}^{1}/_{\lambda^2}\right) \quad (3.7)$$

Where σ_{Eng} is the engineering stress, Y the extrapolated yield stress, G_p strain hardening modulus and λ the extension ratio, λ = extended length/original length[142]. Based on Figure 3.12b, the strain hardening modulus of the fibers drawn at higher stress is larger: 30.6, 39 and 52 for the fibers drawn at stress values of 2.6, 3.7 and 11 MPa respectively.

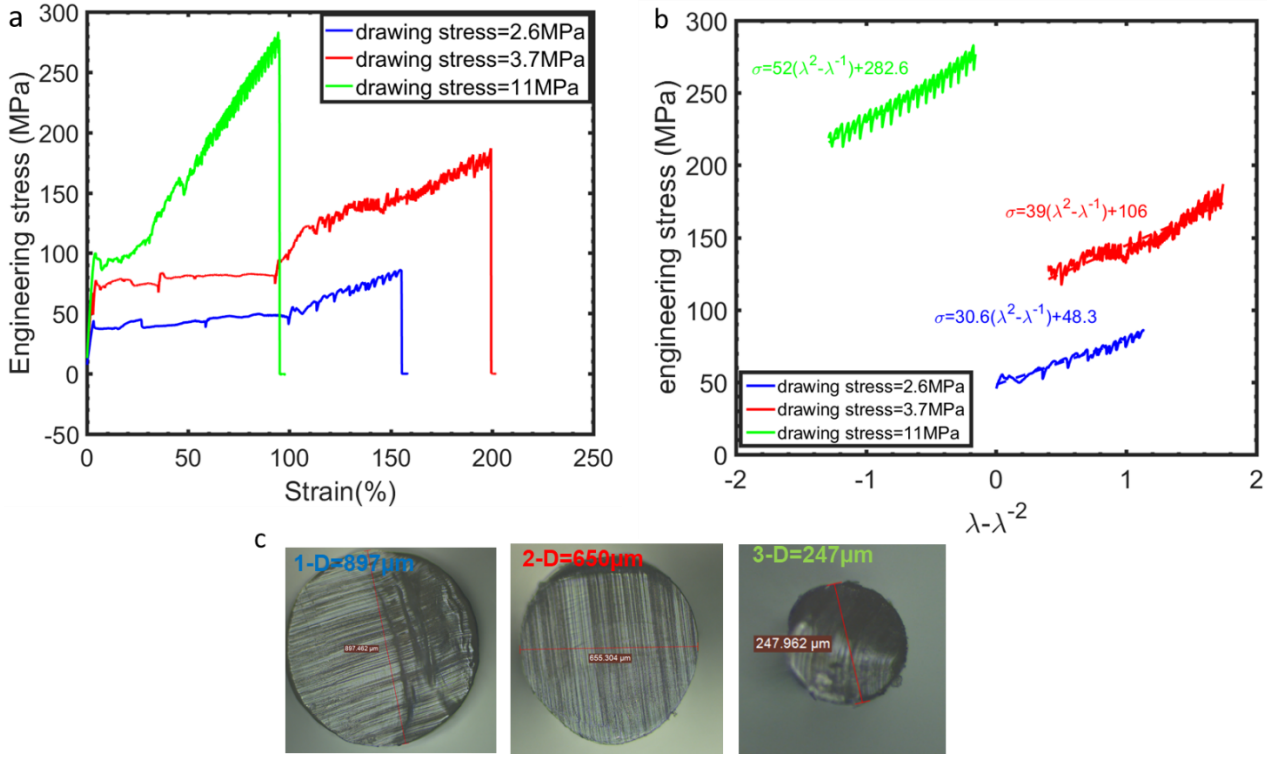

Figure 3.12. The comparison of mechanical properties of the cylindrical PLGA85 fibers drawn at different stresses, a) The tensile curves of the fibers drawn at 2.6, 3.7, and 11 MPa, b) The derivation of strain hardening modulus based on Gaussian equations, c) The optical microscopy images of the three tested PLGA85 fibers with dimensions of 897, 650 and 247µm

The stress-strain curves corresponding to the PLGA85 fibers drawn under relatively high drawing stress (3.7 MPa) are presented in Figure 3.13. As can be seen the tensile curves demonstrate a very good reproducibility at this condition and an average failure stress of 180 MPa was obtained. This implies that the drawing stress was induced evenly during the fabrication and uniform dimensions were obtained all along the fiber.

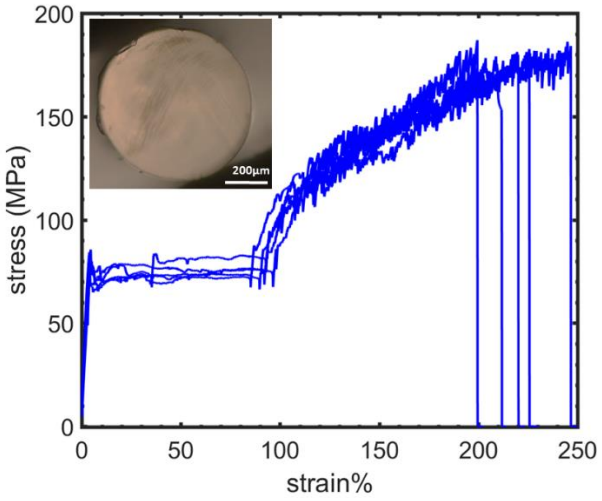

Figure 3.13. The reproducibility of stress-strain curve of 5 cylindrical PLGA85 fibers drawn at drawing stress of 3.7 MPa

3.8 Shrinkage study of PLGA fibers

While the chain orientation by the drawing stress is beneficial for the mechanical properties, such alignment is responsible for unwanted shrinkage of PLGA films or fibers when heated or exposed to different solutions[143], [144]. Table 3.2 shows the shrinkage percentage for PLGA75 fibers which were drawn at a low drawing stress (less than 1 MPa), at different conditions after 2 hours, 1 day and 2 days. Regardless of the type of aqueous solution and the pH, fibers go through significant shrinkage when kept at 37°C. On the other hand, when fibers were kept at 37°C without any solvent, there was no evidence of shrinkage. The analysis also shows the significant impact of temperatures as the fibers in buffer of pH 7.4 at 25°C did not show any shrinkage. Therefore, the two factors of elevated temperature and solvent together lead to enhanced mobility of polymer chains and subsequent shrinkage. Also interestingly, it can be seen that the shrinkage occurs almost immediately in all cases, 40% after 2 hours, and then the increase continues slowly with time: about 55% after 1 day and 60% after 2 days and then stabilizes.

	PH7.4(37˚C)	PH3(37˚C)	Water(37˚C)	PH7.4(25˚C)	Dry fiber(37˚C)
After 2 hours	40%	40%	40%	No change	No change
After 1 day	52%	56%	57%	No change	No change
After 2 days	60%	61%	62%	No change	No change

Table 3.2. Shrinkage percentage of PLGA75 fibers at different environmental conditions at different times

Figure 3.14 shows the cross-section of the corresponding PLGA75 fibers before and after the shrinkage after 4 days of incubation in PBS and at 37°C. As can be seen the changes of dimensions happen proportionally. As the length of the fiber was reduced by almost a factor of 2.5, from 4.2 cm to 1.5 cm, the width and thickness of fibers were also expanded by almost a factor of 2.5; width was increased from 1060 µm to 2388 µm, and thickness from 197 µm to 432 µm. While this shrinkage is considered a problem in our study, this proportional mechanical deformation based on the drawing stress could be exploited to obtain functional devices.

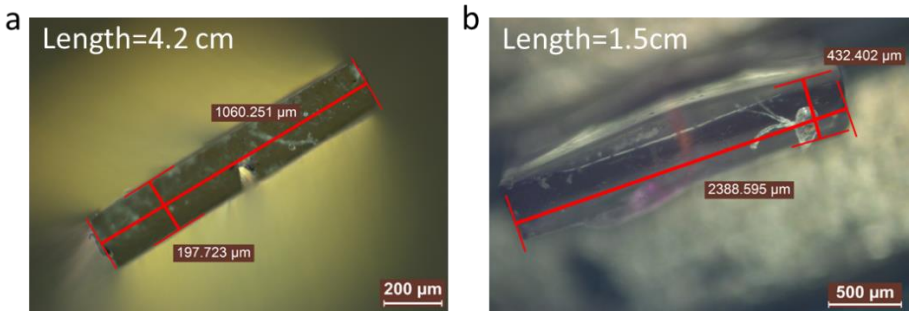

Figure 3.14. Dimensional change of rectangular PLGA75 fibers a) before and b) after 4 days of incubation in PBS at 37°C

3.9 Methods to mitigate the shrinkage of thermally drawn PLGA fibers

The phenomenon of shrinkage was also previously observed in PLGA fibers produced by techniques such as electrospinning. This problem was tackled with different methods such as confining the PLGA fiber mesh inside a polypropylene ring[145] or blending the PLGA with PCL [146]. In this part, we approach this problem by two methods: 1) a heat treatment procedure of the PLGA fibers to relax the residual stress from drawing, and 2) the codrawing of PLGA with a PCL core.

The heat treatment of PLGA-based fibers was done in an oven under controlled temperature and time. The two ends of the fibers were fixed to prevent their shrinkage at elevated temperatures. This treatment was found to be only effective on the fibers drawn at low stress values (less than 1MPa). The fibers drawn at

higher stress values could not resist the high temperature and broke during the heat treatment. The treatment followed this procedure: (10 min at 80°C+10 min at 25°C) x 3 times+ 2 hours at 80°C. In the beginning, the exposure of the fibers at high temperature was interrupted in short intervals to slowly increase the mobility of the chains and thus to prevent breakage. Later, the fibers were left to stay longer at this high temperature. In order to further ensure the stability of the fibers during the heat treatment, this stress relaxation could be done at lower temperature than 80°C and over a longer time.

The shrinkage comparison of PLGA fibers, before and after the heat treatment is analyzed using DMA (Figure 3.15). The two end of the fibers were fixed with a very small force, and their dimensional change (strain%) is measured over a temperature ramp. As can be seen, both fibers started to show a change in their length at 62°C, a temperature close to their T_g: they reach a maximum shrinkage strain of 60% for untreated fibers and 28% for the heat treated fibers. Even though, the result shows that the heat-treated fibers still go through shrinkage, it should be mentioned that the condition of the DMA analysis is different from the one in the release studies. The dimension of the fibers is required to be stable in PBS and 37°C. However, based on our observations of the dimensions of the heat treated fibers after immersing in PBS at 37°C, the shrinkage could be significantly improved or even completely removed.

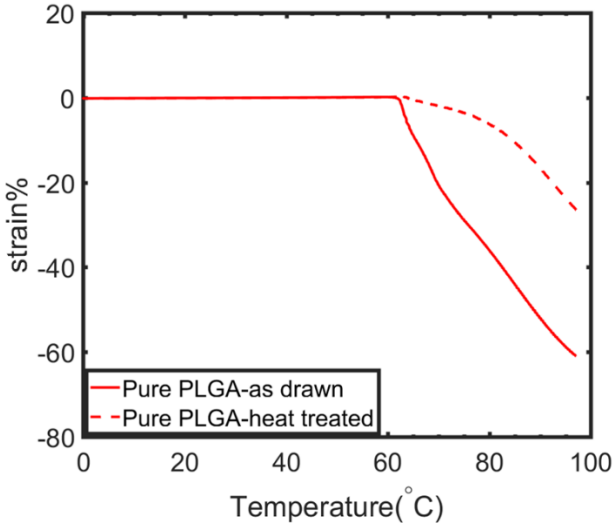

Figure 3.15. DMA measurement for the shrinkage analysis of PLGA75 fibers before and after the heat treatment

To alleviate the shrinkage problem completely without any post-drawing treatment, we established co-drawing of a semicrystalline biodegradable polymer, Polycaprolactone (PCL) with the amorphous PLGA in a core-shell structure. This architecture meets both the requirements of the thermal drawing and the dimensional stability. Since PCL is a semi-crystalline polymer with a melting point of 60°C, it will flow as a liquid with low viscosity during drawing. Therefore, PLGA which is a viscous amorphous polymer with

a T_g of about 60°C should surround the PCL to act as an encapsulant. The picture of the described preform before the drawing is shown in Figure 3.16a where the PCL is the material of the core with a diameter of 1 cm inside a cylindrical PLGA of 2 cm diameter.

The placement of PCL in the core prevents the shrinkage of the PLGA cladding by providing a rigid semicrystalline base for the amorphous PLGA shell at elevated temperature. Figure 3.16b shows the state of PLGA-PCL fibers in 3 different sizes after incubation at 37°C in PBS after 2 days. As can be seen, all the fibers showed almost no dimensional change and only the small fiber exhibited a small curvature. In order to quantitatively show the impact of the PCL core on the shrinkage of PLGA, a DMA analysis was done on PLGA-PCL and hollow core PLGA fibers (Figure 3.16c). In contrast to previous analysis where the dimensional change was measured over a temperature ramp, in this case the measurement was done at an isothermal mode at 50°C to maintain the temperature below the melting temperature of PCL. The two ends of the fibers were fixed at 50°C for 2 hours to prevent any dimensional change, and then this force was removed to allow the fibers to relax. As can be seen the hollow core PLGA fiber showed a shrinkage of 10% while the PLGA-PCL fibers with the same dimension only shrunk by 1% and immediately stabilized. The proportional composition of PCL and PLGA in this architecture can be further optimized to achieve complete mechanical robustness.

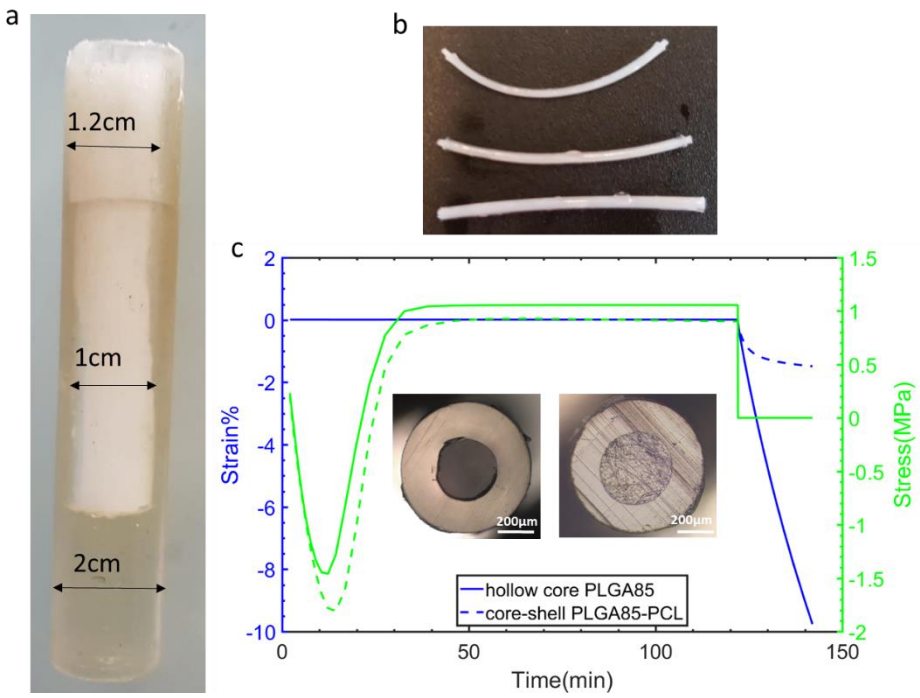

Figure 3.16. The fabrication and shrinkage analysis of PLGA-PCL fibers, a) the corresponding preform structure, b) the obtained fibers in 3 different sizes after incubation for a few days, c) DMA measurement for shrinkage analysis of core-shell PLGA-PCL and hollow core PLGA fibers

Figure 3.17 shows the stress-strain curves from fibers of hybrid core-shell PCL-PLGA85. Even though the tensile curves of the fibers from the same batch showed some discrepancy, a high tensile strength was obtained for all the cases, from 150 MPa to 200 MPa. These values are comparable to the tensile properties of fully PLGA85 fibers therefore it can be inferred that the PLGA85 shell is also highly aligned in this configuration. This result presents a crucial novelty where biodegradable fibers of high mechanical strength with a good mechanical robustness are realized.

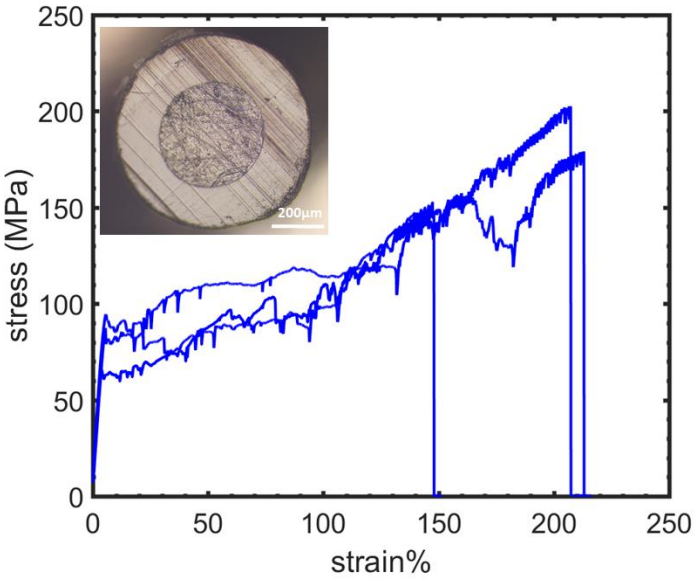

Figure 3.17. The reproducibility of stress-strain curves obtained for 3 PLGA-PCL fibers drawn at the same drawing stress

3.10 Experimental

Materials: Phosphate buffer Saline, PBS, (10×) pH 7.4 was purchased from Thermo Fisher. Fluorescein isothiocyanate(FITC) labeled dextran (MW=70kg/mol) (FD70) was purchased from Sigma-Aldrich.

Preform fabrication:

1) PMMA-PLGA preforms: two PMMA plates of 5.8 mm were hot-pressed (Lauffer Pressen UVL 5.0) together at 130 °C, 10 N cm^{-2} for 20 min to obtain a thicker plate with dimensions of 2.4 cm width,1.2cm thickness and 16cm length. A groove of 4 mm depth×2mm width was milled along the preform. PLGA films were each prepare by hot-pressing predetermined weight of PLGA pellets in a rectangular mold of 2.4×17 cm under conditions of 100 °C, 5 N cm^{-2} under vacuum for 10 min to obtain the desired thickness (1g~300 µm film). The PLGA film and PMMA plate were hot-pressed at 90 °C and 4 N cm^{-2} with presence of a Teflon bar in the channel to prevent the deformation of PLGA film. The Teflon bars were removed prior to drawing.
2) Cylindrical PMMA-PLGA preform: The channels of 2×2 mm were milled symmetrically on the two sides of the PMMA rod. PLGA ribbons of desired thickness was prepared by hot-pressing, and the films were gently pressed on top of the channels on a hot-plate set at 70 °C.
3) Multimaterial 4-channel PLGA preform: The PLGA85 plate was prepared by hot-pressing the flakes at 130 °C, 6 N cm^{-2} for 20min in a rectangular mold to obtain preforms of 2cm×8mm×13cm. The 4channels were produced by milling grooves of 2×2mm.Teflon bars were inserted in the channels and

PLGA films of right dimensions were taped on top of the prescribed channel and hot-pressed at 80°C and 6N cm^{-2} for 10min. After hot-pressing, the Teflon rods were withdrawn prior to drawing.

4) Cylindrical PLGA85: was prepared by filling up a vertical cylindrical mold by the pressed PLGA85 pieces and heating up the mold in a consolidation oven (France Etuves C 3000) at 160°C and under vacuum with a pressure about 10N cm^{-2}.
5) Core-shell PC-PLGA fibers: Firstly, PLGA shell were fabricated in a hollow core mold in the consolidation oven as described before. The mold was taken out and the core was filled with PCl, and heated at about 70°C with frequent pressure.
6) Hollow core PLGA85 fiber: the hollow core PLGA85 cylinder was made in a pre-designed mold with a diameter of 2 cm including a 1cm-dimater rod at the center. The PLGA85 pieces were first grounded to obtain a powder-like consistency. This step was found to help the material to melt efficiently and to prevent the creation of bubbles. The mold was filled with the powder and pressed in a consolidation oven with some heavy weights. The temperature was set at 180°C for one hour and then, it was reduced to 160°C and the consolidation was continued for a few more hours. More material was added progressively upon melting of the material

Thermal drawing: The preforms were drawn with a custom draw tower consisting of a three-zone furnace. The set temperatures PMMA-PLGA preforms were (100-260-90 °C). The PLGA75 preforms were drawn at (70-135-50 °C) while the PLGA85 preforms were drawn at (70-170-50 °C).

Dye injection: The fibers of 3cm-long were injected with FD70 using a vacuum pump (D.V.P). After the injection, the two ends of the fibers were sealed by a water resistance glue (Araldite Rapid) and placed in 4 ml of PBS and incubated at 37 ˚C in a microbiological incubator (XB032) from France Etuves.

Fluorescence spectroscopy: In order to calculate the concentration of released FD70, the fluorescence spectroscopy was performed by LS 50B, Perkin Elmer. The excitation wavelength was set at 493 nm with slit size 9. For all the release measurements corresponding to each type of fibers, 6 fibers were used for each studied thickness.

Thickness measurement: The thickness of PLGA films in PMMA-PLGA fibers were measured by the optical microscopy. The t-test analysis showed that there was a significant difference between the thickness values of thin and thick fibers for all PLGA types: PLGA50, PLGA75blend, and PLGA75 with P-values of 8.05e-10, 3.302e-4, and 1.1265e-5.

Scanning electron microscopy: For each type of PLGA, batches of corresponding PMMA-PLGA fibers were prepared and put in PBS and at 37°C. For each predetermined time of morphology analysis, one fiber with length of 2 cm was assigned as the SEM analysis is a destructive method upon coating. The samples

were coated with 5 nm Iridium by Quorum 150 sputter coater. The SEM images were taken by Gemini SEM 300 operating at 0.5 kV tension and 30 µm aperture size. The analysis was performed on 2-3 batches of PMMA-PLGA75 and PMMA-PLGA50 fibers, and only on 1 batch of PLGA75blend-PMMA fibers. In each batch, one fiber was assigned for the analysis of each predetermined time.

WAXS: experiments were performed with a Bruker Nanostar instrument (Bruker AXS GmbH, Karlsruhe, Germany) equipped with pinhole collimation system and a micro-focused X-ray Cu source (wavelength CuKα 1.5406 Å) providing a beam with a diameter of about 400 µm. The sample-to-detector distance was 5 cm.

Tensile machine: The tensile test was performed on an Electromechanical Universal Testing Machine Series LFM-125 kN using 1 kN load cell. The initial distance was set 10cm and the elongation speed 1mm s^{-1}. For rectangular and cylindrical PLGA85 fibers, tests were performed on 5 fibers for each drawing stress, and for core-shell PLGA85-PCL fibers, 3 fibers for each drawing stress. The linear regression analysis on PLGA85 fibers showed that the increase of tensile strength is the result of increase of drawing stress for rectangular fibers with p-value=7.983e-5 and R^2=0.5265 and for cylindrical fiber with p-value=3.258e-3 and R^2=0.4348.

DMA measurement: The shrinkage analysis on as-drawn and heat-treated PLGA75 fibers was done in controlled force mode where a 0.001N force was applied in a temperature ramp from 0 to 100°C with a temperature ramp of 3°C/min. The shrinkage analysis on the hollow core PLGA85 fiber and core-shell PLGA85-PCL fiber was performed on stress relaxation mode where a displacement of 0.01% and a minimum force of 0.001N were maintained in isothermal condition at 50°C and 20 minutes of recovery was measured.

3.11 Summary and Conclusion

In this work, we first identified the important criteria for the selection of an appropriate drug model such as size and hydrophilicity. Accordingly, FITC-dextran as the representative of hydrophilic macromolecular drugs was selected for the release studies. The release property of thermally drawn PLGA films was characterized in the context of multimaterial fibers of PMMA-PLGA compositions. By using PLGAs of different grades and molecular weights, a variety of the release profiles were obtained. The mechanism of the release kinetics was elucidated based on the morphology of the degrading PLGA films. For the slow degradation rate PLGA such as PLGA75, the importance of heterogeneous bulk degradation on the release kinetics was observed while for the fast degradation rate PLGA such as PLGA50, this effect seemed to be insignificant. Moreover, it was found that the release mechanism could be switched from the erosion-controlled to diffusion-controlled when the high MW PLGAs were blended with low MW PLGAs. In order to mathematically describe the observed release kinetics in relation with the physicochemical properties of

the PLGA, a release equation based on an existing phenomenological degradation model was developed and fitted to the experimental results. The model could encompass some of the important features of release kinetics such as the biphasic regime and the enhanced release due to the bulk degradation. However due to the complexity of the events and the change of release mechanism based on the thickness range, a more complex model is required to fully describe the release profiles.

Based on the results of the studied release barriers, complex multimaterial fibers containing multiple channels with different release barriers are realized in partially and fully biodegradable compositions. As a result, multi-dose release profiles were obtained where each step of the profile could be matched to the release properties of the corresponding barrier. Such fibers present the unique attribute of the thermal drawing process as they offer unprecedented pharmaceutical capability in a single microstructured device through a facile processing procedure.

Moreover, The WAXS analysis on the PLGA films before and after thermal drawing showed no impact on the internal microstructures which suggests the intactness of the biodegradation property upon drawing. This is an important insight as the release results of PLGA in other drug delivery systems could be utilized to predict the release profiles of thermally drawn PLGA fibers in both simple and complex structures.

Lastly, due to the importance of mechanical strength in some biomedical applications such as sutures or implants, the tensile strength of the fibers was improved by increasing the drawing stress. As a result, a tensile strength close to 300 MPa which is comparable to the one of commercial sutures, could be obtained for these amorphous fibers. This is the result of the alignment of polymer chains during thermal drawing. However, polymers with such aligned morphology are prone to shrinkage when exposed to solvents and at temperatures close to their T_g. Therefore, we established a heat treatment procedure to relax the internal stress. This method was found to be particularly effective for the fibers drawn at low stress values (below 1 MPa). Ultimately, when the PLGA fibers were co-drawn with PCL as a semicrystalline polymer in their core, the shrinkage could be completely alleviated, even when the PLGA shell was drawn at high stress. This is an interesting development as PCL is biocompatible and biodegradable and it enables to make a fully biodegradable structure with complex architectures for multi-dose release, while possessing high mechanical strength and high integrity under exposure to temperature or solvents.

Chapter 4 Biodegradable glass composite fibers

While we could demonstrate that PLGAs of high lactic content and molecular weight can be thermally drawn and used in complex control release fibers, we have not addressed two limitations that could restrict possible applications. PLGA polymers indeed possess a slow degradation rate, and the degradation products are acidic which can be harmful for the environment and especially surrounding tissue[77]. As explained in chapter 1, phosphate glasses (PG) have attractive properties which have been exploited in a variety of drug delivery systems. The degradation of PG particles is much faster than PLGA[91], and it consists of series of precipitation/dissolution steps with alkaline byproducts that could help pH neutralization[147]. We therefore proposed to investigate the formation of a polymer composite with a PLGA matrix hosting PG particles. The objective is to exploit the processability of the polymer demonstrated before, while tailoring the degradation rate and controlling the pH environment thanks to the effect of embedded PG particles.

First, we need to identify formulations of biodegradable composites made up of a PLGA matrix loaded with absorbable phosphate glass (PG) particles compatible with the drawing process. Toward this goal, the rheological and viscoelastic properties of these composites in relation to the content and size of PG particles are studied. It is shown that the laser diffraction is the appropriate method for the measurement of size distribution of particles. Thanks to the ideal viscoelastic properties of these composites, fibers of phosphate glass (PG) and PLGA composites with good dispersion are thermally drawn. The degradation properties of the composites are studied through the pH and weight measurements and in parallel, the morphology of the degrading composite fiber with different PG content is analyzed during their degradation time. Lastly, multimaterial drug delivery fibers using the composites as the release barriers are fabricated. We elucidate the structure-function relationship of the composite barriers by correlating the macroscopic release data to their degradation behavior. Versatile release kinetics by the variation of PG content are obtained and the effect of thickness for each type of release kinetic is investigated. Moreover, the DMA measurement showed that the incorporation of PG particles in the PLGA fibers could reduce the shrinkage compared to pure PLGA fibers.

4.1 Rheology and viscoelastic characterization of PLGA/PG composites

Many properties in composite systems depend on the interaction between the polymer matrix and the fillers. Three types of interaction could be described: 1) when the filler is physically present in a non-polar polymer matrix with no interaction at all, 2) when there is an affinity between the polymer and filler and causes a friction during the movement, 3) when a chemical bond is created between the filler and the polymer matrix[148]. While in case 1 the filler could even weaken the matrix, in case 2 and 3 the filler has a

strengthening effect. Factors such as filler geometry, volume fraction, filler surface and wettability influence this interaction[148]. In our particular case, the nature of interaction between the PG particles and polymer matrix is analyzed through rheology and DMA analyses.

The main criteria for a compatible composite with the thermal drawing is to maintain a high viscosity at high temperatures, however incorporation of high content of fillers often stiffens the polymer or lead to the agglomeration of fillers at high temperatures. The proportion and size of the fillers are the two key parameters in controlling the flow of the composites at high temperature[149]–[151].While highly filled composite materials have attracted significant interest from industry in realizing targeted properties[151], the size of the particles could be manipulated in order to maintain processability of the original matrix. Therefore, in this work large particles with average size of 26 μm are utilized to have the minimal impact on the rheological property of the PLGA matrix.

The composites of various PG contents are fabricated and their rheological properties are investigated to verify their compatibility with the thermal drawing process. As can be seen in Figure 4.1, the complex viscosity of all contents of PG composites decreases smoothly with temperature, which is an essential criterion for the thermal drawing. As opposed to nano-fillers[149] which most of the time increase the viscosity of polymers, it is shown here that microscale fillers have almost no impact on the viscosity of polymers. Only by the incorporation of high content of the particles (40%) a slight increase of viscosity could be observed. This trend supports the previous claims where the interparticle interaction was seen in concentrations above (20% volume) for non-agglomerated large particles[152]. Such system can be considered as a suspension of rigid particles in the melt flow. As the size of the particles is larger than the polymer chains and comparable to the length scale of viscous forces[153], the response to the shear deformation is governed by hydrodynamic interaction[154] and not interparticle interaction[148].

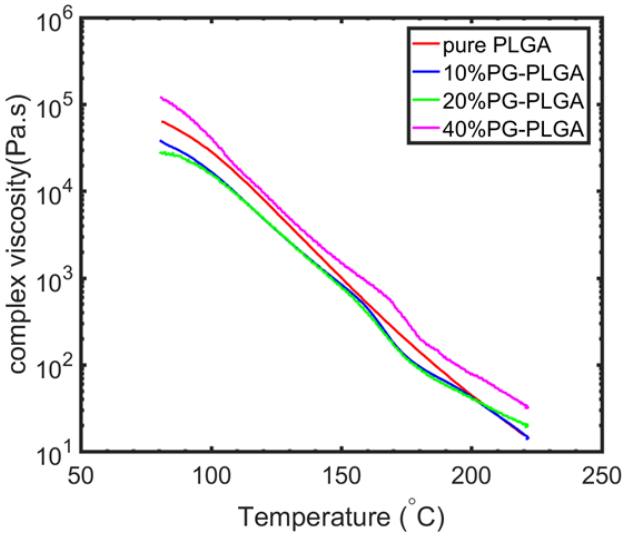

Figure 4.1. The complex viscosity of the pure PLGA and the composite films containing 10%, 20%, and 40% PG microparticles, measured in oscillatory shear rheology

In order to better understand the viscoelastic properties of these composites, dynamic mechanical analysis is performed on various contents of PG composites (Figure 4.2). Below the glass transition temperature, composites of higher PG content show higher storage modulus, which implies stronger intermolecular forces and a strengthening effect of the PG particles at lower temperature. However, this increase is relatively small for such high content of particles which is attributed to the high molecular weight of the PLGA matrix[151]. With the increase of temperature, the composites go through the glass transition temperature as reflected by a drop in storage modulus, and enter the rubbery plateau. In this region, the storage modulus is found to be very similar for composites of various PG content and again only a slight increase is observed for the composites of 40% and 20% PG. This small increase could be attributed to the slow dynamic of bound polymer layer around the particles[155], [156]. This trend confirms the results of complex viscosity obtained in oscillatory shear testing (Figure 4.1). Moreover, as the result of stronger intermolecular interaction, loss modulus and in turn the peak of tan delta decreases for higher content of PG (Figure 4.2b).

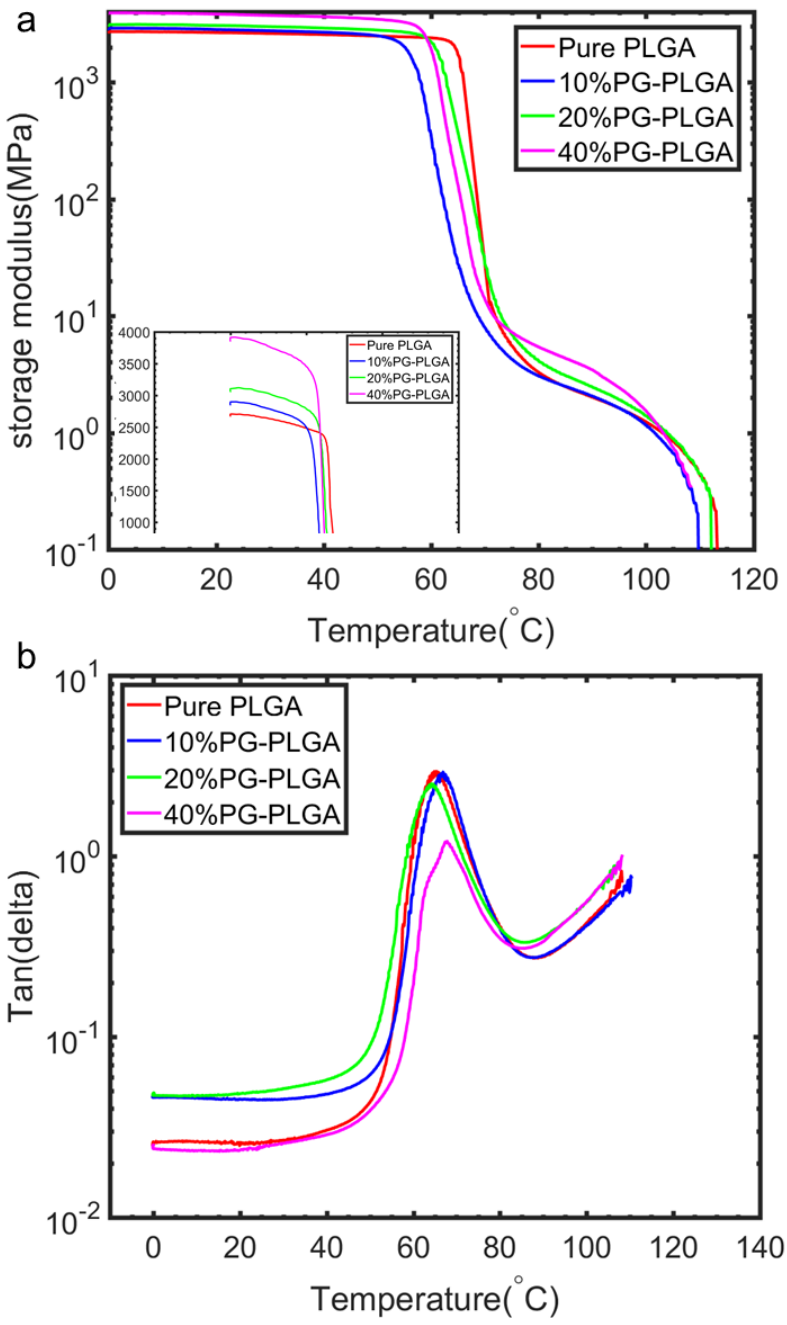

Figure 4.2. Comparison of the storage modulus and loss factor (Tan(delta)) of the pure PLGA and composite films containing 10%, 20%, and 40% PG microparticles

The close proximity of the complex viscosity and modulus over a temperature ramp for different compositions of PG-PLGA composites and the slow decrease of viscosity ensured the feasibility of the thermal drawing process. As the result, the two composites of 10% PG and 20% PG were successfully thermally drawn. Figure 4.3 shows the SEM images of the cross-sections of the two composite fibers in

rectangular geometry. As can be seen despite processing the composites with high content of particles at high temperature, the particles remained well-dispersed and the structure is well-maintained. Such high dispersion of the particles is attributed to zero interaction between the particles [8] and high viscosity of long PLGA chain, which prevented the movement of particles even at high temperatures.

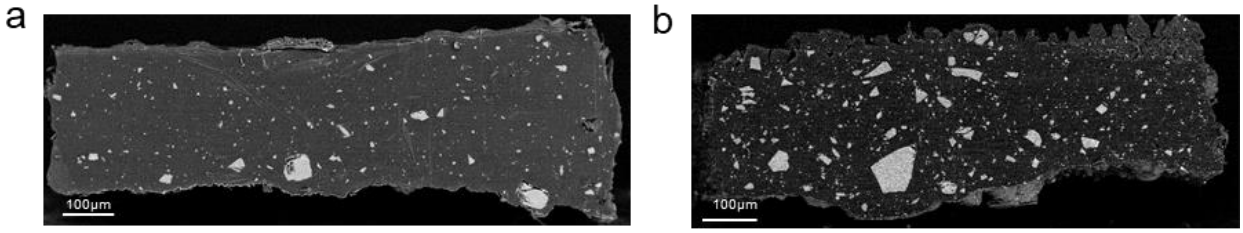

Figure 4.3. Backscattered electron SEM images of the two cross-sections of the composite fibers containing a) 10% and b) 20% PG microparticles after the thermal drawing

4.2 Particle size measurement

Due to the a priori large size of the particles, laser diffraction is the selected method for the particle size measurement. In this technique the particle size is estimated based on the intensity of the scattered light as a function of scattering angle using Mie theory. This is in contrast to dynamic light scattering (DLS) which is based on the Brownian motion and thus suitable for sub-micron particles[157]. Therefore, the ideal range of particles size in laser diffraction is between 50 nanometers to a few thousand microns[157]. In order to reduce multiple scattering of the light from the particles, a low concentration solution of PG particles (0.5g) was prepared in distilled water (40g). Prior to the measurement, 5 minutes of ultrasonication was done on the solution to ensure good dispersion of the particle without dissolving them. The results is presented below in Figure 4.4 and Table 4.1. It should be noted that the technique assumes that the particles have spherical shape so the measured sizes are overestimated. It is shown that 10% of the particles are below 4.89 µm, 50% below 26.92 µm and 90% below 117.39 µm. The results confirm the visual size distribution of particles seen in the SEM image of cross-section of 20% PG-PLGA fiber after the ultramicrothomy (Figure 4.5). The size of a few particles is above 100 microns and the majority of the particles size fall below 50 microns.

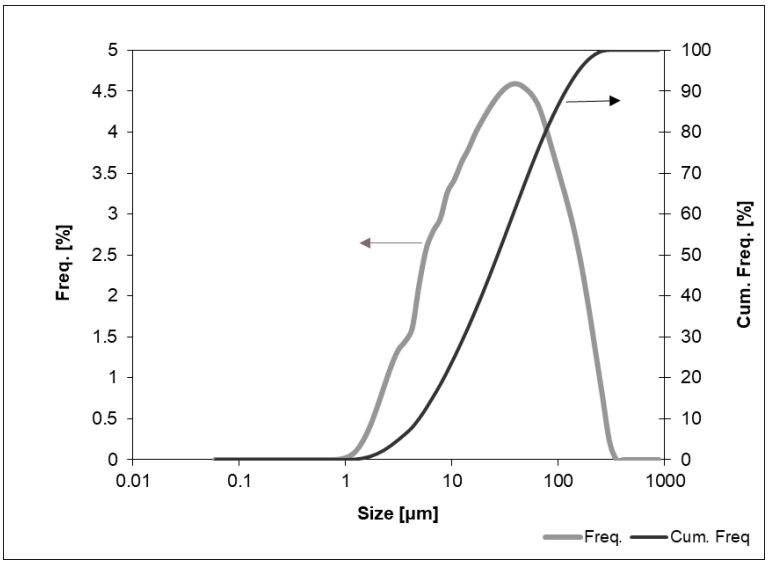

Figure 4.4. The size distribution of PG microparticles measured by laser diffraction

Volume Distributions	
Dv10	4.89µm
Dv50	26.92µm
Dv90	117.39µm

Table 4.1. The maximum particle size below which 10% (Dv10), 50% (Dv50) and 90% (Dv90) of the sample volume exists

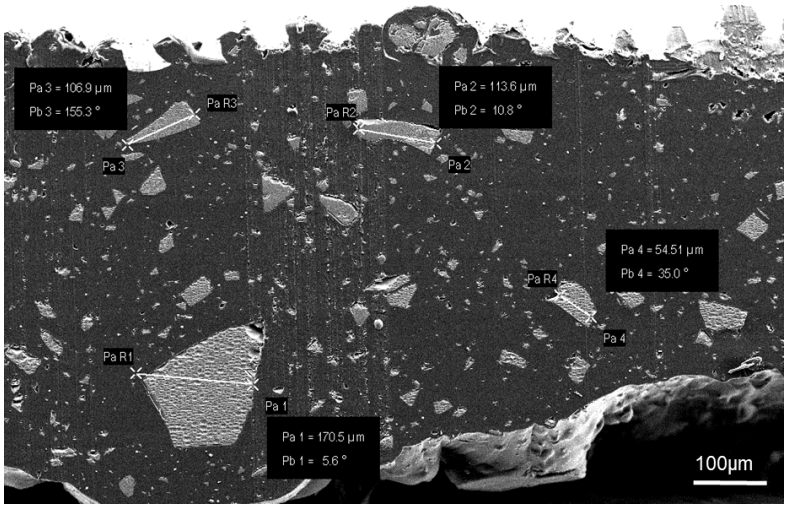

Figure 4.5. The cross-section of 20% PG-PLGA fibers showing the size of PG particles

4.3 Biodegradation characterization of the composites

Biodegradation study was performed on thin films of varying concentrations of PG particles, following a similar procedure as before. The results for pH and weight loss are shown in Figure 4.6a&b respectively. Degradation properties have been significantly changed by the addition of phosphate glass particles. Firstly, it can be noted that the pH drop has been nullified with all the composite cases. With only addition of 5% PG particles, the pH value could be altered to a neutral pH compared to pH 3 obtained in the degradation of PLGA matrix. The drop of pH indicates the release of acidic oligomers confirming the heterogeneous degradation mechanism, while the stable pH in composite films suggests the modification of the degradation mechanism to a more uniform and homogenous manner.

The changes in pH mirrors the changes in weight loss. The composite films go through two stages of degradation, one where the PG particles dissolves (the first drop in mass and pH) and the slower second drop attributed to the degradation of the PLGA matrix. The lack of a large drop in the PLGA matrix is due to the degradation of microparticles which creates a porous like structure in the system, thus decreasing the autocatalytic effect of PLGA[158]. At the same time, the porous structure provides a larger surface area which enhances the rate of biodegradation, as also shown in the work of Isobe[159]. This is a truly useful prospect which can be used for tailoring degradation rates for the PG/PLGA composite and thus a modified diffusion rate for drug delivery, as discussed later.

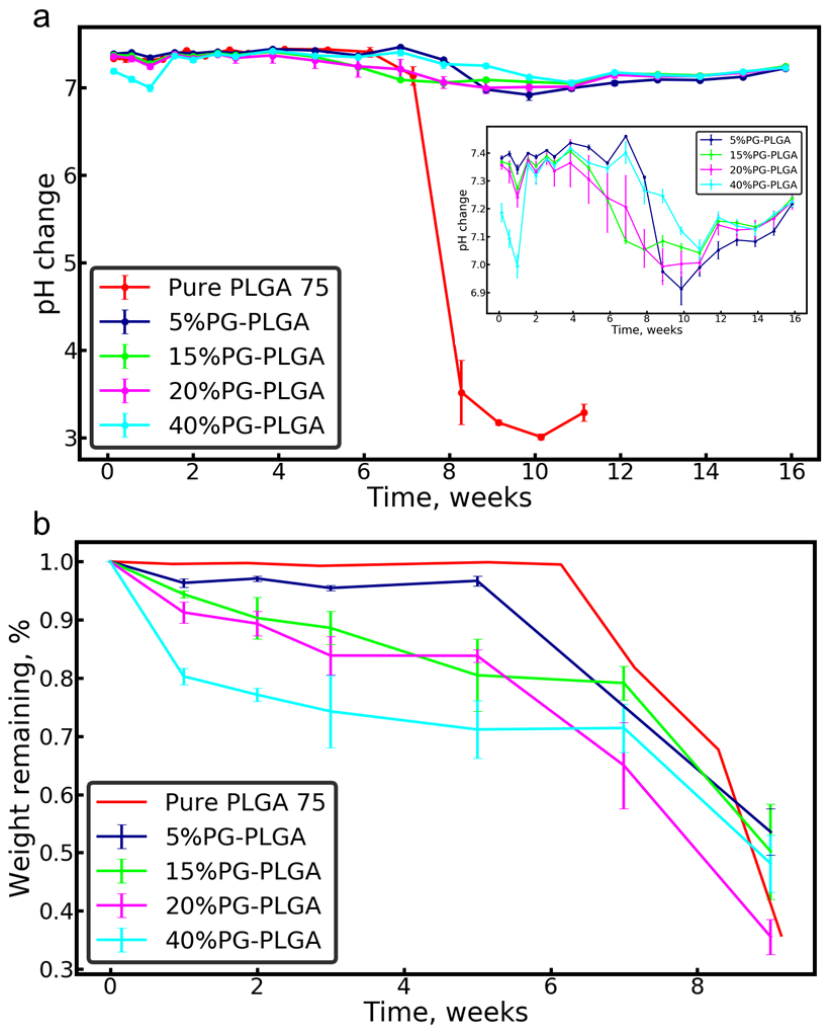

Figure 4.6. The degradation study of the composite films: a) pH measurement and b) weight loss measurement during the degradation period of pure PLGA and composite films containing 5%, 15%, 20%, and 40% PG microparticles

4.4 Evolution of morphology change of degrading composites

In order to elucidate the degradation behavior of the composite fibers, the morphology of the cross-section of the fibers for the two compositions of 10% and 20%PG were analyzed by scanning electron microscopy during the degradation period. It is found that the degradation of PG particles not only affects the overall degradation of the fiber structure, but also affects the degradation of polymer matrix. Different contents of PG showed this impact differently. As can be seen in Figure 4.7, the complete dissolution of PG particles occurred by week 2 where the pores and cavities are formed. At this stage, the polymer matrix is not affected by the PG dissolution and therefore a porous structure is created. Then, early dissolution of PG leads to

absorption of water in the polymer matrix which further accelerates the degradation of PLGA. This is indicative of the presence of bulk degradation even with the creation of pores. As can be seen in week 4 for the fiber containing 10% of PG microparticles, pores seem to be coalescing and getting closed up due to the higher mobility and solubility of created low MW PLGA and eventually on week 5, the number of pores dramatically reduces. The investigation of morphology was stopped after this stage due to the high degradation of PLGA which gave a jelly/gluey texture to the fiber.

Figure 4.7 shows the morphology change during the degradation of 20% PG-PLGA fibers. The dissolution of PG particles in 20% PG content is evident in the SEM images of week 1 and week 2 where the voids and pores are created. In this composition, in contrast with the unfolding of degradation of the 10% PG composition, the effect of PLGA degradation is not seen. On week 3, when the complete dissolution of PG occurs, the fiber loses its integrity and collapses, due to the high content of particles. Clearly, the parts of the fiber containing larger particle size is more prone to this collapse. At this stage, the PLGA is not fully degraded, and the loss of mechanical integrity is responsible for the collapse due to excessive porosity, rather than biodegradation mechanisms.

In order to confirm the leaching of the ions out of the fiber upon their dissolution, energy-dispersive X-ray spectroscopy was performed on the samples to map the different elements. Figure 4.8 shows mapping of phosphorous for the 10% PG-PLGA fibers during the degradation period. Clearly, the phosphorous is present at particle sites after the drawing. During their dissolution and pore creation, they start dissolving from the center of the cavities and remain in the surrounding of the inner wall of the pores. Finally, upon the closure of the pores from week 4, very little amount of phosphorous remains in the structure.

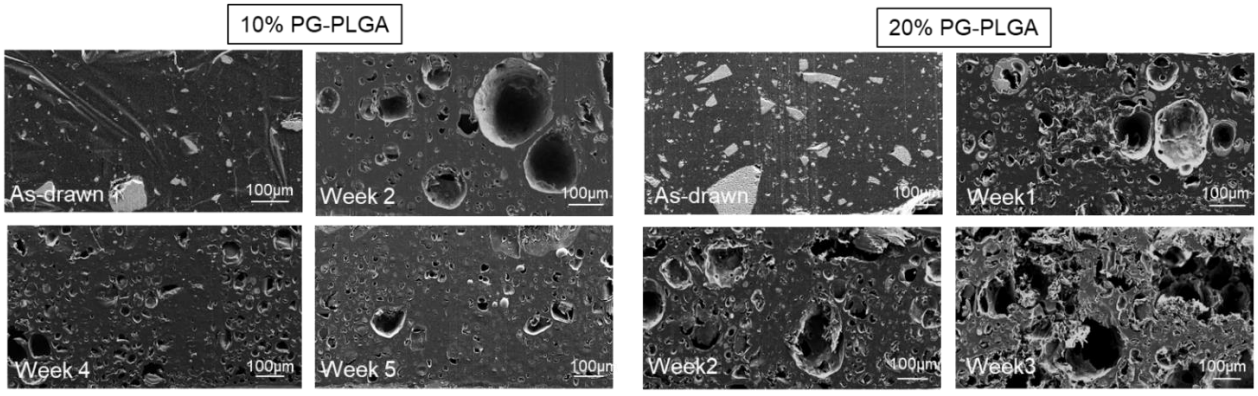

Figure 4.7. Secondary electron SEM images of cross-sections of the fibers containing 10% and 20% PG microparticles during their degradation period

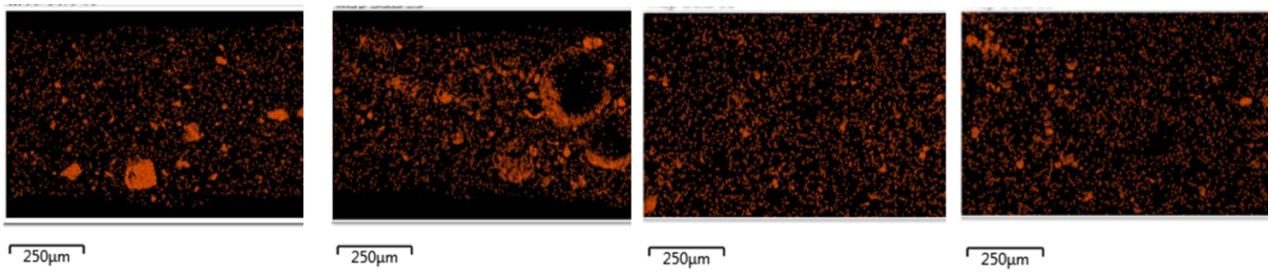

Figure 4.8. EDX images showing Phosphorous mapping of the cross -section of 10% PG/PLGA composite fiber at different stages of the degradation

4.5 Release kinetics shifts by composite barriers

In order to illustrate the tunability of release kinetics in complex structures, hybrid PMMA-PG/PLGA multimaterial drug delivery fibers are fabricated via thermal drawing, as illustrated in the schematic in Figure 4.9a. . PMMA is placed in the bulk to ensure the integrity of the fiber structure and a channel is inserted for drug encapsulation. The composite film is placed on top of the channels to serve as the release barrier. As can be seen in Figure 4.9b, the structure of the fiber is well preserved and the composite film kept its shape with minimal deformation. This structure was obtained for composites of 10% PG content. The fibers were injected with a hydrophilic macromolecule drug model, Fluorescein isothiocyanate (FITC) labeled dextran, FD70, and fluorescence spectroscopy measurements were performed at prescribed times.

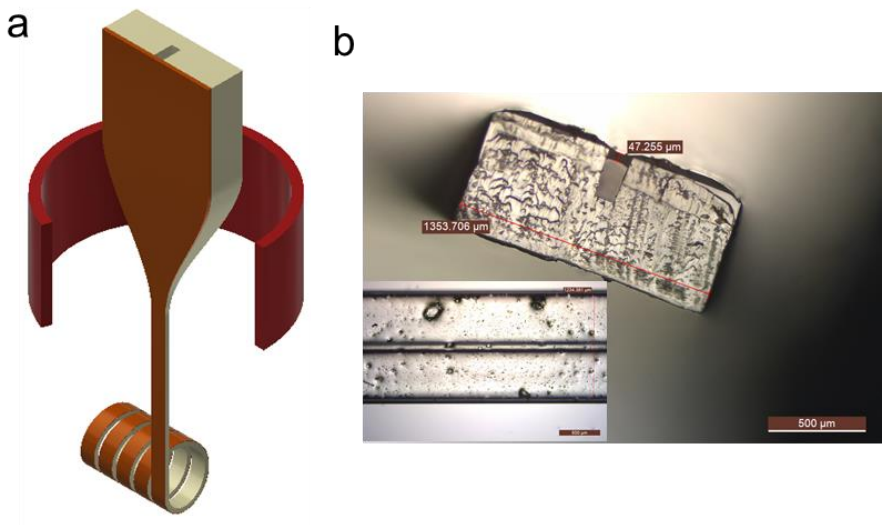

Figure 4.9. Multimaterial drug delivery fiber obtained by the thermal drawing, a) The schematic of thermal drawing of PMMA-PLGA/PG fiber, and b) the optical microscopy image of cross-sectional and top view of the corresponding fiber after the drawing process

Interestingly, the desired release profile could be engineered by adjusting the content of PG particles within the composite matrix. Figure 4.10 shows the release profiles obtained from PMMA/PLGA and PMMA/PG-PLGA fibers of 15%, 20%, and 40% PG composite barriers. A sustained release profile was obtained for all the fibers. As it has been demonstrated in the chapter 2, the release profiles consists of two phases governing by two mechanisms: 1) slow release due to diffusion through degrading polymer chains, 2) fast release due to diffusion through created pores upon degradation[50], [160]. By incorporating PG particles in the PLGA film, not only could we accelerate the release but also modify the nature of the release kinetics. By increasing the PG content, the release profiles deviate from degradation-controlled mechanism evident in the sigmoidal profile of pure PLGA to diffusion-controlled mechanism evident in the exponentially decreasing release profile[161] of 40% PG composite. The sigmoidal profile of pure PLGA is described by a diffusion phase up to day 65 followed by a fast release phase due to the degradation of PLGA. However, when incorporating 15% PG particles, the diffusion phase is accelerated and the fast release phase is decelerated, resembling a zero order release profile. The deceleration of this phase is due to the presence of a high number of cavities and pores, which provide an increased number of diffusion pathways for the acidic oligomer to exit out of the film. This subsequently suppresses the bulk degradation of PLGA. It should be indicated that such linear release profiles have been the target of many research work since it allows the administration of the drug in a sustained and constant manner over a long period. Based on the obtained release profiles, it can be concluded that the rate of PLGA degradation plays an important role in defining the shape of release profiles of pure PLGA and 15% PG-PLGA composites.

The release profiles of both 20% and 40% PG composites resemble the first order release kinetics which is diffusion-controlled and its rate depends on the concentration of encapsulated drug [162]. The release profile of 40% PG composites is characterized by a sharp increase up to week 3 after which the release starts to slow down significantly. This interval of the sharp release coincides well with the expected duration of PG particle dissolution in the previous study[84] as well as the timeline of PG dissolution in SEM analysis of 10% and 20% PG-PLGA composites (Figure 4.7). The slow release from week 3 onwards in 20% and more clearly in 40% can be explained by the tortuosity of new diffusion pathways which slow down the drug transport[161]. Therefore, it is shown that the first steep release phase depends on the PG dissolution rate and the second slow phase on the PLGA degradation rate.

Moreover, it is shown that the film thickness can have different effects on the release rate depending on the nature of the release kinetics. Faster degradation of thicker films in pure PLGA is known to be due to the bulk degradation effect[163], [164]. Here, 15% PG composite film with relatively linear release profile also exhibited faster degradation rate for thicker films, which confirms the important influence of PLGA degradation in this composition. However, as it can be seen, this difference is very small, whereas a large difference in release rate was observed for pure PLGA with just a few micron variation in thickness[165], [166]. In contrast, for 40% PG composite film with diffusion-controlled release kinetics, thinner films exhibited faster release. This is attributed to the presence of short diffusion pathways that facilitate drug transport.

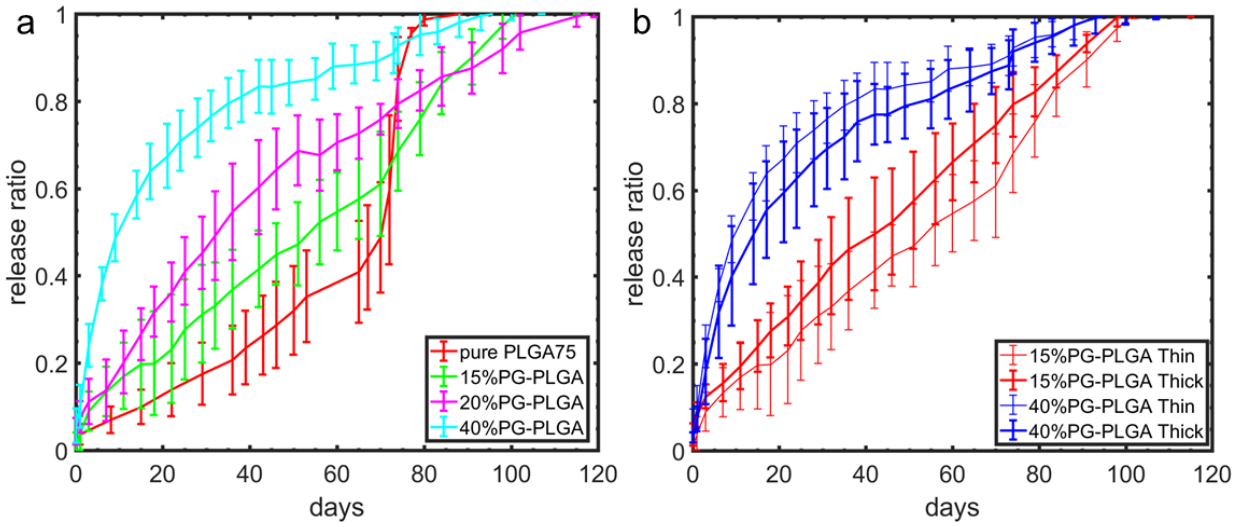

Figure 4.10. Cumulative release profile of FD70 from PMMA-PLGA/PG fibers from the release barriers of a) pure PLGA and composites films containing 15%, 20%, and 40% PG microparticles, b) composite films of 15% and 40% in two thicknesses of thin (70µm) and thick (100µm)

4.6 Improvement of the shrinkage property of fibers by composites

As discussed in chapter 3, the shrinkage of polymer is a common problem in the processing techniques which induces chain alignment such as cold drawing[167] and electrospinning[168]. The incorporation of fillers inside the polymer matrix is an effective method to prevent or reduce this shrinkage[169]–[171]. During thermal drawing, fibers go through a high stress and therefore polymer chains are highly aligned. It was shown in chapter 3 that a heat treatment procedure around the glass transition temperature over a long period of time is effective in relaxing the frozen stress. To evaluate the effect of the PG particles, two batches of fibers composed of purely PLGA and 20% PG-PLGA were drawn at a same drawing stress, and the heat treatment was done at 50°C for 1 day and subsequently at 60°C for 2 days. In order to compare the built-in stress of the two batches, dynamic mechanical analysis (DMA) was performed. The test measured the shrinkage strain of all fibers before and after the heat treatment under a fixed force over a temperature ramp. The results are shown below in Figure 4.11. As can be seen, all the fibers started to show a change in their length at 62°C, a temperature around the T_g of PLGA. Both types of freshly drawn fibers exhibited significant shrinkage due to the alignment of polymer chains during the drawing, however this shrinkage is more pronounced for the pure PLGA fibers (61%) compared to 20% PG-PLGA fibers (47%). This shows the inhibiting effect of the particles on the movement of polymer chains to get aligned. Even though the two types were drawn at the same drawing stress, the induced residual stress in PLGA matrix is less for the composite fibers than the pure PLGA fibers. After the heat treatment procedure, the two fibers exhibited

less deformation, yet it can be observed that the heat treatment has a much stronger impact on the composite fiber, to the extent that the shrinkage is almost completely removed and the fiber even starts to thermally expand upon further increase of the temperature. This is while the shrinkage of pure PLGA fibers could be reduced to 26%.

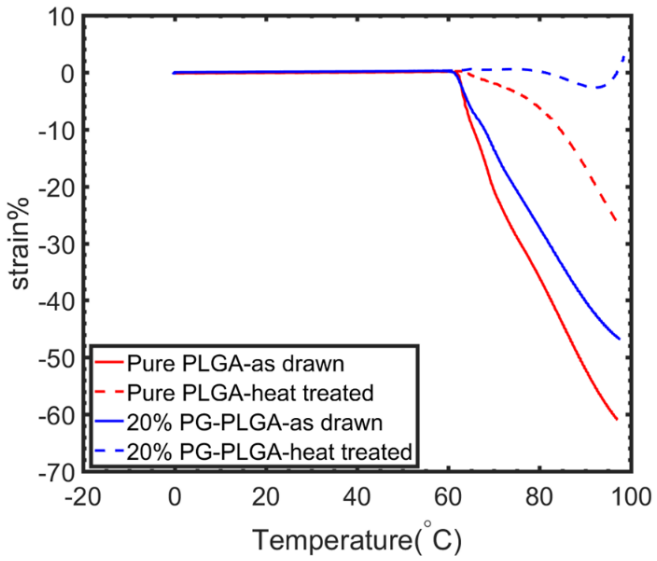

Figure 4.11. DMA-fixed force analysis showing the shrinkage behavior of pure PLGA and 20% PG-PLGA composite fibers when they are as-drawn and heat-treated

4.7 Experimental

Composite fabrication: Poly(DL-lactic-co-glycolic acid) (PLGA) of ratio 75:25 (Purasorb PDLG 7507, Corbion Purac, Amsterdam, Netherlands) was used in this study. Phosphate glass micro-particles were synthesized with conventional melt-quenching method (nominal glass composition is (in mol%) 50% - P_2O_5, 23% - MgO, 11.5% - Na_2O, 10% - CaO, 3% - SiO_2 and 2.5% - B_2O_3) [1], and then milled into a fine powder, around 26 µm average size. Solvent for PLGA was dichloromethane with 99.9% purity (Sigma-Aldrich, St. Louis, Missouri, USA).

Varying compositions of the composite films for fiber drawing were fabricated using the solvent casting procedure. A 10% by weight solution with a range of PLGA75 (75% lactide and 25% glycolide) and phosphate glass mixtures (5, 10, 20 and 40% phosphate glass with PLGA) were dissolved in DCM (dichloromethane). The solution was mixed for 1 hour on a magnetic stirrer as well as sonicated for 10 more minutes, until all ingredients had homogeneously blended together. The solution was then homogeneously spread onto a Teflon film, at about a 150µm thickness. DCM was let to evaporate under a fume hood for

24h in room temperature, after which it was put into a 60°C oven for 24 more hours for complete removal of DCM.

Oscillatory shear rheology: Oscillatory shear testing was done to measure the complex viscosity of composites and to compare with that of pure PLGA. The measurement was done by a AR 2000ex series rheometer, TA Instruments, New Castle, USA with geometry 25mm Aluminum parallel plate. The temperature ramp was set over 30°C to 220°C with the ramp rate of 5°C/min, the fixed frequency of 1 Hz and strain of 1%.

Dynamic mechanical analysis: The viscoelastic response of composites was measured with the clamp for tension of rectangular films. The measurement was done in the module of multi-frequency-strain in the temperature range of 0°C to 120°C with heating ramp of 3°C/min. The static force was set at 0.01 N, frequency at 1 Hz and oscillatory strain at 0.01%.

The shrinkage tests on the pure and composite PLGA fibers were performed in the module for controlled force with the clamp for tension of films. The measurement was done in the temperature ramp from 0°C to 100°C with heating rate of 3°C/min. The static force was set at 0.001 N to just provide a sufficient force to hold the sample.

*Preform fabrication***:**

1) PG/PLGA-PMMA preforms: two PMMA plates of 5.8mm were hot-pressed (Lauffer Pressen UVL 5.0) together at 130°C, 10 Ncm^{-2} for 20 min to obtain a thicker plate with dimensions of 2.4 cm width 1.12 cm thickness and 16 cm length. A groove of 4 mm depth and 2 mm width was milled along the preform. The PG/PLGA composite films were hot-pressed together at 100°C, 7 Ncm^{-2}, for 20 min to obtain a plate of desired thickness of about 0.8 mm. The PLGA film and PMMA plate were hot-pressed at 90°C and 5 Ncm^{-2} with presence of a Teflon bar in the channel to prevent the deformation of PLGA film.
2) PG/PLGA preforms: The PG/PLGA composite films were hot-pressed together at 100°C, 7 Ncm^{-2}, for 30 min to obtain a plate of desired dimensions of 2x2 mm.

Thermal drawing process: The preforms were drawn with a custom draw tower consisting of a three-zone furnace, with a thermostat in each zone. The temperatures set for the PG/PLGAPMMA preforms were 100-260-90°C. The PG/PLGA preforms were drawn at 70-135-50°C temperatures.

pH measurement and weight measurement: The thin films (prepared in section 1) were cut into 2x2cm large squares with 150µm thickness. All the weights for the films were measured separately and they were placed into a phosphate buffered saline solution (PBS) with 7.4pH. The PBS medium was changed weekly to represent the ever changing and balancing environment of a live system. Twice every week for the first

three weeks and then once a week the pH was measured to determine the pH change as a function of time and degradation. Weight measurements were carried out weekly, the thin composite film was removed from the PBS medium, dried at room temperature at atmospheric conditions and weighted.

Scanning mechanical analysis: The morphology of the thermally drawn fibers was examined under SEM to verify the dispersion of the particles. The cross-sections of the fibers were prepared by ultramicrothomy and were coated with a 10-15nm of carbon. The secondary electron detector was used in order to analyze the topography of the samples, and the backscattered electron detector (VP BSD1) was used to analyze the distribution of particles by the chemical contrast. The tension was 10 kV and the aperture size was 60 µm.

EDX: In order to map the distribution of the elements in the cross section of the fibers at different stage of the degradation, energy-dispersive X-ray spectroscopy was performed on the sample. The same fibers analyzed in other SEM detectors were used for Carbon was chosen as the coating as it is a light element and allows the EDX measurements. The EHT was set at 7.5 kV as Ca has the highest energy among the present elements in the particle. The gun mode was changed to analytical and the current was set to 800 pA to prevent charging of the samples.

Release study of the drug delivery fibers: Thermally drawn fibers with the of PMMA-PLGA/PG compositions, were cut into 3 mm long pieces, with two different PG/PLGA thicknesses about 70 and 100 µm. 15, 20 and 40% compositions, each with 12 samples (6 thin, 6 thick) were filled with fluorescent dye (Fluorescein isothiocyanate-dextran, Sigma Aldrich, St. Louis Missouri, USA, average molecular weight 70000 g/mol) and the sides were glued with epoxy resin glue. The fibers were placed in 4ml of PBS solution. Twice per week the solution was measured with a luminescence spectrometer (LS 50B, Perkin Elmer, Waltham, Massachusetts, USA) with the excitation wavelength of 493nm and slit length of 9. The PBS solution changed after each measurement.

4.8 Summary and Conclusion

Biocomposites composed of PLGA polymer and phosphate glass particles are developed which are compatible with the thermal drawing process. The cumulative degradation properties of the PLGA and PG resulted in favorable release properties. The structure-function relationship of the fibers was elucidated through the analysis of their morphology during the degradation. Such facile method of tailoring the release kinetics over a large span of rates and timescale could be highly advantageous in pharmaceutical applications. Moreover, the little influence of the PG particles on the viscoelastic properties of high molecular weight pure thermoplastics, enables to apply a variety of drawing conditions to reach similarly complex structures as demonstrated before. In future studies however, the impact of the release of metallic

ions in the surrounding biological environment should be investigated as the biocompatibility and toxicity of the recently developed biomaterials has yet to be established.

Chapter 5 Heat-triggered release in fibers

In this final chapter, we propose a configuration for a multi-material fiber capable of control release on-demand via an external stimulus. We chose to present preliminary results using joule heating, via passing a current through embedded metallic electrodes, as a proof of concept for this paradigm. Temperature is indeed an effective stimuli used to induce release in different drug delivery systems. In order to be able to engineer such devices, it is crucial to first understand the effect of temperature on the biodegradation kinetics and to couple it with the release kinetics. While the effect of temperature on the degradation of PLGA has been widely studied[172], [173], its impact on the release kinetics could differ significantly depending on the formulation[174], [175]. The dependence of degradation reaction to temperature can be described using the Arrhenius equation[172]:

$$k = A \cdot exp\left(-{}^{E_a}/_{RT}\right) \quad (5.1)$$

Where k, T and E_a are the reaction rate constant, temperature, and the activation energy, respectively. A is a constant and R is the universal gas constant.

We performed this study over a wide range of temperatures to fully understand the release mechanism. Moreover, since PLGA degradation differs significantly below and above its glass transition temperature (T_g)[172], this behavior can be manifested differently in their release profiles. Above T_g, amorphous polymers transform from the glassy state to rubbery state, therefore it could be expected that the release mechanism would be governed by the increase in the mobility of polymer chains and thus by diffusion.

In this part, the release profiles of PLGA drug delivery fibers degraded at different temperatures were measured. Simultaneously, the T_g of thermally drawn PLGAs during the degradation was measured at various times. The results of the two measurements are correlated and the underlying mechanism for the release and degradation at elevated temperatures are elucidated. After this first study, our ultimate objective is to fabricate electrically active drug delivery fibers which respond to an electrical input inducing a joule effect and an increase of temperature. The generation of heat via electric current could however introduce different effects from the ones induced by heating in an oven. An oven induces the heat more uniformly and externally while the electrodes are in direct contact with PLGA and could generate heat internally, locally and rapidly[176]. Moreover, it has been demonstrated that the presence of an electric field could cause different behaviors in the materials such as electroporation[176] and mechanical deformation[177]. Therefore, we aim to investigate the presence of these effects in our fibers and their possible impact on the release. The fabrication procedure of such fibers containing electrodes, a drug reservoir and the PLGA release barrier in polymeric matrix is demonstrated. As a first step the challenges with the fabrication process

will be discussed. Next, it will be shown that steady temperature could be achieved in the fibers by the application of different voltages, and finally the release study is performed upon the application of current for 30 minutes.

5.1 The Effect of Temperature on the release kinetics

PMMA-PLGA50 and PMMA-PLGA75 fibers were injected with FD70 and their release behavior was studied at different temperatures in an oven. In parallel, the degradation mechanism was explored using differential scanning calorimetry (DSC). The architecture is the same as initial fibers used in chapter 3 to characterize thermally drawn PLGA films. The thickness of PLGA75 is about 70µm and PLGA50 about 55µm.

The cross-section of PMMA-PLGA50 fibers and the corresponding release profiles at 37, 42, 50 and 60°C are shown in Figure 5.1. The T_g of PLGA50 and PLGA75 after thermal drawing are 56 and 60°C, respectively. Therefore, we chose four temperatures that lie under, at and above the T_g values of the investigated polymers. The release profiles maintained their characteristic sigmoidal shape at all temperatures which include a diffusion-controlled phase and an erosion-controlled phase. This is in contrast to the previous studies on other formats of PLGA delivery systems where the disappearance of the diffusion phase at elevated temperatures was reported[174]. The rate of diffusion phase seems to be increasing with the increase of temperature at 37, 42, and 50°C, however at 60°C, this rate seems to be diminishing. Looking at the SEM images of the PLGA50 after 3 days of degradation at the three temperatures of 42, 50, and 60°C (Figure 5.1c), fewer number of pores at 60°C is formed. This observation explains the slower rate of diffusion phase at 60°C which is in contrary to our initial assumption regarding the enhanced diffusion at higher temperature. As a matter of fact, the onset of fast release phase is shifted to earlier times occurring on day 16, 7, 6, and 2 at 37, 42, 50 and 60°C respectively, indicating the pronounced effect of temperature on the PLGA degradation. In particular, at 60°C, the PLGA degrades much faster than the characteristic diffusion time. As the fast release phase reflects the erosion in PLGA film, the significant acceleration of the degradation at elevated temperature is confirmed.

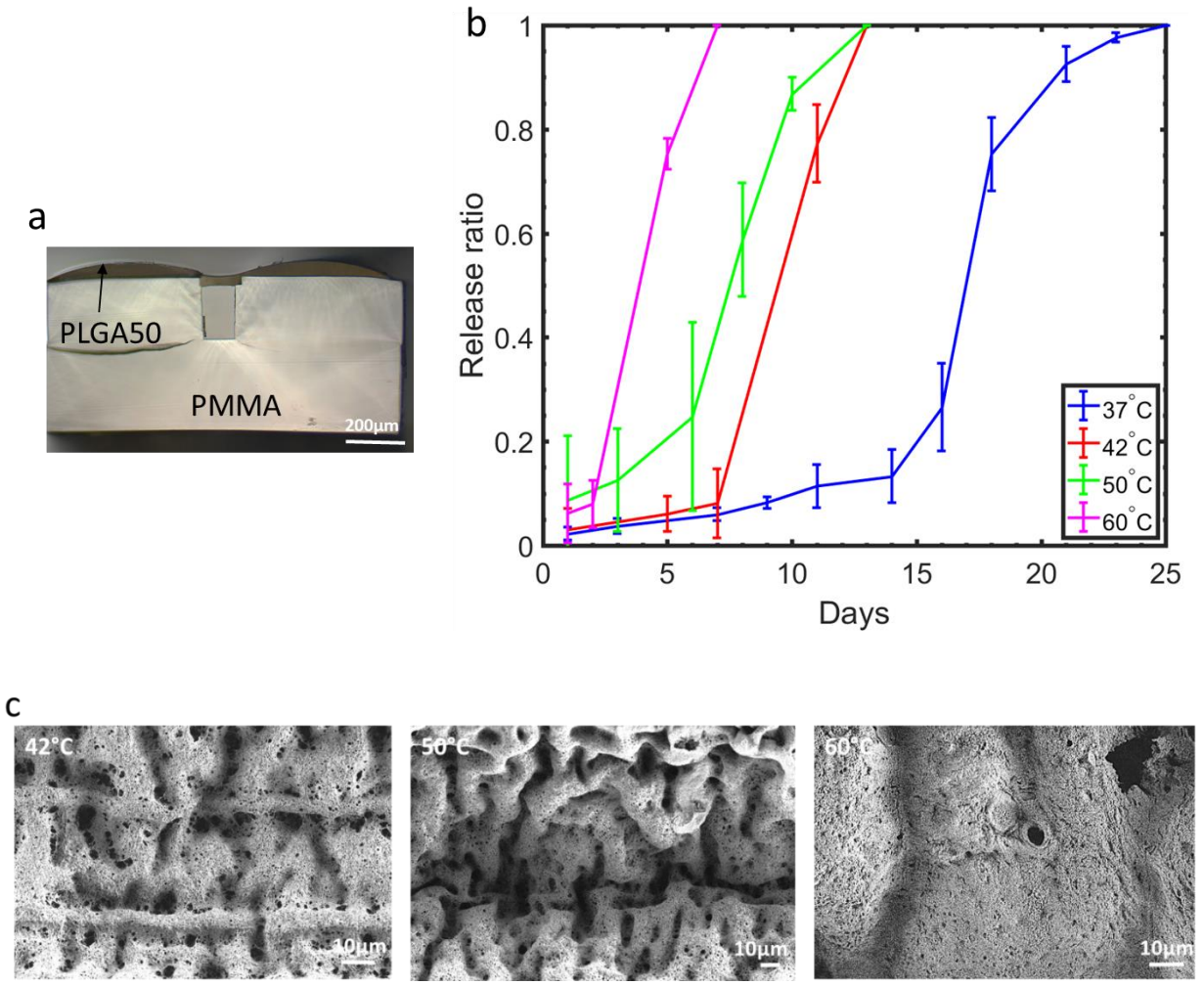

Figure 5.1. Effect of the temperature on the release property of PLGA50 barrier, a) Cross-section of PMMA-PLGA50 drug delivery fiber, b) The obtained release profiles from the corresponding fibers at 37, 42, 50 and 60°C, c) SEM images of PLGA50 after 3 days of degradation at 42, 50, and 60°C

Figure 5.2 shows the cross section of PMMA-PLGA75 fibers with their release profiles at two temperatures of 37 and 50°C. The release profile is again characterized with a biphasic profile at the two temperatures. As can be seen the total release timeline was reduced to 35 days at 50°C compared to 88 days at 37°C. This reduction is due to the higher diffusion rate in the slow release phase as well as the earlier start of the fast release phase. However, the slope of fast release phase appears to be similar in both cases. This similarity could be explained by the degradation mechanism, which is governed by a rupture in the film, thus providing the same release pathway in both cases.

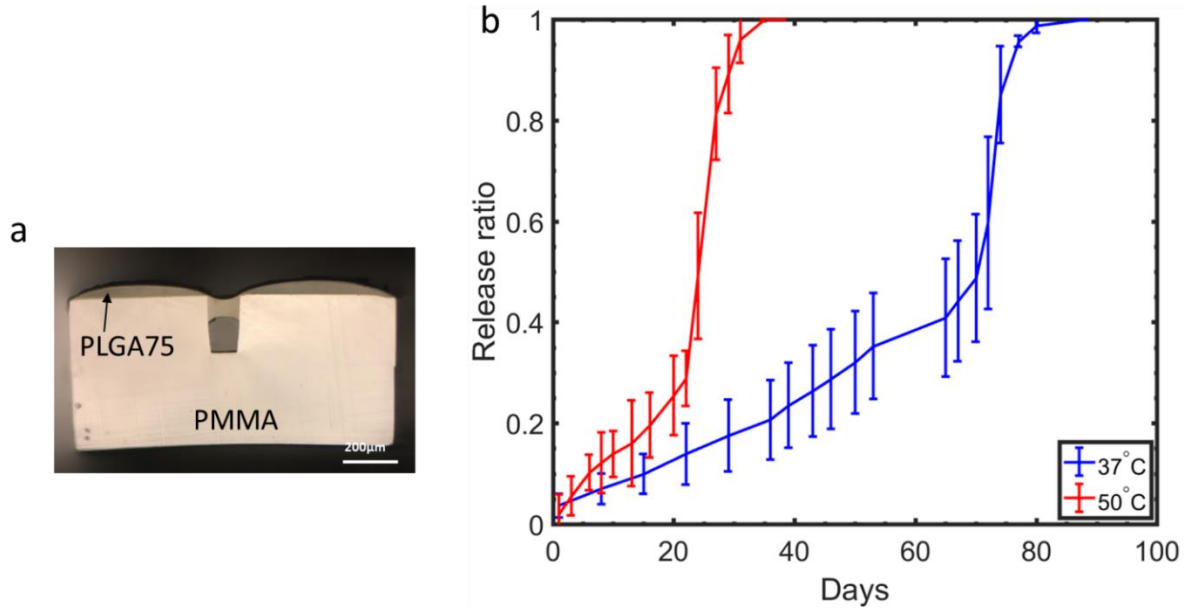

Figure 5.2. Effect of the temperature on the release property of PLGA75 barrier, a) Cross-section of PMMA-PLGA75 drug delivery fiber, b) The obtained release profiles at 37 and 50 °C

5.2 Effect of temperature on the biodegradation kinetics

Differential scanning calorimetry(DSC) was performed on PMMA-PLGA fibers at predetermined times and the T_g of PLGA was extracted at each measurement time during its degradation period. The obtained thermal graphs contained two glass transition temperatures for both PLGA and PMMA. Figure 5.3 shows the obtained DSC curves for PLGA50 at different degradation times. As can be seen, the glass transition of PLGA does not appear as a smooth step but is accompanied with a small deep, which reflects the thermal history of PLGA explained in chapter 2. The measurements were stopped when no sign of glass transition appeared for PLGA, this was assumed to indicate full degradation and dissolution of PLGA chains.

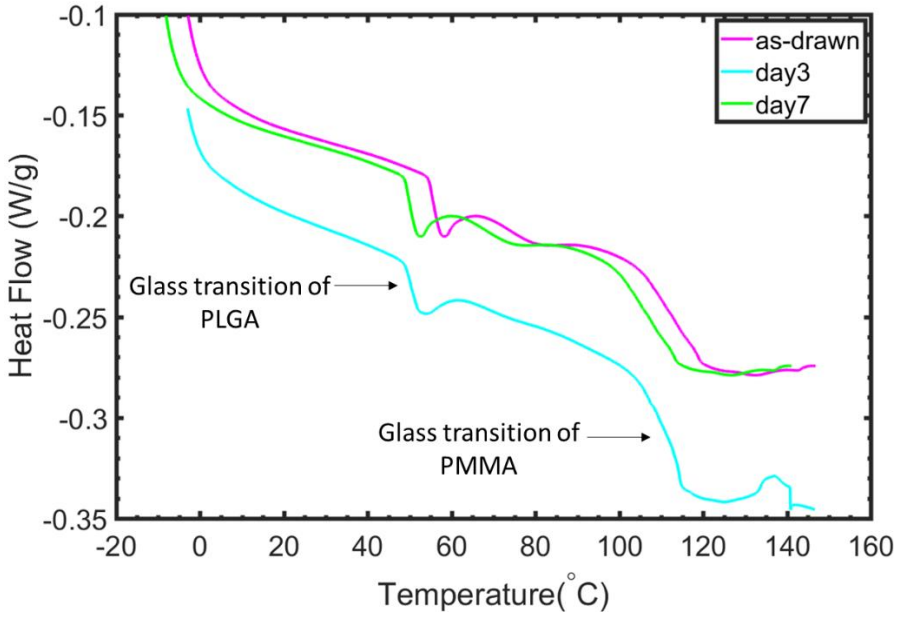

Figure 5.3. DSC curves of PMMA-PLGA50 fibers at different times during the degradation period of PLGA50 at 50°C

The extracted T_g values with respect to the degradation time were plotted for PLGA50 and PLGA75 at different temperatures (Figure 5.4). Just shortly after the incubation in PBS, the T_g values dropped for all the cases, however unexpectedly, the T_g values started to increase again. Such a trend could be attributed to the heterogeneous degradation of PLGA. As T_g has a direct relation with the molecular weight and represents the increased mobility of polymer chains, the lower molecular weight polymers possess lower T_g. The initial drop of T_g is correlated with the PLGA chain scission by hydrolysis. Due to the autocatalytic effect, the bulk of PLGA experiences a more rapid chain scission. When the degradation is advanced enough, the molecular weight becomes small enough to be soluble in water and to diffuse out of the PLGA film, thus leaving behind higher MW chains which leads to the increase of T_g again. This result is consistent with the work of Vey et al.[173] where they observed sudden release of acidic degradation products through pH, T_g and MW measurements. Another explanation that can be proposed [173] for such trend is the preferential degradation of glycolic unit which results in the enrichment of lactic content in the later stage of degradation and thus the increase of T_g.

The onset of the increase of T_g for PLGA50 at 42, 50, and 60°C in Figure 5.4 infers the earlier release of acidic oligomers at higher temperatures. For PLGA75 degraded at 50°C, the T_g first drops sharply, and then the rate gets slower until the T_g experiences a sharper decrease and consecutive increase. The presence of different rates in the drop of T_g in correlation with the degradation mechanism should be further explored. However, the immediate drop of T_g in PLGA75 could be explained by the plasticizing effect of PBS at 37°C

which causes a change in conformational behavior of the polymer and thus higher chain mobility. This decrease is not attributed to the PLGA chain scission since the T_g values after the day 2 do not show the same decreasing rate. This observation aligns well with a degradation study on PLGA95[173], a polymer with a slow degradation rate, where no reduction of MW was observed upon the decrease of T_g.

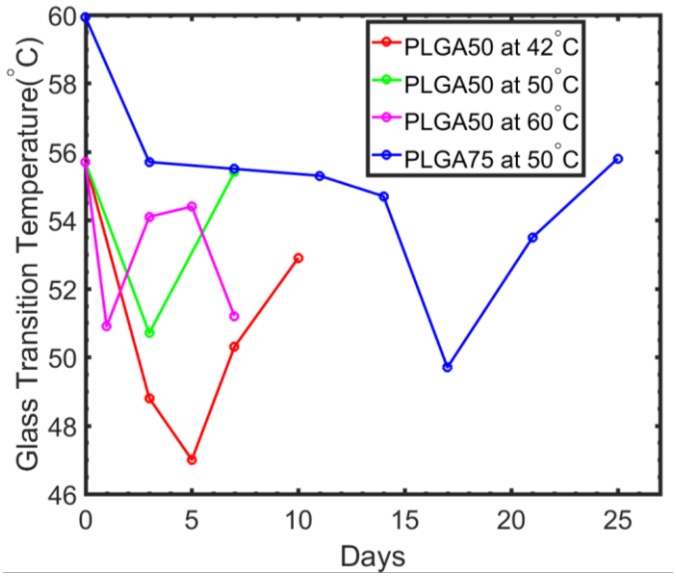

Figure 5.4. The trend of measured T_g during the degradation period of PLGA50 at 42, 50, 60°C and PLGA75 at 50°C

5.3 Coupling the degradation and release kinetics

The obtained trend of T_g values throughout the degradation period not only confirmed the heterogeneous degradation in PLGA films but also elucidated the underlying release mechanism. The clear decrease and increase of T_g represent the sudden release of acidic oligomers. Figure 5.5a&b show the correlation seen in the trend of T_g values and the cumulative release curves for PLGA50 at 42, 50, and 60°C and PLGA75 at 50°C. As can be seen, interestingly, the increase in T_g values occurs at the same time as the onset of the fast release phase for all the cases. It means that the created pathway for the release of acidic oligomers allowed the release of FD70 which led to a faster release rate. Another implication is that a certain amount of hydrophilic FD70 was trapped in the bulk of PLGA on the site of autocatalysis, which was released with the acidic oligomers. Any interaction between FD70 and the acidic PLGA should be further investigated as the degradative effect of some drug types on PLGA degradation has been reported[175].

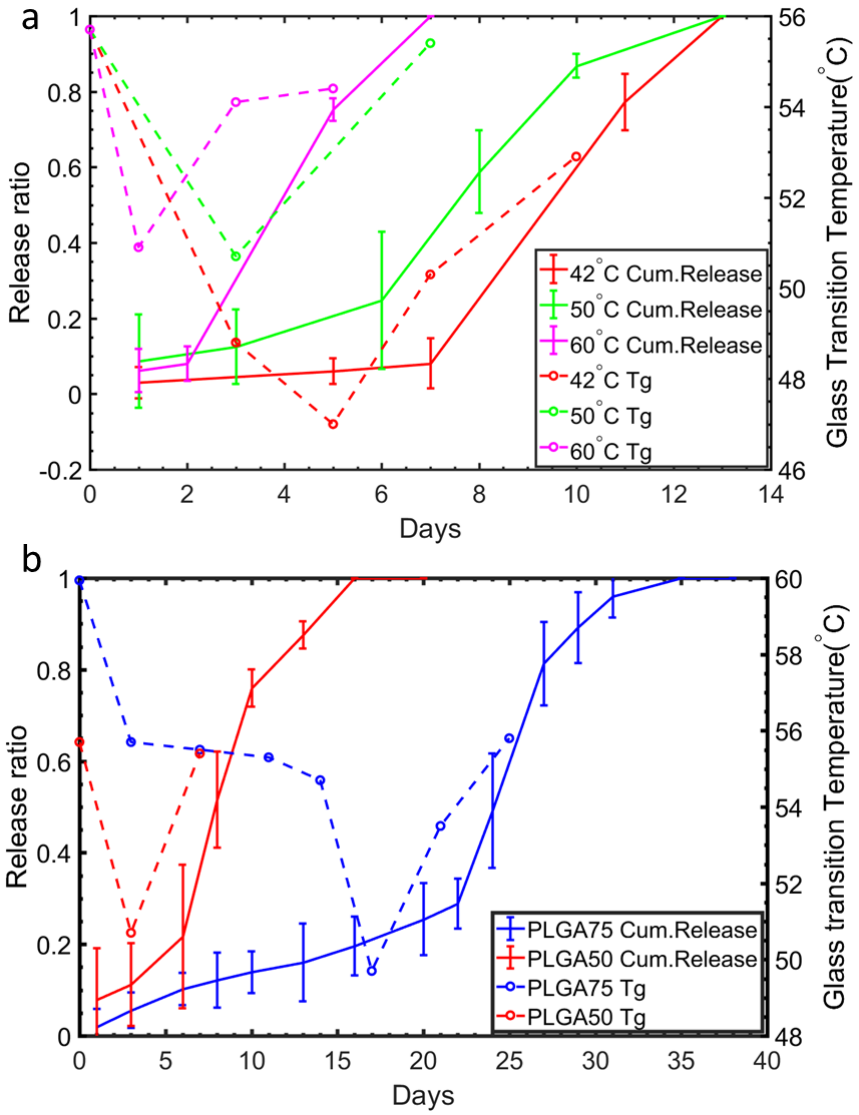

Figure 5.5. The correlation of T_g values with the release kinetics of a) PMMA-PLGA50 fibers at 42,50, and 60°C, b) PMMA-PLGA50 and PMMA-PLGA75 at 50°C

5.4 Fabrication of electrically active drug delivery fibers

After investigating the behavior of degradation at higher temperatures, we turn to the fabrication of electrically active biodegradable fibers. We chose stainless steel wires as the material for the electrodes because they have a high conductivity and are biocompatible. Two stainless steel wires are integrated inside the fiber through wire feeding, or convergence drawing[27], [178], via two wheels on top of the drawing tower. To do so, two hollow channels are milled inside the PMMA plate and the wires are fed inside them (Figure 5.6). With the right drawing speed, the dimensions of the channel are set be reduced to match the

dimension of the wires. If the milled channel has a diameter of 1.5mm and the wires 0.08mm, the draw-down ratio should be 18.75. The drawing speed with the fixed feeding speed of 1 mm/min is calculated based on this equation:

$$D^2 = \frac{V_F}{V_D} \quad (5.2)$$

Where D is the draw-down ratio, V_F is the feeding speed and V_D, the drawing speed. Based on this formula, the drawing speed was set at 0.35 m/min. Upon softening the preform at this drawing speed, the wires are encapsulated inside the channels and pulled with the drawing.

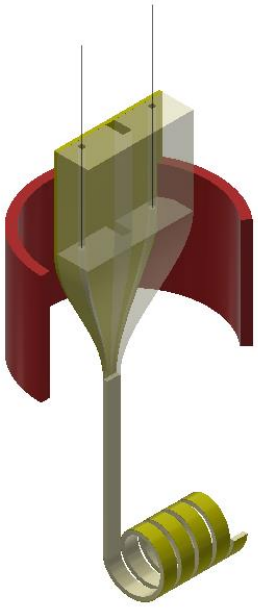

Figure 5.6 . Schematic of thermal drawing of electrically active fibers with wire feeding

Figure 5.7 shows the schematics of cross-sections of the attempted fibers and their obtained structure after thermal drawing. In Figure 5.7a, a PMMA with a MW lower than that of the bulk PMMA plate is employed to seal the inserted channels. However, as shown, this design led to the complete break-up of both PLGA film and low MW PMMA film. This is because the low MW PLGA had a very low viscosity at the drawing temperature and due to the high surface tension with the low MW PMMA, both dewetted significantly on the surface of the PMMA plate and formed a droplet-shape. To overcome this problem, the low MW PMMA is replaced by a higher MW grade PMMA (same as the bulk PMMA plate) as increasing the MW decreases the surface tension ($\gamma \propto MW^{-2/3}$)[179]. The cross-section of the obtained fiber can be seen in Figure 5.7b, however this time a thinner PMMA plate was employed in the bulk. The high tension during the drawing, because in part of the wire feeding, caused the plate to bend and the PLGA to collapse in the drug reservoir.

Therefore, in the last attempt (Figure 5.7c), the thick PMMA plate with the same composition was thermally drawn. The integrity of the film could be successfully preserved albeit with the evidence of dewetting on the surface of PMMA.

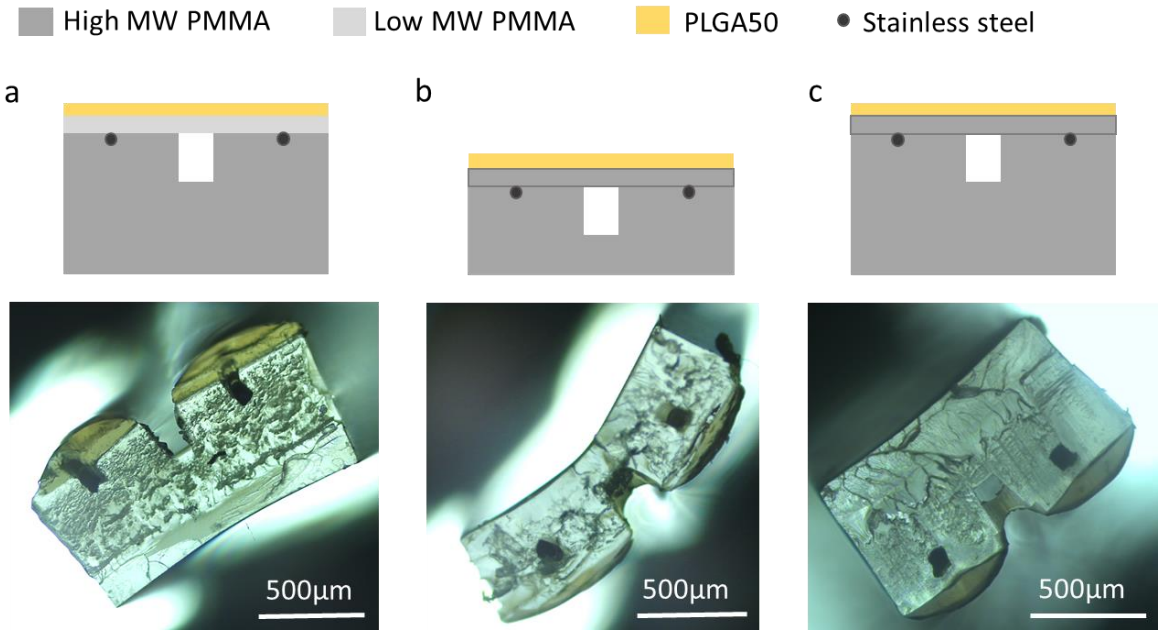

Figure 5.7. Schematics and corresponding cross-sections of thermally drawn fibers comprising stainless steel wires as electrodes and PLGA film as the release barrier: a) low and high MW PMMA with a thick PMMA plate (∼ 8 mm), b) high MW PMMA with a thin PMMA plate (∼ 4 mm), and c) high MW PMMA with a thick PMMA plate

5.5 Control of temperature via electric current in the fibers

In order to produce a circuit via the electrical wires, the two wires from one end of the fiber were exposed and knotted to be in contact with each other. At the other end of the fiber, PMMA and PLGA surrounding the wires were dissolved for 7cm to expose the wires. Next, four alligator probes were clipped on the wires for 4-probe measurement. A constant voltage was applied to the wires, and the produced current was recorded by a Keithley. At the same time, thermal photographs of the fiber were taken in the intervals of 1 minute via an infrared (IF) camera. Figure 5.8a shows the correlation between the current and temperature at three voltages of 1, 2 and 3V measured at room temperature. As can be seen, immediately after the application of voltage, the temperature rises and interestingly exhibits almost a stable value for the whole measurement period. The stability of temperature implies the equilibrium of heat exchange between the wire and the surrounding. Interestingly, the temperature follows all the fluctuation trend of the measured current

which is more clearly seen at 3V. Such a correlation shows a good control of the temperature via the applied current. As shown in Figure 5.8b, there is a slight difference in temperature along the fiber as the two ends exhibit the hottest spots. The temperature at the center of the fiber was selected as the representative temperature for each condition. The generated temperature at 1, 2, and 3V are found to be 30, 48 and 74°C, respectively. It should be noted that the applied voltage values are significantly higher than the values predicted by the theoretical heat exchange equation for achieving these temperatures. The reason behind is the significant losses of electrical energy to the surrounding. Since the temperature is stable at each applied voltage, these losses could be simulated using software such as COMSOL Multiphysics.

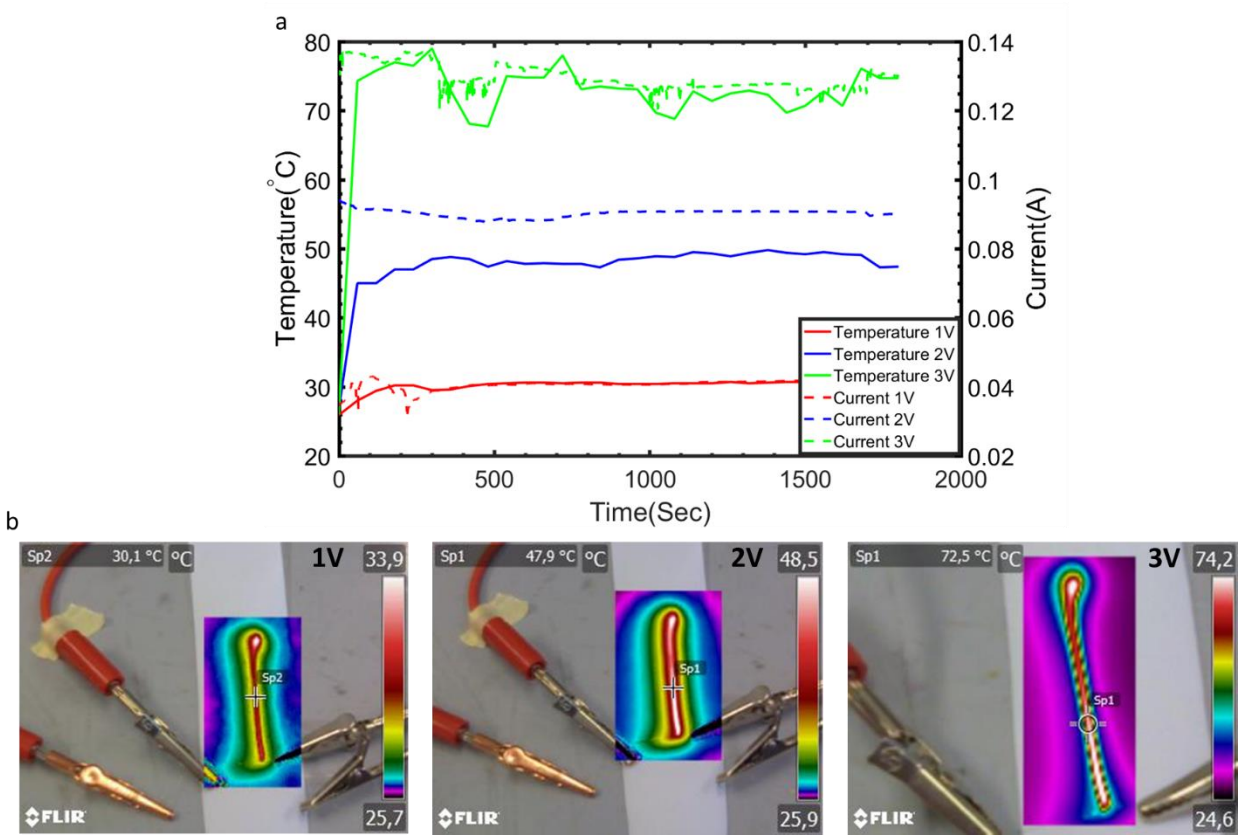

Figure 5.8. The heat generation in the fibers in air by the application of current, a) the correlation between the measured current and temperature, b) The thermal graph of fibers with application of 1V, 2V and 3V

In order to stimulate the aqueous environment of the body, the fibers were put in a container with water and bent to have the two ends of the fiber exposed in air. Then, the same procedure as the measurements in air was applied for the connections of the wires. Figure 5.9a shows the correlation between the current and temperature for the measurements in water at three voltages of 2, 3, and 4V. Figure 5.9b shows the representative thermal photographs at each voltage. As can be seen, the temperature distribution along the fiber varies a lot since only the center of the fiber is immersed in water. As water has a high heat capacity,

the obtained temperatures are much lower than the measured temperatures in air. However, the temperature still exhibits a relatively stable trend for the entire period of measurement: 27, 34 and 38°C at 2, 3 and 4V, respectively. The correlation between the changes in current and temperature is less clear compared to measurements in air. This could be explained by the higher losses originated from cooling by water as well as the lower obtained temperatures which make the fluctuations less pronounced.

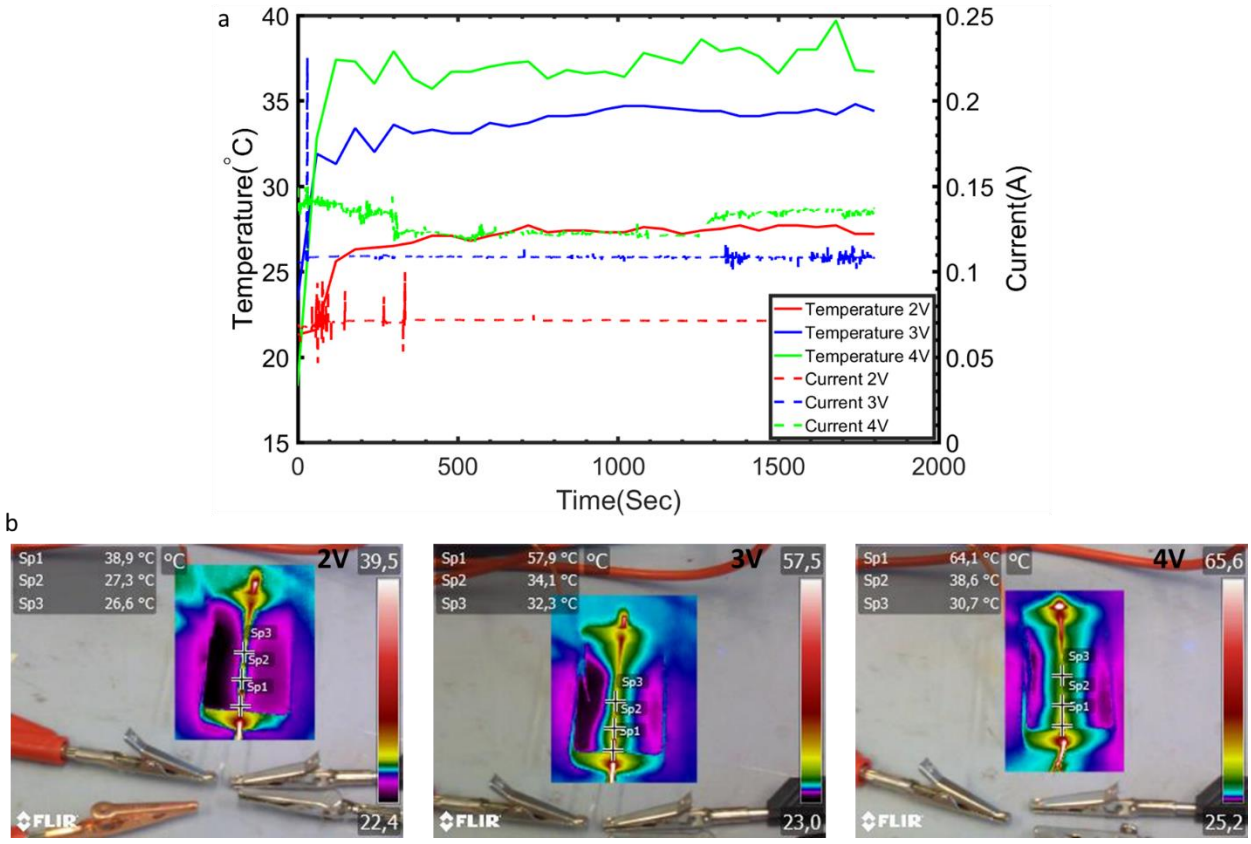

Figure 5.9. The heat generation in the fibers in water by the application of current, a) the correlation between the measured current and temperature, b) The thermal graph of fibers with application of 2V, 3V and 4V

5.6 Release study of electrically triggered fibers

In order to explore the release behavior of PLGA upon applying an electric current through the electrodes, the hollow channels were injected with FD70. The two ends of the fibers were glued while in one end the wires were exposed for the connection. No release was observed by applying voltage values of 4 and 5 V for 30min. The release at high temperatures during a short time, 30 minutes, compared to days of incubation in the oven, was speculated to be through the diffusion mechanism, however no clear release was observed upon the application of such high voltages. One reason could be due to the rapid morphological change of the polymer chains. As the chain mobility increases upon heating, the chains tend to form a coil-shape

structure and this could potentially lead to the inhibition of the release. In a previous work on low MW PLGA microspheres, a reduction of release was also observed at higher temperature due to the same reason[174]. Further release measurements over a longer period of time at such high temperature as well as at temperatures below T_g should be performed. Moreover, it would be interesting to investigate different parameters in the same measurements such as a drug model of smaller size and PLGA films of lower molecular weight or smaller thickness.

5.7 Experimental

Preform fabrication:

1) PMMA-PLGA preforms: two PMMA plates of 5.8 mm were hot-pressed (Lauffer Pressen UVL 5.0) together at 130 °C, 10 N cm^{-2} for 20 min to obtain a thicker plate with dimensions of 2.4 cm width,1.2 cm thickness and 16 cm length. A groove of 4 mm depth×2 mm width was milled along the preform. The PLGA film and PMMA plate were hot-pressed at 90 °C and 4 N cm^{-2} with presence of a Teflon bar in the channel to prevent the deformation of PLGA film. The Teflon bars were removed prior to drawing.

2) electrically active fibers: The preforms had a width of 24 mm and the length of 160 mm. Stainless steel wires (316 L) with a diameter of 80 µm and a density of 8000 kg/m^3 were incorporated in the preform via wire feeding. After milling hollow passages for the wires, the PMMA film was pressed on the PMMA plate at 200°C and under pressure of 10N/cm^2. After the preparation of the PLGA film of the desired thickness, it was hot-pressed on PMMA at 150°C and 6 N/cm^2.

DSC: After the fibers were taken from PBS, they were kept in the vacuum for a few days to fully evaporate the absorbed water. Then the DSC measurement was performed by a DSC Q100 TA on 10-15 mg samples of the entire fiber. The samples were heated from -10°C to 150°C at a constant speed of 10°C/min. The T_g value of the samples for each measurement was determined with "Universal Analysis" software.

SEM: The fibers were left to dry for a few days in a vacuum oven after they were taken out of the PBS. The fibers were coated with 5nm of Iridium, and the SEM was done with a secondary electron detector, with a tension of 0.5 kV and 30 µm aperture size.

Fluorescence spectroscopy: Fluorescence spectroscopy was performed on the PBS containing the fiber for the verification of released FD70. The excitation and emission wavelength were set at 493 and 516 nm, respectively and the slit length at 9nm.

Infrared camera: The temperature measurements were done using FLR-T62101. In the setting, the emissivity was set at 0.9, typically used for polymers.

Electric source: The voltage was applied using a Keithley DMM7510 7 ½ multimeter, and the generated current and resistance were recorded.

5.8 Summary and conclusion

A significant acceleration of release kinetics by increasing the degradation temperature was observed. The underlying degradation mechanism was elucidated by the measurement of thermal properties of PLGA during its degradation period. The heterogeneous bulk degradation of PLGA was confirmed and its kinetics was revealed. More interestingly, a clear correlation between the degradation and release kinetics was found. The obtained release profiles for the PLGAs degraded at different temperatures could be used as a reference to predict or to interpolate the degradation kinetics at different temperatures. This could be done through the correlation of temperature and activation energy using the slopes of release profiles as the indicator of degradation kinetics. Further measurements of T_g values during the degradation at 37°C is required. As 37°C lies well below the T_g, the degradation could follow different mechanisms from the PLGAs degraded at higher temperatures.

Finally integrating active components inside passive drug delivery systems is demonstrated through simultaneous processes of wire feeding and thermal drawing of polymers. Thanks to this co-processing, we could integrate materials of different physicochemical properties inside one device. Different designs of attempted fibers elucidated the weakness and strengths of the technique and led us to an effective material and geometry system for the successful drawing. As a result, stable temperatures below and above the glass transition of PLGA were achieved upon application of current as an external stimulus. Such systems allow us to determine the release mechanism of our drug delivery fibers, from diffusion-controlled to erosion-controlled, through the application of current in different periods of time.

Chapter 6 Conclusion and outlook

In this thesis, we demonstrated innovative materials and fabrication platform that reconciles processing of biodegradable polymers at high viscosity, with the precise tailoring of biodegradation kinetics of thin polymer films in a fiber form. Based on the scalable thermal drawing process traditionally used to make optical fibers, we designed, fabricated and characterized fibers with different biodegradable polymers, of different shapes and feature sizes down to micrometers, and encapsulating a prescribed array of microchannels that can contain a variety of substances. This study constitutes a novel paradigm for the design of biodegradable fibers as one dimensional capsules with multiple reservoirs and unprecedented release profiles of multiple drugs.

Our results consist of several breakthroughs both in scientific and technological perspectives:

- We proposed a unique materials selection criteria that balances the need for proper rheological properties during processing, the resulting mechanical properties of the fabricated fiber, and the biodegradability of the various polymers that will control release properties.
- As a result, we demonstrated biodegradable fibers with unprecedented complex architectures of different materials and microchannels, resulting in the most advanced release profiles, possibly of multiple drugs.
- The control release we demonstrated span a wide range from weeks to several months.
- We used modeling to understand and then design fibers with complex release profile. In this process, we reassessed the degradation and release mechanism of PLGA polymers that has been studied in the last decades.
- A composite system was proposed to enhance the biodegradation property of PLGA and to offer even more versatile release profiles, including zero order kinetics which is the target of many pharmaceutical systems.
- A facile fabrication method for active drug delivery systems was proposed to alter the polymer behavior upon applying an external trigger.
- The fabricated fibers have high mechanical properties, and can be textured, woven, or sustain knots, which makes them ideal candidates for a variety of applications in bioengineering and health care.

Below the highlights of scientific achievements and the future outlooks for each topic is presented in details:

6.1 Release kinetics of thermally drawn PLGAs

In order to provide a selection of polymers with different degradation rate for the realization of complex multimaterial fibers, PLGA polymers of different compositions and molecular weights were employed and their release behavior was characterized. The results of the release kinetics shined light on the complexity of coupling of PLGA degradation and release kinetics. The morphological analysis of the PLGA revealed evidences of pores, swelling and rupture at different times throughout the degradation period which could be matched very accurately to the release results. Moreover, it was found that the effect of thickness in PLGA delivery system is not straightforward and it highly depends on the composition and molecular weight of PLGA. In our study, the thickness values lie below 100 microns which is much thinner than the previously studied thicknesses in reservoir-type systems. Therefore, these release results pave the way towards the further miniaturization of complex drug delivery systems. In order to quantitatively describe the release profiles and to elucidate the underlying release mechanisms, a release model coupled to an existing phenomenological degradation model was developed. The proposed release equation is able to describe the shift of mechanism ranging from thinner films attributed to the diffusion-controlled release to thicker films attributed to erosion-controlled release. More strikingly, the developed release equation was able to show a faster release in thicker films for slow degradation rate polymers such as PLGA75, such capability was not demonstrated by previous models. After providing the prerequisites of release prediction, complex biodegradable fiber devices capable of prolonged administration of drugs in temporal-spatial controlled dosages were successfully applied via thermal drawing. In contrast to previously demonstrated thermally drawn fibers, this is the first time that the biodegradation property of the comprising materials is exploited to produce a function. The integration of such complex drug delivery functions with precise control over their released dosage in biomedical fibers and fabrics paves the way towards exciting opportunities in wound dressing, implantable scaffolds, smart sutures and medical textiles.

For future prospects, it is necessary to perform the in-vivo release study to confirm the results obtained in vitro. The physiological condition is much more complex than PBS as the presence of proteins, cells and enzyme could impact the release profiles. One step closer to the in vivo study could be to use body fluid, such as saliva, blood serum or intestinal fluid in the vitro studies[46]. Consequently, it is essential to develop models to take into account the present parameters in vivo, such as osmotic pressure, cellular reactions and enzymes[47]. Moreover, more parameters should be experimentally determined to strengthen the model. For example, the diffusion coefficient of the drug inside the polymer can be experimentally measured by nuclear magnetic resonance or fluorescence correlation spectroscopy [11]. The pores can be further characterized by non-mercury porosimetry and three-dimensional confocal microscopy to have statistics of their size and density. In order to analyze the extent of autocatalysis and the distribution of acidic by-products in the PLGA film, the micro-pH could be monitored via electron paramagnetic resonance and laser confocal microscopic imaging. Finally, a release model capable of illustrating the complexity of multi-

component drug delivery systems should be developed to describe the multi-dose release kinetics obtained in our fibers.

6.2 Mechanical property of biodegradable fibers

The developed drug delivery fibers via thermal drawing offer the advantage of high mechanical strength compared to the microstructured drug delivery devices developed by other techniques. Just by the adjustment of the drawing parameters, the tensile strength of the fibers could be improved by more than 3 times (from 80MPa to 275MPa), an improvement factor unprecedented in the other fiber technologies. In order to confirm the applicability of our results in real applications, the effect of tensile force on the integrity of the release barriers as well as the fiber core during their degradation period should be verified. Furthermore, we could find a compromise between the two desired properties of appropriate degradation rate and mechanical robustness by co-drawing a semi-crystalline PCL core within a micro-structured PLGA cladding. This is a striking result as PCL is in rubbery state at room temperature and just its crystalline part is responsible for the prevention of the shrinkage of highly aligned PLGA chains. In terms of fundamental aspects of the mechanical properties, it would be interesting to further study the behavior of the composite, particularly looking at interface effects. This method could be also utilized in other polymer processing methods as a coating layer of PCL for tackling the common problem of shrinkage.

6.3 Composite of phosphate glass and PLGA

A composite system of phosphate glass particles of fast absorbable rate within a matrix of PLGA with a slow degradation rate and high viscoelastic properties was discussed. It was found that with a large size of inorganic particles (average of 25μm), the content of particles will have almost no impact on the viscoelastic property of the parent matrix except at very high contents (40%). Such composites were able to tailor the degradation properties of PLGA while maintaining a neutral pH with the incorporation of just 5% of PG particles. This neutral pH is to be compared to the pH 3 obtained when pure PLGA degrades. This is an important achievement as this neutralization allows the exploitation of PLGA in a wider range of applications. Moreover, the integration of these composites with different PG contents resulted in versatile release profiles ranging from first-order, zero-order, and sigmoidal-profile. The underlying mechanism of these release profiles was revealed through structure-function relationship for each composition. In the future, it would be interesting to study the impact of smaller size particles (a few microns) on both the viscoelastic property and the release kinetics of biodegradable fiber composites. Such composite drug delivery fibers containing phosphate glasses with antimicrobial properties could be an ideal material system

for wound dressings. The release of antibacterial ions upon PG dissolution in combination with the delivery of antimicrobial agent as the encapsulated drug is highly beneficial in the treatment of severe burns and infected surgical , for example[93].

6.4 Electrically active drug delivery fibers

In the last part we established an intriguing fabrication method to realize active drug delivery fibers through which the physicochemical properties of the polymer could be altered by an external stimulus. Toward this goal, we carried out a deep analysis of the effect of temperature on the release kinetics of PLGA. All the release profiles obtained for PLGAs degraded at different temperatures exhibited the typical PLGA sigmoidal shape. However, the total release timeline could be accelerated from a few weeks to just a few days with the increase of temperature from 37 to 60°C. Electrically active drug delivery fibers were developed which could achieve higher stable temperature upon the application of a current through embedded metallic electrodes. Release experiments of fibers at 4V for 30 min showed no trace of released drug. As the generated temperature was above the Tg of PLGA, it was hypothesized that the rubbery state of the polymer led to the inhibition of the drug diffusion. Nevertheless, this study helped us to elucidate some of the effective parameters of the stimulus and the release barrier in this configuration to be able to stimulate the release in a timely manner. These parameters include the value of applied voltage, time intervals of voltage application, drug size, PLGA molecular weight and thickness which should be further investigated.

An appealing alternative to PLGA for the development of stimuli-responsive drug delivery fibers is the use of hydrogels, as they have a high sensitivity to temperature and pH. However, a challenge regarding the integration of hydrogels is the development of novel formulations which are compatible with the thermal drawing process. Another promising method for the generation of heat inside the fibers could be the use of super paramagnetic nanoparticle (SPIONs) from which controlled temperature could be obtained upon the application of a high frequency magnetic field. Such a heat source has the advantage of remote application and targeted delivery. At last, one main concern that should be addressed in the future studies is the biocompatibility, biodegradability and non-toxicity of the smart drug delivery systems during their serving period. Therefore, it is required to identify biodegradable conductive materials to be integrated in the thermal drawing process.

Reference

[1] M. Grassi and G. Grassi, "Mathematical modelling and controlled drug delivery: matrix systems," *Curr Drug Deliv*, vol. 2, no. 1, pp. 97–116, Jan. 2005, doi: 10.2174/1567201052772906.

[2] L.-M. Zhu and D. G. Yu, "9 - Drug delivery systems using biotextiles," in *Biotextiles as Medical Implants*, M. W. King, B. S. Gupta, and R. Guidoin, Eds. Woodhead Publishing, 2013, pp. 213–231.

[3] V. Albright *et al.*, "Micelle-Coated, Hierarchically Structured Nanofibers with Dual-Release Capability for Accelerated Wound Healing and Infection Control," *Advanced Healthcare Materials*, vol. 7, no. 11, p. 1800132, 2018, doi: 10.1002/adhm.201800132.

[4] D. P. Pioletti, O. Gauthier, V. A. Stadelmann, B. Bujoli, J. Guicheux, and P.-Y. Z. and J.-M. Bouler, "Orthopedic Implant Used as Drug Delivery System: Clinical Situation and State of the Research," *Current Drug Delivery*, Dec. 31, 2007. http://www.eurekaselect.com/66184/article (accessed Jul. 31, 2019).

[5] A. Kumar and J. Pillai, "Chapter 13 - Implantable drug delivery systems: An overview," in *Nanostructures for the Engineering of Cells, Tissues and Organs*, A. M. Grumezescu, Ed. William Andrew Publishing, 2018, pp. 473–511.

[6] S. Shadman *et al.*, "Microstructured Biodegradable Fibers for Advanced Control Delivery," *Advanced Functional Materials*, vol. 30, no. 13, p. 1910283, Mar. 2020, doi: 10.1002/adfm.201910283.

[7] M. Ramchandani and D. Robinson, "In vitro and in vivo release of ciprofloxacin from PLGA 50:50 implants," *Journal of Controlled Release*, vol. 54, no. 2, pp. 167–175, Jul. 1998, doi: 10.1016/S0168-3659(97)00113-2.

[8] S. Mao, J. Xu, C. Cai, O. Germershaus, A. Schaper, and T. Kissel, "Effect of WOW process parameters on morphology and burst release of FITC-dextran loaded PLGA microspheres," *International Journal of Pharmaceutics*, vol. 334, no. 1–2, pp. 137–148, Apr. 2007, doi: 10.1016/j.ijpharm.2006.10.036.

[9] T. G. Park, "Degradation of poly (lactic-co-glycolic acid) microspheres: effect of copolymer composition," *Biomaterials*, vol. 16, no. 15, pp. 1123–1130, 1995.

[10] F. Danhier, E. Ansorena, J. M. Silva, R. Coco, A. Le Breton, and V. Préat, "PLGA-based nanoparticles: An overview of biomedical applications," *Journal of Controlled Release*, vol. 161, no. 2, pp. 505–522, Jul. 2012, doi: 10.1016/j.jconrel.2012.01.043.

[11] K. Khoshnevisan *et al.*, "Cellulose acetate electrospun nanofibers for drug delivery systems: Applications and recent advances," *Carbohydrate Polymers*, vol. 198, pp. 131–141, Oct. 2018, doi: 10.1016/j.carbpol.2018.06.072.

[12] S. Chakraborty, I.-C. Liao, A. Adler, and K. W. Leong, "Electrohydrodynamics: A facile technique to fabricate drug delivery systems," *Adv. Drug Deliv. Rev.*, vol. 61, no. 12, pp. 1043–1054, Oct. 2009, doi: 10.1016/j.addr.2009.07.013.

[13] E. Mathiowitz, D. M. Lavin, and R. A. Hopkins, "Wet spun microfibers: potential in the design of controlled-release scaffolds?," *Therapeutic Delivery*, vol. 4, no. 9, pp. 1075–1077, Sep. 2013, doi: 10.4155/tde.13.73.

[14] D. Shahriari *et al.*, "Scalable Fabrication of Porous Microchannel Nerve Guidance Scaffolds with Complex Geometries," *Advanced Materials*, vol. 31, no. 30, p. 1902021, 2019, doi: 10.1002/adma.201902021.

[15] Z. X. Meng *et al.*, "Preparation and characterization of electrospun PLGA/gelatin nanofibers as a potential drug delivery system," *Colloids and Surfaces B: Biointerfaces*, vol. 84, no. 1, pp. 97–102, May 2011, doi: 10.1016/j.colsurfb.2010.12.022.

[16] D. b. Keck, R. d. Maurer, and P. c. Schultz, "On the ultimate lower limit of attenuation in glass optical waveguides," *Appl. Phys. Lett.*, vol. 22, no. 7, pp. 307–309, Apr. 1973, doi: 10.1063/1.1654649.

[17] Y. Qu *et al.*, "Superelastic Multimaterial Electronic and Photonic Fibers and Devices via Thermal Drawing," *Advanced Materials*, vol. 30, no. 27, p. 1707251, Jul. 2018, doi: 10.1002/adma.201707251.
[18] T. Nguyen-Dang, A. G. Page, Y. Qu, M. Volpi, W. Yan, and F. Sorin, "Multi-material micro-electromechanical fibers with bendable functional domains," *J. Phys. D: Appl. Phys.*, vol. 50, no. 14, p. 144001, Mar. 2017, doi: 10.1088/1361-6463/aa5bf7.
[19] C. Dong, A. G. Page, W. Yan, T. Nguyen-Dang, and F. Sorin, "Microstructured Multimaterial Fibers for Microfluidic Sensing," *Advanced Materials Technologies*, vol. 4, no. 10, p. 1900417, 2019, doi: 10.1002/admt.201900417.
[20] T. Zhang *et al.*, "High-performance, flexible, and ultralong crystalline thermoelectric fibers," *Nano Energy*, vol. 41, pp. 35–42, Nov. 2017, doi: 10.1016/j.nanoen.2017.09.019.
[21] A. Leber *et al.*, "Compressible and Electrically Conducting Fibers for Large-Area Sensing of Pressures," *Advanced Functional Materials*, vol. 0, no. 0, p. 1904274, doi: 10.1002/adfm.201904274.
[22] W. Yan *et al.*, "Semiconducting Nanowire-Based Optoelectronic Fibers," *Advanced Materials*, vol. 29, no. 27, p. 1700681, Jul. 2017, doi: 10.1002/adma.201700681.
[23] F. Sordo *et al.*, "Microstructured Fibers for the Production of Food," *Advanced Materials*, vol. 31, no. 14, p. 1807282, 2019, doi: 10.1002/adma.201807282.
[24] D. Shahriari *et al.*, "Scalable Fabrication of Porous Microchannel Nerve Guidance Scaffolds with Complex Geometries," *Advanced Materials*, vol. 0, no. 0, p. 1902021, doi: 10.1002/adma.201902021.
[25] R. A. Koppes *et al.*, "Thermally drawn fibers as nerve guidance scaffolds," *Biomaterials*, vol. 81, pp. 27–35, Mar. 2016, doi: 10.1016/j.biomaterials.2015.11.063.
[26] T. Nguyen-Dang *et al.*, "Controlled Sub-Micrometer Hierarchical Textures Engineered in Polymeric Fibers and Microchannels via Thermal Drawing," *Advanced Functional Materials*, vol. 27, no. 10, p. 1605935, Mar. 2017, doi: 10.1002/adfm.201605935.
[27] G. Loke *et al.*, "Structured multimaterial filaments for 3D printing of optoelectronics," *Nature Communications*, vol. 10, no. 1, pp. 1–10, Sep. 2019, doi: 10.1038/s41467-019-11986-0.
[28] S. Park *et al.*, "One-step optogenetics with multifunctional flexible polymer fibers," *Nature Neuroscience*, vol. 20, no. 4, pp. 612–619, Apr. 2017, doi: 10.1038/nn.4510.
[29] R. D. Maurer and P. C. Schultz, "Fused silica optical waveguide." May 02, 1972.
[30] D. B. Keck, R. D. Maurer, and P. C. Schultz, "On the ultimate lower limit of attenuation in glass optical waveguides," *Applied Physics Letters*, vol. 22, pp. 307–309, Apr. 1973, doi: 10.1063/1.1654649.
[31] M. Bayindir *et al.*, "Metal–insulator–semiconductor optoelectronic fibres," *Nature*, vol. 431, no. 7010, pp. 826–829, Oct. 2004, doi: 10.1038/nature02937.
[32] F. Sorin *et al.*, "Exploiting Collective Effects of Multiple Optoelectronic Devices Integrated in a Single Fiber," *Nano Letters*, vol. 9, no. 7, pp. 2630–2635, Jul. 2009, doi: 10.1021/nl9009606.
[33] M. Bayindir, A. F. Abouraddy, J. Arnold, J. D. Joannopoulos, and Y. Fink, "Thermal-Sensing Fiber Devices by Multimaterial Codrawing," *Adv. Mater.*, vol. 18, no. 7, pp. 845–849, Apr. 2006, doi: 10.1002/adma.200502106.
[34] S. Egusa *et al.*, "Multimaterial piezoelectric fibres," *Nature Materials*, vol. 9, no. 8, pp. 643–648, Aug. 2010, doi: 10.1038/nmat2792.
[35] A. Gumennik *et al.*, "All-in-Fiber Chemical Sensing," *Advanced Materials*, vol. 24, no. 45, pp. 6005–6009, Nov. 2012, doi: 10.1002/adma.201203053.
[36] C. Lu *et al.*, "Polymer Fiber Probes Enable Optical Control of Spinal Cord and Muscle Function In Vivo," *Adv. Funct. Mater.*, vol. 24, no. 42, pp. 6594–6600, Nov. 2014, doi: 10.1002/adfm.201401266.
[37] F. Sorin *et al.*, "Multimaterial Photodetecting Fibers: a Geometric and Structural Study," *Adv. Mater.*, vol. 19, no. 22, pp. 3872–3877, Nov. 2007, doi: 10.1002/adma.200700177.

[38] W. Yan *et al.*, “Advanced Multimaterial Electronic and Optoelectronic Fibers and Textiles,” *Advanced Materials*, vol. 31, no. 1, p. 1802348, Jan. 2019, doi: 10.1002/adma.201802348.
[39] G. Loke, W. Yan, T. Khudiyev, G. Noel, and Y. Fink, “Recent Progress and Perspectives of Thermally Drawn Multimaterial Fiber Electronics,” *Advanced Materials*, vol. 32, no. 1, p. 1904911, Jan. 2020, doi: 10.1002/adma.201904911.
[40] D. Shahriari *et al.*, “Scalable Fabrication of Porous Microchannel Nerve Guidance Scaffolds with Complex Geometries,” *Advanced Materials*, vol. 31, no. 30, p. 1902021, 2019, doi: 10.1002/adma.201902021.
[41] B. Grena, J.-B. Alayrac, E. Levy, A. M. Stolyarov, J. D. Joannopoulos, and Y. Fink, “Thermally-drawn fibers with spatially-selective porous domains,” *Nature Communications*, vol. 8, no. 1, pp. 1–8, Aug. 2017, doi: 10.1038/s41467-017-00375-0.
[42] L. K. Fung and W. M. Saltzman, “Polymeric implants for cancer chemotherapy,” *Advanced Drug Delivery Reviews*, vol. 26, no. 2, pp. 209–230, Jul. 1997, doi: 10.1016/S0169-409X(97)00036-7.
[43] S. Kyotani *et al.*, “A study of embolizing materials for chemo-embolization therapy of hepatocellular carcinoma: antitumor effect of cis-diamminedichloroplatinum(II) albumin microspheres, containing chitin and treated with chitosan on rabbits with VX2 hepatic tumors,” *Chem. Pharm. Bull.*, vol. 40, no. 10, pp. 2814–2816, Oct. 1992, doi: 10.1248/cpb.40.2814.
[44] W. Bechtel *et al.*, “An experimental evaluation of microcapsules for arterial chemoembolization,” *Radiology*, vol. 161, no. 3, pp. 601–604, Dec. 1986, doi: 10.1148/radiology.161.3.2947261.
[45] G. Roos, P. I. Christensson, I. A. el Hag, B. Jakobsson, H. Teder, and U. Stenram, “Degradable starch microspheres in cytostatic treatment of a liver carcinoma; experimental studies in rats with 5-fluorouracil, tauromustine, carmustine, doxorubicin and RSU-1069,” *Anticancer Res.*, vol. 13, no. 3, pp. 635–641, Jun. 1993.
[46] Y. Fu and W. J. Kao, “Drug Release Kinetics and Transport Mechanisms of Non-degradable and Degradable Polymeric Delivery Systems,” *Expert Opin Drug Deliv*, vol. 7, no. 4, pp. 429–444, Apr. 2010, doi: 10.1517/17425241003602259.
[47] J. Siepmann and A. Göpferich, “Mathematical modeling of bioerodible, polymeric drug delivery systems,” *Adv. Drug Deliv. Rev.*, vol. 48, no. 2–3, pp. 229–247, Jun. 2001, doi: 10.1016/s0169-409x(01)00116-8.
[48] C. Shih, N. Waldron, and G. M. Zentner, “Quantitative analysis of ester linkages in poly(dl-lactide) and poly(dl-lactide-co-glycolide),” *Journal of Controlled Release*, vol. 38, no. 1, pp. 69–73, Jan. 1996, doi: 10.1016/0168-3659(95)00104-2.
[49] X. Wang, S. S. Venkatraman, F. Y. C. Boey, J. S. C. Loo, and L. P. Tan, “Controlled release of sirolimus from a multilayered PLGA stent matrix,” *Biomaterials*, vol. 27, no. 32, pp. 5588–5595, Nov. 2006, doi: 10.1016/j.biomaterials.2006.07.016.
[50] S. J. Siegel, J. B. Kahn, K. Metzger, K. I. Winey, K. Werner, and N. Dan, “Effect of drug type on the degradation rate of PLGA matrices,” *European Journal of Pharmaceutics and Biopharmaceutics*, vol. 64, no. 3, pp. 287–293, Nov. 2006, doi: 10.1016/j.ejpb.2006.06.009.
[51] null Saltzman and null Fung, “Polymeric implants for cancer chemotherapy,” *Adv. Drug Deliv. Rev.*, vol. 26, no. 2–3, pp. 209–230, Jul. 1997, doi: 10.1016/s0169-409x(97)00036-7.
[52] J. Siepmann and F. Siepmann, “Mathematical modeling of drug delivery,” *Int J Pharm*, vol. 364, no. 2, pp. 328–343, Dec. 2008, doi: 10.1016/j.ijpharm.2008.09.004.
[53] P. L. Ritger and N. A. Peppas, “A simple equation for description of solute release II. Fickian and anomalous release from swellable devices,” *Journal of Controlled Release*, vol. 5, no. 1, pp. 37–42, Jun. 1987, doi: 10.1016/0168-3659(87)90035-6.
[54] J. Siepmann and N. A. Peppas, “Higuchi equation: Derivation, applications, use and misuse,” *International Journal of Pharmaceutics*, vol. 418, no. 1, pp. 6–12, Oct. 2011, doi: 10.1016/j.ijpharm.2011.03.051.
[55] B. J. Meister, “Uniting molecular network theory and reptation theory to predict the rheological behavior of entangled linear polymers,” *Macromolecules*, vol. 22, no. 9, pp. 3611–3619, Sep. 1989, doi: 10.1021/ma00199a019.

[56] T. Higuchi, “Rate of release of medicaments from ointment bases containing drugs in suspension,” *Journal of Pharmaceutical Sciences*, vol. 50, no. 10, pp. 874–875, 1961, doi: 10.1002/jps.2600501018.
[57] K. E. Uhrich, S. M. Cannizzaro, R. S. Langer, and K. M. Shakesheff, “Polymeric Systems for Controlled Drug Release,” *Chem. Rev.*, vol. 99, no. 11, pp. 3181–3198, Nov. 1999, doi: 10.1021/cr940351u.
[58] X. Zhu and R. D. Braatz, “A mechanistic model for drug release in PLGA biodegradable stent coatings coupled with polymer degradation and erosion: A Mechanistic Model for Drug Release in PLGA,” *Journal of Biomedical Materials Research Part A*, vol. 103, no. 7, pp. 2269–2279, Jul. 2015, doi: 10.1002/jbm.a.35357.
[59] R. Baker, *Controlled Release of Bioactive Materials*. Elsevier, 2012.
[60] R. P. Batycky, J. Hanes, R. Langer, and D. A. Edwards, “A Theoretical Model of Erosion and Macromolecular Drug Release from Biodegrading Microspheres,” *Journal of Pharmaceutical Sciences*, vol. 86, no. 12, pp. 1464–1477, Dec. 1997, doi: 10.1021/js9604117.
[61] J. L. Cleland *et al.*, “Development of a single-shot subunit vaccine for HIV-1,” *AIDS Res. Hum. Retroviruses*, vol. 10 Suppl 2, pp. S21-26, 1994.
[62] A. G. Thombre and K. J. Himmelstein, “A simultaneous transport-reaction model for controlled drug delivery from catalyzed bioerodible polymer matrices,” *AIChE Journal*, vol. 31, no. 5, pp. 759–766, 1985, doi: 10.1002/aic.690310509.
[63] K. Zygourakis, “Development and temporal evolution of erosion fronts in bioerodible controlled release devices,” *Chemical Engineering Science*, vol. 45, no. 8, pp. 2359–2366, Jan. 1990, doi: 10.1016/0009-2509(90)80116-V.
[64] K. Zygourakis and P. A. Markenscoff, “Computer-aided design of bioerodible devices with optimal release characteristics: a cellular automata approach,” *Biomaterials*, vol. 17, no. 2, pp. 125–135, Jan. 1996, doi: 10.1016/0142-9612(96)85757-7.
[65] Y. Wang, J. Pan, X. Han, C. Sinka, and L. Ding, “A phenomenological model for the degradation of biodegradable polymers,” *Biomaterials*, vol. 29, no. 23, pp. 3393–3401, Aug. 2008, doi: 10.1016/j.biomaterials.2008.04.042.
[66] X. Liu, G. J. Pettway, L. K. McCauley, and P. X. Ma, “Pulsatile release of parathyroid hormone from an implantable delivery system,” *Biomaterials*, vol. 28, no. 28, pp. 4124–4131, Oct. 2007, doi: 10.1016/j.biomaterials.2007.05.034.
[67] A. C. R. Grayson *et al.*, “Multi-pulse drug delivery from a resorbable polymeric microchip device,” *Nature Materials*, vol. 2, no. 11, pp. 767–772, Nov. 2003, doi: 10.1038/nmat998.
[68] S. Kim, J.-H. Kim, O. Jeon, I. C. Kwon, and K. Park, “Engineered Polymers for Advanced Drug Delivery,” *Eur J Pharm Biopharm*, vol. 71, no. 3, pp. 420–430, Mar. 2009, doi: 10.1016/j.ejpb.2008.09.021.
[69] D. Wermeling, R. Vallance, A. Balasubramanian, and B. L. Walcott, “Programmable Multi-Dose Intranasal Drug Delivery Device,” p. 34.
[70] V. Albright *et al.*, “Micelle-Coated, Hierarchically Structured Nanofibers with Dual-Release Capability for Accelerated Wound Healing and Infection Control,” *Adv Healthc Mater*, vol. 7, no. 11, p. e1800132, 2018, doi: 10.1002/adhm.201800132.
[71] H. Jiang, L. Wang, and K. Zhu, “Coaxial electrospinning for encapsulation and controlled release of fragile water-soluble bioactive agents,” *Journal of Controlled Release*, vol. 193, pp. 296–303, Nov. 2014, doi: 10.1016/j.jconrel.2014.04.025.
[72] G. Polacco, M. G. Cascone, L. Lazzeri, S. Ferrara, and P. Giusti, “Biodegradable hollow fibres containing drug-loaded nanoparticles as controlled release systems,” *Polymer International*, vol. 51, no. 12, pp. 1464–1472, 2002, doi: 10.1002/pi.1086.
[73] E. Ural, K. Kesenci, L. Fambri, C. Migliaresi, and E. Piskin, “Poly(d,l-cactide/ε-caprolactone)/hydroxyapatite composites,” *Biomaterials*, vol. 21, no. 21, pp. 2147–2154, Nov. 2000, doi: 10.1016/S0142-9612(00)00098-3.

[74] K. G. Marra, J. W. Szem, P. N. Kumta, P. A. DiMilla, and L. E. Weiss, “In vitro analysis of biodegradable polymer blend/hydroxyapatite composites for bone tissue engineering,” *Journal of Biomedical Materials Research*, vol. 47, no. 3, pp. 324–335, 1999, doi: 10.1002/(SICI)1097-4636(19991205)47:3<324::AID-JBM6>3.0.CO;2-Y.
[75] J. C. Knowles, G. W. Hastings, H. Ohta, S. Niwa, and N. Boeree, “Development of a degradable composite for orthopaedic use: in vivo biomechanical and histological evaluation of two bioactive degradable composites based on the polyhydroxybutyrate polymer,” *Biomaterials*, vol. 13, no. 8, pp. 491–496, 1992, doi: 10.1016/0142-9612(92)90099-a.
[76] R. L. Reis, J. S. Román, and J. S. Román, “Development of Bioactive Composites Based on Biodegradable Systems for Bone Replacement Applications,” *Biodegradable Systems in Tissue Engineering and Regenerative Medicine*, Nov. 29, 2004. https://www.taylorfrancis.com/ (accessed Jan. 21, 2020).
[77] M. V. Jose, V. Thomas, K. T. Johnson, D. R. Dean, and E. Nyairo, “Aligned PLGA/HA nanofibrous nanocomposite scaffolds for bone tissue engineering,” *Acta Biomater*, vol. 5, no. 1, pp. 305–315, Jan. 2009, doi: 10.1016/j.actbio.2008.07.019.
[78] A. Asti *et al.*, “Stem Cells Grown in Osteogenic Medium on PLGA, PLGA/HA, and Titanium Scaffolds for Surgical Applications,” *Bioinorganic Chemistry and Applications*, 2010. https://www.hindawi.com/journals/bca/2010/831031/ (accessed Jan. 29, 2020).
[79] L. L. Hench and J. R. Jones, “Bioactive Glasses: Frontiers and Challenges,” *Front. Bioeng. Biotechnol.*, vol. 3, 2015, doi: 10.3389/fbioe.2015.00194.
[80] M. Scheffler and P. Colombo, Eds., *Cellular ceramics: structure, manufacturing, properties and applications*. Weinheim: Wiley-VCH, 2005.
[81] D. Mohamad Yunos, O. Bretcanu, and A. R. Boccaccini, “Polymer-bioceramic composites for tissue engineering scaffolds,” *J Mater Sci*, vol. 43, no. 13, pp. 4433–4442, Jul. 2008, doi: 10.1007/s10853-008-2552-y.
[82] H. Wang, “Hydroxyapatite degradation and biocompatibility,” 2004.
[83] M. N. Rahaman *et al.*, “Bioactive glass in tissue engineering,” *Acta Biomater*, vol. 7, no. 6, pp. 2355–2373, Jun. 2011, doi: 10.1016/j.actbio.2011.03.016.
[84] E. Ceci-Ginistrelli *et al.*, “Drug release kinetics from biodegradable UV-transparent hollow calcium-phosphate glass fibers,” *Materials Letters*, vol. 191, pp. 116–118, Mar. 2017, doi: 10.1016/j.matlet.2016.12.103.
[85] J. Knowles, “Phosphate based glasses for biomedical applications,” 2003, doi: 10.1039/B307119G.
[86] rer nat Brauer and D. Silke, “Degradable phosphate glasses and composite materials for biomedical applications,” 2005.
[87] C.-K. Loong, K. Suzuya, D. L. Price, B. C. Sales, and L. A. Boatner, “Structure and dynamics of phosphate glasses: from ultra- to orthophosphate composition,” *Physica B: Condensed Matter*, vol. 241–243, pp. 890–896, Dec. 1997, doi: 10.1016/S0921-4526(97)00747-3.
[88] W. H. Zachariasen, “THE ATOMIC ARRANGEMENT IN GLASS,” *J. Am. Chem. Soc.*, vol. 54, no. 10, pp. 3841–3851, Oct. 1932, doi: 10.1021/ja01349a006.
[89] B. C. Bunker, G. W. Arnold, and J. A. Wilder, “Phosphate glass dissolution in aqueous solutions,” *Journal of Non-Crystalline Solids*, vol. 64, no. 3, pp. 291–316, May 1984, doi: 10.1016/0022-3093(84)90184-4.
[90] K. Franks, V. Salih, J. C. Knowles, and I. Olsen, “The effect of MgO on the solubility behavior and cell proliferation in a quaternary soluble phosphate based glass system,” *Journal of Materials Science: Materials in Medicine*, vol. 13, no. 6, pp. 549–556, Jun. 2002, doi: 10.1023/A:1015122709576.
[91] E. Ceci-Ginistrelli *et al.*, “Novel biocompatible and resorbable UV-transparent phosphate glass based optical fiber,” *Opt. Mater. Express, OME*, vol. 6, no. 6, pp. 2040–2051, Jun. 2016, doi: 10.1364/OME.6.002040.

[92] J. C. Knowles and G. W. Hastings, “In vitro and in vivo investigation of a range of phosphate glass-reinforced polyhydroxybutyrate-based degradable composites,” *J Mater Sci: Mater Med*, vol. 4, no. 2, pp. 102–106, Mar. 1993, doi: 10.1007/BF00120377.
[93] E. A. A. Neel and J. C. Knowles, “7 - Biocompatibility and other properties of phosphate-based glasses for medical applications,” in *Cellular Response to Biomaterials*, L. Di Silvio, Ed. Woodhead Publishing, 2009, pp. 156–182.
[94] T. Gilchrist, D. M. Healy, and C. Drake, “Controlled silver-releasing polymers and their potential for urinary tract infection control,” *Biomaterials*, vol. 12, no. 1, pp. 76–78, Jan. 1991, doi: 10.1016/0142-9612(91)90136-X.
[95] T. Gilchrist *et al.*, “In vitro nerve repair — in vivo. The reconstruction of peripheral nerves by entubulation with biodegradeable glass tubes — a preliminary report,” *British Journal of Plastic Surgery*, vol. 51, no. 3, pp. 231–237, Jan. 1998, doi: 10.1054/bjps.1997.0243.
[96] K. J. Toumba and M. E. J. Curzon, “Slow-Release Fluoride,” *CRE*, vol. 27, no. Suppl. 1, pp. 43–46, 1993, doi: 10.1159/000261601.
[97] E. A. El-Meliegy, M. M. Farag, and J. Knowles, “Dissolution and drug release profiles of phosphate glasses doped with high valency oxides,” *Journal of Materials Science: Materials in Medicine*, vol. 27, pp. 1–10, 2016, doi: 10.1007/s10856-016-5711-8.
[98] E. El-Meliegy, M. M. Farag, A. M. El-Kady, M. S. Mohamed, H. K. Abdelhakim, and M. Moaness, “Evaluation of solubility and cytotoxicity of lanthanum-doped phosphate glasses nanoparticles for drug delivery applications,” *Journal of Non-Crystalline Solids*, vol. 475, pp. 59–70, Nov. 2017, doi: 10.1016/j.jnoncrysol.2017.08.034.
[99] M. Fernández *et al.*, “Acrylic-phosphate glasses composites as self-curing controlled delivery systems of antibiotics,” *J Mater Sci Mater Med*, vol. 13, no. 12, pp. 1251–1257, Dec. 2002, doi: 10.1023/a:1021135314619.
[100] C. Ding, L. Tong, J. Feng, and J. Fu, “Recent Advances in Stimuli-Responsive Release Function Drug Delivery Systems for Tumor Treatment,” *Molecules*, vol. 21, no. 12, Dec. 2016, doi: 10.3390/molecules21121715.
[101] M. Stubbs, P. M. McSheehy, and J. R. Griffiths, “Causes and consequences of acidic pH in tumors: a magnetic resonance study,” *Adv. Enzyme Regul.*, vol. 39, pp. 13–30, 1999, doi: 10.1016/s0065-2571(98)00018-1.
[102] A. A. Aimetti, A. J. Machen, and K. S. Anseth, “Poly(ethylene glycol) hydrogels formed by thiol-ene photopolymerization for enzyme-responsive protein delivery,” *Biomaterials*, vol. 30, no. 30, pp. 6048–6054, Oct. 2009, doi: 10.1016/j.biomaterials.2009.07.043.
[103] R. Tang, R. N. Palumbo, W. Ji, and C. Wang, “Poly(ortho ester amides): Acid-labile Temperature-responsive Copolymers for Potential Biomedical Applications,” *Biomacromolecules*, vol. 10, no. 4, pp. 722–727, Apr. 2009, doi: 10.1021/bm9000475.
[104] B. Shen, Y. Ma, S. Yu, and C. Ji, “Smart Multifunctional Magnetic Nanoparticle-Based Drug Delivery System for Cancer Thermo-Chemotherapy and Intracellular Imaging,” *ACS Appl. Mater. Interfaces*, vol. 8, no. 37, pp. 24502–24508, Sep. 2016, doi: 10.1021/acsami.6b09772.
[105] L.-L. Tan, N. Song, S. X.-A. Zhang, H. Li, B. Wang, and Y.-W. Yang, “Ca2+, pH and thermo triple-responsive mechanized Zr-based MOFs for on-command drug release in bone diseases,” *J. Mater. Chem. B*, vol. 4, no. 1, pp. 135–140, Dec. 2015, doi: 10.1039/C5TB01789K.
[106] S. E. Naleway, W. Lear, J. J. Kruzic, and C. B. Maughan, “Mechanical properties of suture materials in general and cutaneous surgery: An Update on Mechanical Properties of Suture Materials,” *Journal of Biomedical Materials Research Part B: Applied Biomaterials*, vol. 103, no. 4, pp. 735–742, May 2015, doi: 10.1002/jbm.b.33171.
[107] A. J. Tsugawa and F. J. M. Verstraete, “Chapter 7 - Suture materials and biomaterials,” in *Oral and Maxillofacial Surgery in Dogs and Cats*, F. J. Verstraete and M. J. Lommer, Eds. Oxford: W.B. Saunders, 2012, pp. 69–78.
[108] W. Yan *et al.*, “Advanced Multimaterial Electronic and Optoelectronic Fibers and Textiles,” *Advanced Materials*, vol. 31, no. 1, p. 1802348, 2019, doi: 10.1002/adma.201802348.

[109] M. A. Schmidt, A. Argyros, and F. Sorin, “Hybrid Optical Fibers – An Innovative Platform for In-Fiber Photonic Devices,” *Advanced Optical Materials*, vol. 4, no. 1, pp. 13–36, 2016, doi: 10.1002/adom.201500319.
[110] M. Bayindir, A. F. Abouraddy, F. Sorin, J. D. Joannopoulos, and Y. Fink, “Detectors,” *Optics & Photonics News, OPN*, vol. 15, no. 12, pp. 24–24, Dec. 2004, doi: 10.1364/OPN.15.12.000024.
[111] R. L. Kronenthal, “Biodegradable Polymers in Medicine and Surgery,” in *Polymers in Medicine and Surgery*, R. L. Kronenthal, Z. Oser, and E. Martin, Eds. Boston, MA: Springer US, 1975, pp. 119–137.
[112] S. J. Holland, B. J. Tighe, and P. L. Gould, “Polymers for biodegradable medical devices. 1. The potential of polyesters as controlled macromolecular release systems,” *Journal of Controlled Release*, vol. 4, no. 3, pp. 155–180, Oct. 1986, doi: 10.1016/0168-3659(86)90001-5.
[113] R. K. Gupta, *Polymer and Composite Rheology, Second Edition,*. CRC Press, 2000.
[114] A. Franck, “Viscoelasticity and dynamic mechanical testing,” p. 7.
[115] “Introducing the Temperature Modulated DSC,” p. 8.
[116] L. C. Thomas, T. Instruments, L. Drive, and N. Castle, “Modulated DSC® Paper #2 Modulated DSC® Basics; Calculation and Calibration of MDSC® Signals,” p. 9.
[117] L. C. Thomas, T. Instruments, L. Drive, and N. Castle, “Modulated DSC® Paper #3 Modulated DSC® Basics; Optimization of MDSC® Experimental Conditions,” p. 10.
[118] R. Fu *et al.*, “Implantable and Biodegradable Poly(l-lactic acid) Fibers for Optical Neural Interfaces,” *Advanced Optical Materials*, vol. 6, no. 3, p. 1700941, 2018, doi: 10.1002/adom.201700941.
[119] R. Casasola, N. L. Thomas, A. Trybala, and S. Georgiadou, “Electrospun poly lactic acid (PLA) fibres: Effect of different solvent systems on fibre morphology and diameter,” *Polymer*, vol. 55, no. 18, pp. 4728–4737, Sep. 2014, doi: 10.1016/j.polymer.2014.06.032.
[120] T. Nguyen Dang, I. Richard, E. Goy, F. Sordo, and F. Sorin, “Insights into the fabrication of sub-100 nm textured thermally drawn fibers,” *Journal of Applied Physics*, vol. 125, no. 17, p. 175301, May 2019, doi: 10.1063/1.5089022.
[121] M. J. Ellis and J. B. Chaudhuri, “Poly(lactic-co-glycolic acid) hollow fibre membranes for use as a tissue engineering scaffold,” *Biotechnol. Bioeng.*, vol. 96, no. 1, pp. 177–187, Jan. 2007, doi: 10.1002/bit.21093.
[122] K. D. Nelson and B. B. Crow, “Drug releasing biodegradable fiber for delivery of therapeutics,” US7033603B2, Apr. 25, 2006.
[123] D. Klose, F. Siepmann, K. Elkharraz, and J. Siepmann, “PLGA-based drug delivery systems: Importance of the type of drug and device geometry,” *International Journal of Pharmaceutics*, vol. 354, no. 1–2, pp. 95–103, Apr. 2008, doi: 10.1016/j.ijpharm.2007.10.030.
[124] L. Lu, C. A. Garcia, and A. G. Mikos, “In vitro degradation of thin poly(DL-lactic-co-glycolic acid) films,” *J. Biomed. Mater. Res.*, vol. 46, no. 2, pp. 236–244, Aug. 1999.
[125] A. Djemai, L. F. Gladden, J. Booth, R. S. Kittlety, and P. R. Gellert, “MRI investigation of hydration and heterogeneous degradation of aliphatic polyesters derived from lactic and glycolic acids: a controlled drug delivery device,” *Magnetic resonance imaging*, vol. 19, no. 3, pp. 521–523, 2001.
[126] A. C. R. Grayson, M. J. Cima, and R. Langer, “Size and temperature effects on poly(lactic-co-glycolic acid) degradation and microreservoir device performance,” *Biomaterials*, vol. 26, no. 14, pp. 2137–2145, May 2005, doi: 10.1016/j.biomaterials.2004.06.033.
[127] S. Siegel, J. Kahn, K. Metzger, K. Winey, K. Werner, and N. Dan, “Effect of drug type on the degradation rate of PLGA matrices,” *European Journal of Pharmaceutics and Biopharmaceutics*, vol. 64, no. 3, pp. 287–293, Nov. 2006, doi: 10.1016/j.ejpb.2006.06.009.
[128] L. K. Chiu, W. J. Chiu, and Y.-L. Cheng, “Effects of polymer degradation on drug released — mechanistic study of morphology and transport properties in 50:50 poly(dl-lactide-co-glycolide),” *International Journal of Pharmaceutics*, vol. 126, no. 1, pp. 169–178, Dec. 1995, doi: 10.1016/0378-5173(95)04119-2.

[129] A. Charlier, B. Leclerc, and G. Couarraze, “Release of mifepristone from biodegradable matrices: experimental and theoretical evaluations,” *Int J Pharm*, vol. 200, no. 1, pp. 115–120, Apr. 2000.
[130] J. Siepmann and N. A. Peppas, “Higuchi equation: Derivation, applications, use and misuse,” *International Journal of Pharmaceutics*, vol. 418, no. 1, pp. 6–12, Oct. 2011, doi: 10.1016/j.ijpharm.2011.03.051.
[131] A. C. Dumitru *et al.*, “In situ nanomechanical characterization of the early stages of swelling and degradation of a biodegradable polymer,” *Nanoscale*, vol. 7, no. 12, pp. 5403–5410, 2015, doi: 10.1039/C5NR00265F.
[132] E. L. Cussler and E. L. Cussler, *Diffusion: Mass Transfer in Fluid Systems*. Cambridge University Press, 1997.
[133] P. Gunatillake, R. Mayadunne, and R. Adhikari, “Recent developments in biodegradable synthetic polymers,” in *Biotechnology Annual Review*, vol. 12, M. R. El-Gewely, Ed. Elsevier, 2006, pp. 301–347.
[134] F. P. La Mantia, M. Ceraulo, M. C. Mistretta, and M. Morreale, “Effect of cold drawing on mechanical properties of biodegradable fibers,” *J Appl Biomater Funct Mater*, vol. 15, no. 1, pp. e70–e76, Jan. 2017, doi: 10.5301/jabfm.5000328.
[135] M. Kanik *et al.*, “Strain-programmable fiber-based artificial muscle,” *Science*, vol. 365, no. 6449, pp. 145–150, Jul. 2019, doi: 10.1126/science.aaw2502.
[136] P. Nitti *et al.*, “Influence of Nanofiber Orientation on Morphological and Mechanical Properties of Electrospun Chitosan Mats,” *Journal of Healthcare Engineering*, 2018. https://www.hindawi.com/journals/jhe/2018/3651480/ (accessed Oct. 25, 2019).
[137] H. C. Kim, D. Kim, J. Y. Lee, L. Zhai, and J. Kim, “Effect of Wet Spinning and Stretching to Enhance Mechanical Properties of Cellulose Nanofiber Filament,” *Int. J. of Precis. Eng. and Manuf.-Green Tech.*, vol. 6, no. 3, pp. 567–575, Jul. 2019, doi: 10.1007/s40684-019-00070-z.
[138] W. Okumura, Y. Ohkoshi, Y. Gotoh, M. Nagura, H. Urakawa, and K. Kajiwara, “Effects of the drawing form and draw ratio on the fiber structure and mechanical properties of CO2-laser-heated-drawn poly(ethylene terephthalate) fibers,” *Journal of Polymer Science Part B: Polymer Physics*, vol. 42, no. 1, pp. 79–90, 2004, doi: 10.1002/polb.10673.
[139] I. Cantat and O. Pitois, “Stokes experiment in a liquid foam,” *Physics of Fluids*, vol. 18, no. 8, p. 083302, Aug. 2006, doi: 10.1063/1.2267062.
[140] G. Porte, J.-F. Berret, and J. L. Harden, “Inhomogeneous Flows of Complex Fluids: Mechanical Instability Versus Non-Equilibrium Phase Transition,” 1997, doi: 10.1051/jp2:1997138.
[141] D. A. Müller, J. G. Snedeker, and D. C. Meyer, “Two-month longitudinal study of mechanical properties of absorbable sutures used in orthopedic surgery,” *Journal of Orthopaedic Surgery and Research*, vol. 11, no. 1, Dec. 2016, doi: 10.1186/s13018-016-0451-5.
[142] R. N. Haward, “Strain hardening of thermoplastics,” *Macromolecules*, vol. 26, no. 22, pp. 5860–5869, Oct. 1993, doi: 10.1021/ma00074a006.
[143] T. Pakula and M. Trznadel, “Thermally stimulated shrinkage forces in oriented polymers: 1. Temperature dependence,” *Polymer*, vol. 26, no. 7, pp. 1011–1018, Jul. 1985, doi: 10.1016/0032-3861(85)90221-6.
[144] C. Ru, F. Wang, M. Pang, L. Sun, R. Chen, and Y. Sun, “Suspended, Shrinkage-Free, Electrospun PLGA Nanofibrous Scaffold for Skin Tissue Engineering,” *ACS Applied Materials & Interfaces*, vol. 7, no. 20, pp. 10872–10877, May 2015, doi: 10.1021/acsami.5b01953.
[145] C. Ru, F. Wang, M. Pang, L. Sun, R. Chen, and Y. Sun, “Suspended, Shrinkage-Free, Electrospun PLGA Nanofibrous Scaffold for Skin Tissue Engineering,” *ACS Appl. Mater. Interfaces*, vol. 7, no. 20, pp. 10872–10877, May 2015, doi: 10.1021/acsami.5b01953.
[146] “CONTROL OF DIMENSIONAL STABILITY AND DEGRADATION RATE IN ELECTROSPUN COMPOSITE SCAFFOLDS COMPOSED OF POLY(D,L-LACTIDE-co-GLYCOLIDE) AND POLY(ε-CAPROLACTONE),” *Chinese Journal of Polymer Science*, no. 01, pp. 63–71, 2008.

[147] S. Verrier, J. E. Gough, and A. R. Boccaccini, “7 - Bioactive glass containing composites for bone and musculoskeletal tissue engineering scaffolds,” in *Bioactive Glasses*, H. O. Ylänen, Ed. Woodhead Publishing, 2011, pp. 162–188.
[148] A. V. Shenoy, *Rheology of Filled Polymer Systems*. Springer Netherlands, 1999.
[149] C. G. Robertson, C. J. Lin, M. Rackaitis, and C. M. Roland, “Influence of Particle Size and Polymer−Filler Coupling on Viscoelastic Glass Transition of Particle-Reinforced Polymers,” *Macromolecules*, vol. 41, no. 7, pp. 2727–2731, Apr. 2008, doi: 10.1021/ma7022364.
[150] K. A. Schulze, A. A. Zaman, and K.-J. M. Söderholm, “Effect of filler fraction on strength, viscosity and porosity of experimental compomer materials,” *J Dent*, vol. 31, no. 6, pp. 373–382, Aug. 2003, doi: 10.1016/s0300-5712(03)00091-5.
[151] V. Hristov and J. Vlachopoulos, “Effects of polymer molecular weight and filler particle size on flow behavior of wood polymer composites,” *Polymer Composites*, vol. 29, no. 8, pp. 831–839, 2008, doi: 10.1002/pc.20455.
[152] J. Gurland, Brown University, Division of Engineering, and U.S. Atomic Energy Commission, *An estimate of contact and continuity of dispersions in opaque samples*. Providence, R.I.: Division of Engineering, Brown University, 1965.
[153] Z. Zapryanov and S. Tabakova, “Hydrodynamic Interaction between Particles and Effective Viscosity of Suspensions and Emulsions,” in *Dynamics of Bubbles, Drops and Rigid Particles*, Z. Zapryanov and S. Tabakova, Eds. Dordrecht: Springer Netherlands, 1999, pp. 307–336.
[154] A. V. Shenoy, *Rheology of Filled Polymer Systems*. Springer Netherlands, 1999.
[155] R. C. Picu and M. S. Ozmusul, “Structure of linear polymeric chains confined between impenetrable spherical walls,” *The Journal of Chemical Physics*, vol. 118, no. 24, pp. 11239–11248, Jun. 2003, doi: 10.1063/1.1576216.
[156] M. A. Osman and A. Atallah, “Effect of the particle size on the viscoelastic properties of filled polyethylene,” *Polymer*, vol. 47, no. 7, pp. 2357–2368, Mar. 2006, doi: 10.1016/j.polymer.2006.01.085.
[157] M. Li, D. Wilkinson, and K. Patchigolla, “Comparison of Particle Size Distributions Measured Using Different Techniques,” *Particulate Science and Technology*, vol. 23, no. 3, pp. 265–284, Jul. 2005, doi: 10.1080/02726350590955912.
[158] E. Vey *et al.*, “Degradation mechanism of poly(lactic-co-glycolic) acid block copolymer cast films in phosphate buffer solution,” *Polymer Degradation and Stability*, vol. 93, no. 10, pp. 1869–1876, Oct. 2008, doi: 10.1016/j.polymdegradstab.2008.07.018.
[159] M. Isobe, T. Amagasa, S. Oida, Y. Yamazaki, K. Ishihara, and N. Nakabayashi, “Bone morphogenetic protein encapsulated with a biodegradable and biocompatible polymer,” *Journal of Biomedical Materials Research*, vol. 32, no. 3, pp. 433–438, 1996, doi: 10.1002/(SICI)1097-4636(199611)32:3<433::AID-JBM17>3.0.CO;2-H.
[160] M. Ramchandani and D. Robinson, “In vitro and in vivo release of ciprofloxacin from PLGA 50:50 implants,” *Journal of Controlled Release*, vol. 54, no. 2, pp. 167–175, Jul. 1998, doi: 10.1016/S0168-3659(97)00113-2.
[161] S. Muschert, F. Siepmann, B. Leclercq, B. Carlin, and J. Siepmann, “Prediction of drug release from ethylcellulose coated pellets,” *Journal of Controlled Release*, vol. 135, no. 1, pp. 71–79, Apr. 2009, doi: 10.1016/j.jconrel.2008.12.003.
[162] D. Wójcik-Pastuszka, J. Krzak, B. Macikowski, R. Berkowski, B. Osiński, and W. Musiał, “Evaluation of the Release Kinetics of a Pharmacologically Active Substance from Model Intra-Articular Implants Replacing the Cruciate Ligaments of the Knee,” *Materials (Basel)*, vol. 12, no. 8, Apr. 2019, doi: 10.3390/ma12081202.
[163] D. Klose, F. Siepmann, K. Elkharraz, and J. Siepmann, “PLGA-based drug delivery systems: importance of the type of drug and device geometry,” *Int J Pharm*, vol. 354, no. 1–2, pp. 95–103, Apr. 2008, doi: 10.1016/j.ijpharm.2007.10.030.
[164] A. Djemai, L. F. Gladden, J. Booth, R. S. Kittlety, and P. R. Gellert, “MRI investigation of hydration and heterogeneous degradation of aliphatic polyesters derived from lactic and glycolic acids: a

controlled drug delivery device," *Magn Reson Imaging*, vol. 19, no. 3–4, pp. 521–523, May 2001, doi: 10.1016/s0730-725x(01)00283-1.
[165] A. C. R. Grayson, M. J. Cima, and R. Langer, "Size and temperature effects on poly(lactic-co-glycolic acid) degradation and microreservoir device performance," *Biomaterials*, vol. 26, no. 14, pp. 2137–2145, May 2005, doi: 10.1016/j.biomaterials.2004.06.033.
[166] L. Lu, C. A. Garcia, and A. G. Mikos, "In vitro degradation of thin poly(DL-lactic-co-glycolic acid) films," *Journal of Biomedical Materials Research*, vol. 46, no. 2, pp. 236–244, 1999, doi: 10.1002/(SICI)1097-4636(199908)46:2<236::AID-JBM13>3.0.CO;2-F.
[167] T. Pakula and M. Trznadel, "Thermally stimulated shrinkage forces in oriented polymers: 1. Temperature dependence," *Polymer*, vol. 26, no. 7, pp. 1011–1018, Jul. 1985, doi: 10.1016/0032-3861(85)90221-6.
[168] C. Ru, F. Wang, M. Pang, L. Sun, R. Chen, and Y. Sun, "Suspended, Shrinkage-Free, Electrospun PLGA Nanofibrous Scaffold for Skin Tissue Engineering," *ACS Appl Mater Interfaces*, vol. 7, no. 20, pp. 10872–10877, May 2015, doi: 10.1021/acsami.5b01953.
[169] M. Skovgaard, K. Almdal, B. F. Sørensen, S. Linderoth, and A. van Lelieveld, "Shrinkage reduction of dental composites by addition of expandable zirconia filler," *Journal of Composite Materials*, vol. 45, no. 26, pp. 2817–2822, Dec. 2011, doi: 10.1177/0021998311401936.
[170] C. J. Soares *et al.*, "Polymerization shrinkage stress of composite resins and resin cements – What do we need to know?," *Brazilian Oral Research*, vol. 31, Aug. 2017, doi: 10.1590/1807-3107bor-2017.vol31.0062.
[171] N. Malhotra, K. M, and S. Acharya, "Strategies to Overcome Polymerization Shrinkage − Materials and Techniques. A Review," *Dent Update*, vol. 37, no. 2, pp. 115–125, Mar. 2010, doi: 10.12968/denu.2010.37.2.115.
[172] C. m. Agrawal, D. Huang, J. p. Schmitz, and K. a. Athanasiou, "Elevated Temperature Degradation of a 50:50 Copolymer of PLA-PGA," *Tissue Engineering*, vol. 3, no. 4, pp. 345–352, Dec. 1997, doi: 10.1089/ten.1997.3.345.
[173] E. Vey *et al.*, "The impact of chemical composition on the degradation kinetics of poly(lactic-co-glycolic) acid copolymers cast films in phosphate buffer solution," *Polymer Degradation and Stability*, vol. 97, no. 3, pp. 358–365, Mar. 2012, doi: 10.1016/j.polymdegradstab.2011.12.010.
[174] B. S. Zolnik, P. E. Leary, and D. J. Burgess, "Elevated temperature accelerated release testing of PLGA microspheres," *J Control Release*, vol. 112, no. 3, pp. 293–300, May 2006, doi: 10.1016/j.jconrel.2006.02.015.
[175] S. D'Souza, J. A. Faraj, R. Dorati, and P. P. DeLuca, "Enhanced Degradation of Lactide-co-Glycolide Polymer with Basic Nucleophilic Drugs," *Advances in Pharmaceutics*, 2015. https://www.hindawi.com/journals/ap/2015/154239/ (accessed Feb. 24, 2020).
[176] M. C. Knirsch, C. Alves dos Santos, A. A. Martins de Oliveira Soares Vicent, and T. C. Vessoni Penna, "Ohmic heating – a review," *Trends in Food Science & Technology*, vol. 21, no. 9, pp. 436–441, Sep. 2010, doi: 10.1016/j.tifs.2010.06.003.
[177] L. A. Dissado and J. C. Fothergill, *Electrical degradation and breakdown in polymers*. London: P. Peregrinus, 1992.
[178] M. Rein *et al.*, "Diode fibres for fabric-based optical communications," *Nature*, vol. 560, no. 7717, pp. 214–218, Aug. 2018, doi: 10.1038/s41586-018-0390-x.
[179] D. G. Legrand and G. L. Gaines, "The molecular weight dependence of polymer surface tension," *Journal of Colloid and Interface Science*, vol. 31, no. 2, pp. 162–167, Oct. 1969, doi: 10.1016/0021-9797(69)90322-1.

Curriculum Vitae

Shahrzad Shadman Yazdi

Phone number: 0041 78 725 75 03
shahrzad.shadman@epfl.ch
shadman.shahrzad@gmail.com

EDUCATION

- **Ecole Polytechnique Federale de Lausanne (EPFL), Switzerland** May 2016- May 2020

Doctoral Program in Materials Science and Engineering
Project: Microstructured biodegradable fibers for controlled release
Advisor: Professor Fabien Sorin

- **Ecole Polytechnique Federale de Lausanne (EPFL), Switzerland** 2013-2015

Master in Materials Science and Engineering (in English)
Orientation in microelectronic and microtechnology

- **Budapest University of Technology and Economics (BME), Hungary** 2011-2013

Bachelor of Science in Chemical Technology and Biotechnology (in English)
Branch in Chemical and Process Engineering

- **American University of Sharjah (AUS), United Arab Emirates** 2008-2010

Bachelor of Science in Chemical Engineering (in English)

HONORS AND AWARDS

- On 20% scholarship at Budapest University of Technology (GPA> 4.5/5) 2012-2013
- On Dean's List at American University of Sharjah (GPA > 3.5/4)

RESEARCH EXPERIENCE

Laboratory for Semiconductor Materials (LMSC), EPFL October 2015-April 2016

- Internship on electrical characterization of Zn_3As_2 and Zn_3P_2 nanowires

Laboratory for Nanostructured Energy Conversion Devices, UM March 2015-August 2015
(University of Michigan, US)

- Master's Thesis: Hybrid fiber integrated transistors

Laboratory for Advanced Materials Processing, EMPA, Thun August 2014-January 2015
(Swiss Federal Laboratories for Materials Science and Technology)

- Internship on laser source influence on plasma composition determining weld quality of titanium

Department of Microtechnology, (Mta-mfa Kfki)
(Institute or Technical Physics and Materials Science, Hungary) December 2012- May 2013

- Bachelor's thesis: Fabrication and characterization of novel hybrid organic/inorganic solar cells using hierarchical ZnO nanostructures

TEACHING EXPERIENCE

- Fulltime tutor — February-July 2011
  International Training Institute, Knowledge Village, Dubai — Limited Duration Contract
  (Teaching Math and Chemistry in preparation for SAT and GED)
- Math tutor — September-December 2010
  Math Learning Center, American University of Sharjah — Limited Duration Contract
  (Teaching Calculus 1&2)

SKILLS

Languages:
Persian (native)
English (C1)
French (B2)

Computing: (intermediate)
MS Offices (Word, Excel, and Power Point)
MATLAB
Mathematica
Inventor

Technical:
Fiber fabrication
Polymer Processing
Polymers characterization
Biomaterials
Device design
Microscopy techniques
Chemical Analytical techniques

Soft Skills:
Strong interpersonal skills
Critical observation
Solution oriented
Lateral thinking
Autonomous
Persistent
Adaptive and flexible

SELECTED PUBLICATIONS AND CONFERENCE PROCEEDINGS

- "Microstructured biodegradable fibers for advanced drug delivery "; Sh. Shadman Yazdi, T. Ngyuyen-Dang,…, F. Sorin; *Advanced Functional Materials (2020),* p.1910283, doi: 10.1002/adfm.201910283.
- "Microstructured biodegradable Fibers via Thermal Drawing"; Sh. Shadman Yazdi, T. Ngyuyen-Dang,…, F. Sorin; European Materials Research Society(EMRS), Spring 2019
- "Compressible and Electrically Conducting Fibers for Large-Area Sensing of Pressures," A.Leber,…Sh. Shadman Yazdi, F. Sorin.; *Advanced Functional Materials (2019),* p. 1904274, doi: 10.1002/adfm.201904274.
- Investigation and in situ removal of spatter generated during laser ablation of aluminium composites; A.C. Popescu,… S. Shadman, M. Leparoux *; Applied Surface Science* 378 (2016) 102-103